Doctoral Dissertation (Shinshu University)

Study on the functionality of thermoplastic epoxy and its applications

(熱可塑性エポキシの機能性とその応用に関する研究)

September 2022

HU BAOJI

CONTENTS

Abstract I

Chapter 1: General introduction 1

1.1 Shape memory materials 1

1.1.1 Polymer based shape memory materials 3

1.1.2 Fiber type shape memory materials 5

1.2 Epoxy resins 6

1.2.1 Shape memory epoxy resins 7

1.2.2 Modification for epoxy resins 9

1.3 PEG for polymer modification 11

1.4 The purpose and significance of this work 13

1.5 The outline of this dissertation 15

Reference 18

Chapter 2: Shape memory thermoplastic epoxy filaments 38

2.1 Introduction 38

2.2 Materials and Methods 40

2.2.1 Materials 40

2.2.2 Fabrication of EP-TP and SMEF-TP 41

2.2.3 Characterization of chemical structure 42

2.2.4 Thermal analysis 43

2.2.5 Static and dynamic mechanical analysis 43

2.2.6 Shape memory experiments 44

2.3 Results and Discussion 46

2.3.1 Chemical structure 46

2.3.2 Thermal properties 47

2.3.3 Static and dynamic mechanical properties 49

2.3.4 Mechanism of shape memory for SMEF-TP 51

2.3.5 Cyclic test of shape memory process 55

2.3.6 Shape recovery stress of SMEF-TP 58

2.3.7 Application of SMEF-TP in thermal actuation 61

2.4 Conclusions 63

References 64

Chapter 3: Multifunctional shape memory epoxy-PEG films 70

3.1 Introduction 70

3.2 Materials and Methods 72

3.2.1 Materials 72

3.2.2 Fabrication of epoxy-PEG film 73

3.2.3 Water contact angle test 74

3.2.4 Impedance test 74

3.2.5 DSC test 75

3.2.6 FTIR test 75

3.2.7 TGA test 75

3.2.8 Tensile test 76

3.2.9 Dynamic mechanical test 76

3.2.10 Static thermo-mechanical test 76

3.3 Results and Discussion 77

3.3.1 Dispersion of PEG in thermoplastic epoxy 77

3.3.2 Thermal analysis of polymerization process 82

3.3.3 FTIR analysis of thermoplastic epoxy-PEG 84

3.3.4 Thermal stability analysis of thermoplastic epoxy-PEG 88

3.3.5 Mechanical property analysis 89

3.3.6 Dynamic mechanical property analysis 93

3.3.7 Shape memory properties 95

3.3.8 Observation for shape memory and healable properties 99

3.4 Conclusions 102

References 103

Chapter 4: Heat-stimuli controllable shape memory epoxy-PEG filaments 111

4.1 Introduction 111

4.2 Materials and Methods 113

4.2.1 Materials 113

4.2.2 Fabrication of TEP–PEG pellets and TEP–PEG filaments 114

4.2.3 Chemical structure analysis by FTIR 116

4.2.4 Thermal analysis 117

4.2.5 Tensile and dynamic mechanical analysis 117

4.2.6 Shape memory experiments 118

4.3 Results and Discussion 120

4.3.1 FTIR analysis 120

4.3.2 Thermal analysis 124

4.3.3 Mechanical analysis 128

4.3.4 Shape memory performance 131

4.3.4.1 Investigation and selection of prestress and tensile stress 131

4.3.4.2 Investigation of shape memory function 135

4.3.4.3 Recovery stress in shape recovery process 139

4.3.5 Discussion in thermal actuation 143

4.4. Conclusions 147

References 148

Chapter 5: General conclusions 155

List of publications 159

Scientific presentation 160

Acknowledgements 161

Abstract

In this study, the shape memory, thermal actuation, and self-healing functionality of thermoplastic epoxy resins are investigated, and their applications in artificial muscles, smart textiles, and flexible smart films are discussed. The main results obtained in this study are shown as follows.

(1) Development of thermoplastic epoxy filament for thermal actuation with excellent shape memory properties

An epoxy resin mixture composed of epoxy and phenol monomers is used to prepare thermoplastic epoxy polymer through a polymerization reaction and shape memory thermoplastic epoxy filament was successfully developed for the first time through a melt-drawing process. Tensile tests showed that the yield stress of the developed shape memory thermoplastic epoxy filament reached 63 MPa, which is an increase of 54% compared with thermoplastic epoxy films. Shape memory experiments showed that the developed shape memory thermoplastic epoxy filament has excellent shape memory performance, with a shape fixation rate of 97%, a shape recovery rate of over 97%, and good stability in cycling. Based on the shape memory performance analysis, the shape recovery stress of the shape memory thermoplastic epoxy filament was characterized. Shape recovery stress responded to temperature stability and increased with the increase of strain, reaching 1.45 MPa at a strain of 35%. The shape memory

thermoplastic epoxy filament can reach an energy density of 0.066 J/cm^3 during thermal actuation and shows greater application potential when processed into textiles. In addition, the chemical structure, thermal performance, and dynamic mechanical performance of shape memory thermoplastic epoxy filaments are analyzed. The developed shape memory thermoplastic epoxy filament shows excellent shape memory performance, and the output shape recovery stress is more than 5 times that of thermoplastic epoxy film, which provides huge application potential in the fields of artificial muscles and smart textiles.

(2) Development of shape memory thermoplastic epoxy films with human skin temperature response and self-healing function through the regulation of thermal and mechanical properties by PEG

In order to expand the application scope of thermoplastic epoxy resins, epoxy-polyethylene glycol (PEG) films with controllable thermal and mechanical properties were prepared by dispersing PEG, and their multifunctional shape memory properties were explored. PEG has excellent compatibility with unpolymerized epoxy resin because of the existence of a large number of C-O bonds and hydroxyl groups. A uniform and stable epoxy-PEG colloidal-like mixture can be obtained through environmentally friendly melt dispersion, and the PEG molecules are uniformly and stably wrapped in the polymerized epoxy molecular chain. The dispersion of PEG with different contents enables epoxy-PEG films to

be regulated between rigid and flexible without significantly reducing the thermal stability of epoxy-PEG, which greatly expands the application range of epoxy resin. Epoxy-PEG films with different PEG contents all have excellent shape memory properties with shape recovery rates between 92% to 100%, and can be regulated by heat-stimuli between original and temporary shapes. In addition, based on the regulation of T_g of epoxy-PEG films by PEG, the heat-stimuli temperature of epoxy-PEG films can also be adjusted to meet different application requirements. With increasing PEG content, epoxy-PEG films are able to achieve shape memory with human skin temperature response, self-healing, and heating-based adhesive functions. The epoxy-PEG films with controllable thermal and mechanical properties prepared by dispersion of PEG show greater application potential in the fields of shape memory and flexible smart materials.

(3) Development of shape memory thermoplastic epoxy filament with controllable heat-stimuli temperature for adapting thermal actuation of different temperature responses

Shape memory thermoplastic epoxy-polyethylene glycol (PEG) filaments were prepared for the first time based on the research of PEG-modified thermoplastic epoxy, and the heat-stimuli controllability of shape memory function was innovatively endowed by adding PEG in an environmentally friendly way. PEG regulates the T_g of PEG-modified

thermoplastic epoxy without interfering with the polymerization reaction of epoxy. The melt spinning temperature of PEG-modified thermoplastic epoxy is also reduced from 300 °C to 220 °C, and the spinning effect is improved. After PEG modification, Young's modulus of PEG-modified thermoplastic epoxy filaments drawn from PEG-modified thermoplastic epoxy pellets was higher at room temperature. The developed PEG-modified thermoplastic epoxy filaments have excellent shape memory effect with high shape recovery rates of 93.1%–99.0%, and shape fixation rates ranging from 95.8% to 99.1% are also improved after PEG modification. Furthermore, PEG-modified thermoplastic epoxy filaments have controllable stimuli temperatures of shape memory ranging from 69 °C to 105 °C. Additionally, the recovery stress of PEG-modified thermoplastic epoxy filaments after PEG modification was increased to 1.77 MPa, and the recovery temperature of the maximum recovery stress is reduced from 97 °C to 58 °C as PEG content increases to 15 wt%. The problems of difficult melt processing and uncontrollable stimuli temperature for thermoplastic epoxy were solved in this study. The developed PEG-modified thermoplastic epoxy filaments with heat-stimuli controllability of the shape memory function demonstrated excellent thermal actuation capabilities and have shown greater application potential in thermal actuation, smart textiles, and artificial muscles.

In conclusion, from the development of thermoplastic epoxy shape

memory filaments to the development of multifunctional epoxy-PEG including shape memory by dispersing PEG, and further to the development of thermally controlled shape memory epoxy-PEG, this research developed multifunctional thermoplastic epoxy-PEG material in an environment-friendly and low-cost way base on the revealing the dispersing mechanism of PEG in thermoplastic epoxy. In terms of textiles, the developed pure thermoplastic epoxy filaments show great thermal actuation ability on the basis of excellent shape memory properties. The further developed thermoplastic epoxy-PEG filaments can respond to heat-stimuli at different temperatures on the basis of maintaining the excellent shape memory properties of pure epoxy filaments, showing an excellent controllable heat-stimuli shape memory function. In terms of film materials, the developed thermoplastic epoxy-PEG films with more PEG content showed a change from rigid to flexible with increasing PEG content and showed shape memory with human skin temperature response, self-healing, and adhesion performance, which was extremely greatly improved the application range of thermoplastic epoxy.

Chapter 1: General introduction

1.1 Shape memory materials

Smart materials that can produce significant performance changes due to external stimuli are the necessary basis for realizing the concept of intelligence in the fourth industrial revolution, which has recently attracted much attention [1]. As a class of smart materials, shape memory materials (SMMs) have gradually been applied in various fields due to their advanced versatility [2]. SMMs are able to dynamically switch between primitive and temporary shapes through a variety of external stimuli to perform their functions in different application domains [3].

External stimuli usually refer to changes in the external environment, the ability to respond to specific or multiple external environmental changes is considered a prerequisite for SMMs, and the actual ability to achieve executive functions according to the response is a key factor for SMMs to be defined as smart materials [4]. The original shape of SMMs, also known as the permanent shape, is usually the shape processed by the preparation method [5]. The initial shape is changed to a temporary shape by specific or predefined external conditions, and this temporary shape can perform some functions that the original shape could not perform well [6]. Generally, the external conditions that change the initial shape to the

temporary shape are external stress, and the temporary shape from which the external stress is removed can still be well maintained [7]. When no executive function is required, SMMs can be recovery from the temporary shape to the original shape by specific external stimuli, and the process of recovering the temporary shape to the original shape can also be the process of executive function [8]. External stimuli that recovery SMMs from their temporary shape to their original shape generally refer to heating, indirect heating of light and electricity, changes in electromagnetic fields, changes in pH and ions, and changes in humidity [9]. Such non-mechanical external stimuli can induce shape recovery of SMMs based on internal structural changes [10]. In many practical applications, the shape change of materials cannot or is inconvenient to be changed by applying mechanical stress, and shape switching by non-mechanical stimuli shows the intelligence of SMMs [11]. Not only that, SMMs can also be mechanically actuated by outputting mechanical energy during the shape recovery process [12]. This shape recovery with mechanically actuation function through intelligent response without mechanical stimulation undoubtedly expands the application field of SMMs [13].

Awareness of SMMs can be traced back to the 1940s but was not vigorously spread until the 1990s. As its application potential in a wide range of fields gradually showed, it began to attract attention in the late 1990s [14]. The versatile properties of SMMs that can be used in a variety

of geometries have made them attractive to designers and are increasingly used in automotive, packaging engineering, electronics and textiles [15]. In recent years, SMMs, including shape memory alloys, shape memory polymers, and their composites, have been gradually applied in aerospace, biomedicine and artificial intelligence, and the market prospects have gradually expanded while also showing diversification and synergy in design and function [16].

1.1.1 Polymer based shape memory materials

As one type of SMMs, shape memory polymers (SMPs) have gradually attracted extensive attention in recent years [17]. Generally, SMPs that respond to heat-stimuli have biphasic or multiphase polymer structures with both hard and soft segments [18]. The hard segment and the soft segment are connected to each other through physical and chemical cross-linking, and the formed two-phase or multi-phase structure can show a dynamic change process when the external conditions change back and forth [19]. When the temperature is lower than the glass transition temperature (T_g) of the soft segment, the SMPs can maintain the shape as the original shape [20]. When the temperature is higher than the T_g of the soft segment and lower than the T_g of the hard segment, the soft segment is easily changed into a temporary shape by external stress due to the intensified thermal motion of the molecules, and this temporary shape can

maintain by rapidly changing the temperature to below the T_g of the soft segment due to the rapidly reduced molecule thermal motion [21]. The soft segment provides a prerequisite for SMPs to deform due to changes in external conditions, while the hard segment confines the deformation within a certain range and induces shape recovery [22]. When the temperature is raised to the T_g of the soft segment again, the hard segment induces the shape recovery of the soft segment whose molecular thermal motion is intensified [23]. By design, SMPs generate dynamic changes in shape when external conditions change back and forth to meet different demanding application fields [24].

Compared with shape memory alloys (SMAs), SMPs have attracted more and more attention due to their high flexibility, lightweight, low cost, and high recyclability [25]. They also show great potential in applications such as flexible sensors [26], soft actuators [27], self-healing materials [28], flexible energy harvesters [29], and smart textiles [30]. In recent studies, SMPs obtained better mechanical properties, shorter recovery time, greater recovery stress, and electrical conductivity by doping with inorganic particles such as carbon nanotubes and graphene [31]. Modification by functional particles is an important means to realize the multifunctional application of SMPs [32].

As multifunctional materials, composites based on SMPs have been

reported to be able to be applied in artificial intelligence [33], biomedicine [34], smart textiles [35], etc. by responding to heat [36], electricity [37], humidity [38], light [39], and magnetic fields [40]. In addition, SMPs with functions such as repairable, recyclable, and biodegradable has gradually received more attention in the field of novel functional materials [41,42].

1.1.2 Fiber type shape memory materials

SMPs can be prepared into fiber (including filament and yarn) shape by textile processing [29,43]. Generally, polymers are subjected to mechanical drawing during the process of being processed into fibers [44]. This drawing makes fiber-type SMPs exhibit better mechanical properties due to the high axial orientation of their internal molecular chains [45]. In addition to their better mechanical properties, fiber-type SMPs also exhibit greater recovery stress, which makes them have greater thermal actuation ability [46]. Fiber-based SMPs with high mechanical properties have been reported to be used in artificial muscles and thermal actuation [35,47]. Due to the versatility of SMPs, fiber-type SMPs have also been reported for applications in smart sensors, smart actuators, and other fields [26,48].

The shape of the fibers enables fiber-type SMPs to be further integrated into textiles through textile processing [49]. Through textile processing, fiber-type SMPs can be processed into textiles of different shapes for application in different fields [50]. It has been reported that fiber-type

SMPs have been applied in wearable flexible sensors, smart body temperature regulators, and flexible energy harvesters [51]. In addition to one-way SMPs, fiber-type SMPs that induce high tropism have been reported to be applied to two-way SMPs and exhibit excellent shape recovery ability [52].

In recent years, the development of fiber-type SMPs with high biocompatibility, magnetic response, and body temperature response has gradually become a research hotspot by endowing fibrous materials with versatility [53,54]. It has been reported that fibrous SMPs have been used in biomedical fields such as surgical lines, bionic blood vessels, and bionic bones [51,55]. In conclusion, fiber-type SMPs show great potential for application in the field of actuation with high mechanical requirements such as artificial muscles, and at the same time endow textiles with new applications such as smart wearable textiles [56].

1.2 Epoxy resins

Epoxy resins are a kind of polymer commonly used in many industrial fields [57]. Epoxy resins before curing all have epoxy rings in the molecular structure, and this epoxy ring can be opened by the promotion of the catalyst, and then react with other components to form a high molecular weight epoxy resin [58]. Although the epoxy groups are no longer present after the reaction, the reacted resin is often referred to as an

epoxy resin [59]. Among epoxy resins, thermosetting epoxy resins commonly used on the market today were first reported to be in commercial production in 1947 [60].

Thermosetting epoxy resin is formed by epoxy ring-opening and cross-linking with other components and has a three-dimensional network structure, so they have excellent mechanical properties [61], durability [62], and dimensional stability [63]. Thermosetting epoxy resins have also been reported to have more properties such as electrical insulation [64], corrosion resistance [59,62], and chemical resistance [65]. Depending on the type and number of chemical groups, epoxy resins with different properties have been reported for a wide range of applications such as coatings [66], adhesives [67], and composites [31,68].

Despite the many advantages of thermoset epoxy resins, there are drawbacks in reprocessing and recycling that limit their application [69,70]. Compared to thermosetting epoxy resins, thermoplastic epoxy resins have the advantages of melt reprocessing and recycling [71,72]. Despite the great application potential of thermoplastic epoxy resins, there are still few reports on thermoplastic epoxy resins.

1.2.1 Shape memory epoxy resins

As a widely used polymer material, shape memory epoxy resin

polymers (SMEPs) have become a more promising smart material due to their excellent mechanical [73], thermal [74], and electrical properties [75], and play a more important role in the field of SMPs [76]. In recent years, research on imparting epoxy resin which is a kind of multifunctional material shape memory function in the field of composites has gradually increased [77]. Epoxy resins have been reported for the development of various forms of SMMs, such as in the form of films [78], foams [79], and scaffolds [80], with applications in aerospace [81], artificial intelligence [82], civil engineering [83].

The low molecular weight state of epoxy resins before curing is favorable for being dispersed by various modifiers for modification, and this high variability performance endows epoxy resins with potential applications in the field of multifunctional SMMs [84]. Based on the modification treatment, it has been reported that epoxy resins can make shape memory responses to external stimuli such as heat [85], electricity [31,86], light [87], and play an important role in actuation [88], artificial muscles [89], and composite materials [36,90]. Notably, most SMEPs are thermosetting polymers [91], and studies on thermoplastic shape memory epoxy resins are rarely reported. Although thermosetting epoxy resins have advantages in mechanical strength and dimensional stability [92], their three-dimensional network molecular chain structure makes their deformability relatively low, which limits the application range of

thermosetting shape memory epoxy to some extent [41,93].

Different from thermosetting epoxy resins, thermoplastic epoxy resins have a linear molecular chain structure and thus have greater deformability [71], which endows thermoplastic shape memory epoxy resins with greater toughness. When the temperature reaches the T_g, the storage modulus of thermoplastic epoxy resins decreases rapidly [94], which is favorable for the shape memory performance with large deformability. In addition, thermoplastic epoxy resins can be transformed from rubbery to melt at a certain high temperature [95], which endows thermoplastic shape memory epoxy resins with the advantages of melt reprocessing and convenient recycling.

1.2.2 Modification for epoxy resins

Epoxy resin is a versatile material with excellent thermal properties, mechanical properties, chemical and corrosion resistance, electrical insulation, and adhesion properties [96,97]. Epoxy resins are generally in a liquid state before curing, which is convenient for them to meet various shapes and sizes, and then form high molecular weight epoxy resins with high mechanical properties and stability through a curing reaction [98,99]. However, some special requirements such as high toughness and high impact resistance cannot be achieved by curing epoxy resin alone [100]. According to reports, the epoxy resin has problems of poor toughness and

crack resistance after curing [101]. Therefore, modification treatments such as epoxy resin toughening have gradually become a research hotspot [102].

Elastomers, thermoplastics, inorganic particles, etc. have been reported to be mixed with epoxy resins for modification [103]. However, it is difficult to impart new properties to epoxy resins or improve the performance of epoxy resins through modification without reducing the strength of epoxy resins [104]. It has been reported that elastomeric materials can significantly toughen epoxy resins, but greatly reduce the thermal stability and mechanical properties of epoxy resins [105,106].

The epoxy resin before curing has low viscosity and good compatibility with many plasticizers [107]. In recent years, it has become an effective method to modify epoxy resin by dispersing modifiers such as plasticizers and modified fillers in the liquid matrix before epoxy resin curing [108]. The plasticizer can be physically mixed with the epoxy resin to achieve a relatively uniform dispersion state [109,110]. Then through the curing of the epoxy resin, a stable epoxy-plasticizer composite system is formed [111]. The storage modulus and loss modulus of the epoxy-plasticizer composite system can be adjusted by the content of the plasticizer [112]. In addition, it has been reported that the epoxy resin can be further modified by modifying the curing agent as an effective method [113]. The

feasibility of modifying epoxy resin to prepare high-performance and multi-functional composite materials expands the application scope of epoxy resin [114]. Composite materials based on epoxy resin modification have also gradually attracted attention [115,116].

1.3 PEG for polymer modification

Polyethylene glycol (PEG) is commonly used as a plasticizer for its unique physical and chemical properties [117]. The molecular weight of PEG is usually lower than 20,000. In order of molecular weight from low to high, PEG is in liquid, semi-solid, and solid states, respectively [118]. The higher the molecular weight, the higher its crystallinity and melting point [119].

As an important plasticizer, PEG is usually added to the polymer in the dispersion way of blending and solution mixing, which has the function of increasing the flexibility of the polymer [120]. The compatibility of PEG with the polymer is a key factor affecting the blending [121]. The good compatibility of PEG with the plasticized polymer allows the mixed system to have a single-phase, homogeneous structure [122]. The compatibility of PEG and polymer determines the final properties of the blend [123]. Notably, PEG is reported to have good compatibility with many polymers and thus is widely used in blend-based polymer modification treatments [124]. In addition, the lower melting temperature of PEG itself also enables

it to be blended at lower temperatures [125]. PEG has good compatibility with a variety of organic solvents, so it is often used to modify polymers by solution dispersion [126].

Molecular weight has a great influence on PEG in plasticizing applications [127]. In general, relatively small molecular weight PEG is often used for blending due to its low crystallinity, better dispersion, and solubility [128]. Although PEG can toughen the polymer, it reduces the strength of the composite system [129]. Therefore, it is difficult to increase the flexibility of the polymer while simultaneously maintaining the overall mechanical properties of the composite system [130]. Grafting and copolymerization have also been reported to be used for the performance regulation of polymer-PEG composite systems [131]. PEG is also reported to be commonly used to lower the T_g of polymers [132]. PEG with relatively small molecular weight can have larger molecular thermal motion and flowability at a lower temperature, which reduces the T_g of the polymer-PEG composite system and actually can also reduce the melt processing temperature of the composite system [133–135]. In addition, PEG has good biocompatibility, biodegradability, and hydrophilicity, so it is often used in the modification of biological materials [136,137]. The performance advantages of small molecular weight, good compatibility, good biocompatibility, and good hydrophilicity make PEG more and more important in the field of polymer modification [138].

1.4 The purpose and significance of this work

This research aims to develop multifunctional, multimodal SMMs that have applications in thermal actuation, artificial muscles, smart textiles, flexibility and healable materials based on thermoplastic epoxy resins by investigating the thermal and mechanical properties of PEG-modified thermoplastic epoxy. This study fills a gap in current research on thermoplastic epoxy shape memory. In future research, PEG-modified thermoplastic epoxy is expected to develop higher performance, composite materials for more functions and applications.

Thermoplastic epoxy resins not only have excellent mechanical properties but can also be melt-processed into filaments. To the best of our knowledge, there are no other reports on the shape memory properties of thermoplastic epoxy filaments. Based on the research on the thermal properties, mechanical properties, and shape memory properties of pure thermoplastic epoxy, the developed shape memory epoxy filament with excellent recovery stress output ability shows great application potential in the fields of artificial muscles and smart textiles.

Although thermoplastic epoxy filaments exhibit excellent thermal stability, mechanical properties, shape memory properties, and thermal actuation potential, they have high shape memory heat-stimuli temperature. The higher shape memory heat-stimuli temperature is due to the higher T_g

of thermoplastic epoxy, which is an advantage in itself, such as higher thermal stability properties. But the higher heat-stimuli temperature limits its practical scope, such as in applications that require lower stimulation temperatures.

Aiming at the problem of the high T_g of thermoplastic epoxy, this study solved it by dispersing PEG with a molecular weight of 1000 in the thermoplastic epoxy before polymerization. PEG has good compatibility with unpolymerized epoxy resin, and PEG can be uniformly and stably dispersed in epoxy resin by an environmentally friendly melting method. PEG with a molecular weight of 1000 has a lower melting point, and its thermal stability meets the requirements of the polymerization reaction of thermoplastic epoxy at 150 °C. The PEG-modified thermoplastic epoxy gradually changed from high T_g and high strength to low T_g and high flexibility with the increase of PEG content.

To further expand the application range of PEG-modified thermoplastic epoxy, controllable heat-stimuli temperature shape memory epoxy filaments were prepared by melt processing. PEG is evenly distributed in the unpolymerized thermoplastic epoxy and does not hinder the overall polymerization of the epoxy resin. The controllability of PEG on the heat-stimuli temperature of thermoplastic epoxy was successfully applied to shape-memory thermoplastic epoxy filament, and the thermal actuation

ability of PEG-modified thermoplastic epoxy filament was also improved. It has greater application prospects in fields such as thermal actuation and smart textiles.

1.5 The outline of this dissertation

This research fully discusses the performance regulation of thermoplastic epoxy by the dispersion of PEG, so that thermoplastic epoxy can be used in the forms of filament, textile, rigid and flexible film for the fields such as thermal actuation, artificial muscles, smart textiles, healable and adhesive materials. The thermoplastic epoxy resin shows excellent versatility, and the method of PEG-dispersed thermoplastic epoxy shows great potential for application. The research content is summarized into 5 chapters of the dissertation.

In chapter 1, the introduction of this dissertation is presented based on the literature review and summary. The introduction includes four parts: shape memory materials, epoxy resin, PEG for polymer modification, and the purpose and significance of this work. Among them, polymer-based shape memory materials, fiber-type shape memory materials, shape memory epoxy resins, and modification of epoxy resin are also included.

In chapter 2, thermoplastic epoxy filaments with shape memory properties were prepared by the melt drawing process for the first time.

After the filament is drawn during the preparation process, the epoxy filament obtains better mechanical properties. Based on excellent mechanical properties, epoxy filaments not only have excellent shape memory properties but also stably output high recovery stress.

In chapter 3, based on the research on the thermal properties, mechanical properties, and shape memory properties of pure thermoplastic epoxy, the performance regulation of thermoplastic epoxy by the dispersion of PEG was fully discussed. The developed PEG-modified thermoplastic epoxy can be used in the forms of filament, textile, rigid and flexible film for the fields such as thermal actuation, artificial muscles, smart textiles, healable and adhesive materials. The thermoplastic epoxy resin shows excellent versatility, and the method of PEG-dispersed thermoplastic epoxy shows great potential for the application of higher performance and more functions composite materials.

In chapter 4, based on the thermal and mechanical properties of the PEG-modified thermoplastic epoxy, the PEG-modified thermoplastic epoxy particles were successfully prepared into epoxy filaments with different T_g by melt processing. PEG reduces the melt processing temperature of thermoplastic epoxy particles and the T_g of thermoplastic epoxy filaments. The heat-stimuli temperature controllability of shape memory and the greater application potential for PEG-modified thermoplastic epoxy

filaments were fully discussed. The shape memory heat-stimuli temperature of the PEG-modified thermoplastic epoxy filaments can be adjusted according to the content of PEG so that it can be applied to more fields requiring heat-stimuli temperatures.

In chapter 5, the research work and research results of this dissertation are summarized, including the performance and application summary of thermoplastic epoxy shape memory filaments, heat-stimuli controllable thermoplastic epoxy shape memory filaments, and multifunctional thermoplastic epoxy films.

Reference

1. Ashima R, Haleem A, Bahl S, et al. Automation and manufacturing of smart materials in Additive Manufacturing technologies using Internet of Things towards the adoption of Industry 4.0[J]. Materials Today: Proceedings, 2021, 45: 5081-5088.

2. Bahl S, Nagar H, Singh I, et al. Smart materials types, properties and applications: A review[J]. Materials Today: Proceedings, 2020, 28: 1302-1306.

3. Holman H, Kavarana M N, Rajab T K. Smart materials in cardiovascular implants: Shape memory alloys and shape memory polymers[J]. Artificial Organs, 2021, 45(5): 454-463.

4. Subash A, Kandasubramanian B. 4D printing of shape memory polymers[J]. European Polymer Journal, 2020, 134: 109771.

5. Chen Y, Zhao X, Luo C, et al. A facile fabrication of shape memory polymer nanocomposites with fast light-response and self-healing performance[J]. Composites Part A: Applied Science and Manufacturing, 2020, 135: 105931..

6. Li Y J, Zhang F H, Liu Y J, et al. 4D printed shape memory polymers and their structures for biomedical applications[J]. Science China Technological Sciences, 2020, 63(4): 545-560.

7. Sachyani Keneth E, Lieberman R, Rednor M, et al. Multi-Material 3D printed shape memory polymer with tunable melting and glass transition

temperature activated by heat or light[J]. Polymers, 2020, 12(3): 710.

8. Bartkowiak G, Dąbrowska A, Greszta A. Development of smart textile materials with shape memory alloys for application in protective clothing[J]. Materials, 2020, 13(3): 689.

9. Raja M, Ryu S H, Shanmugharaj A M. Influence of surface modified multiwalled carbon nanotubes on the mechanical and electroactive shape memory properties of polyurethane (PU)/poly (vinylidene diflouride)(PVDF) composites[J]. Colloids and Surfaces A: Physicochemical and Engineering Aspects, 2014, 450: 59-66.

10. Bai Y, Zhang J, Wen D, et al. A reconfigurable, self-healing and near infrared light responsive thermoset shape memory polymer[J]. Composites Science and Technology, 2020, 187: 107940.

11. Farber E, Zhu J N, Popovich A, et al. A review of NiTi shape memory alloy as a smart material produced by additive manufacturing[J]. Materials Today: Proceedings, 2020, 30: 761-767.

12. Li W, Liu Y, Leng J. Light-actuated reversible shape memory effect of a polymer composite[J]. Composites Part A: Applied Science and Manufacturing, 2018, 110: 70-75.

13. Wang X, Sparkman J, Gou J. Electrical actuation and shape memory behavior of polyurethane composites incorporated with printed carbon nanotube layers[J]. Composites Science and Technology, 2017, 141: 8-15.

14. Melocchi A, Uboldi M, Cerea M, et al. Shape memory materials and

4D printing in pharmaceutics[J]. Advanced Drug Delivery Reviews, 2021, 173: 216-237.

15. Mahapatra S S, Yadav S K, Yoo H J, et al. Tailored and strong electro-responsive shape memory actuation in carbon nanotube-reinforced hyperbranched polyurethane composites[J]. Sensors and Actuators B: Chemical, 2014, 193: 384-390.

16. Liu K, Tebyetekerwa M, Ji D, et al. Intelligent materials[J]. Matter, 2020, 3(3): 590-593.

17. Xia Y, He Y, Zhang F, et al. A review of shape memory polymers and composites: mechanisms, materials, and applications[J]. Advanced materials, 2021, 33(6): 2000713.

18. Panahi-Sarmad M, Abrisham M, Noroozi M, et al. Programing polyurethane with rational surface-modified graphene platelets for shape memory actuators and dielectric elastomer generators[J]. European Polymer Journal, 2020, 133: 109745.

19. Zhang L, Huang Y, Dong H, et al. Flame-retardant shape memory polyurethane/MXene paper and the application for early fire alarm sensor[J]. Composites Part B: Engineering, 2021, 223: 109149.

20. Liu L Y, Karaaslan M A, Hua Q, et al. Thermo-Responsive Shape-Memory Polyurethane Foams from Renewable Lignin Resources with Tunable Structures–Properties and Enhanced Temperature Resistance[J]. Industrial & Engineering Chemistry Research, 2021, 60(32): 11882-11892.

21. Wang T, Zhao J, Weng C, et al. A bidirectionally reversible light-responsive actuator based on shape memory polyurethane bilayer[J]. Composites Part A: Applied Science and Manufacturing, 2021, 144: 106322.
22. Lashkari R, Tabatabaei - Nezhad S A, Husein M M. Shape Memory Polyurethane as a Drilling Fluid Lost Circulation Material[J]. Macromolecular Materials and Engineering, 2021, 306(11): 2100354.
23. Mehrbakhsh E, Rezaei M, Babaie A, et al. Physical and thermo-mechanical properties of shape memory polyurethane containing reversible chemical cross-links[J]. journal of the mechanical behavior of biomedical materials, 2021, 116: 104336.
24. Kong D, Li J, Guo A, et al. High temperature electromagnetic shielding shape memory polymer composite[J]. Chemical Engineering Journal, 2021, 408: 127365.
25. Liu Y, Du H, Liu L, et al. Shape memory polymers and their composites in aerospace applications: a review[J]. Smart materials and structures, 2014, 23(2): 023001.
26. Guan X, Chen H, Xia H, et al. Flexible energy harvester based on aligned PZT/SMPU nanofibers and shape memory effect for curved sensors[J]. Composites Part B: Engineering, 2020, 197: 108169.
27. Chen H, Liu W, Xia H, et al. Flexible nanopositioning actuators based on functional nanocomposites[J]. Composites Science and Technology,

2020, 186: 107937.

28. Li G, Uppu N. Shape memory polymer based self-healing syntactic foam: 3-D confined thermomechanical characterization[J]. Composites Science and Technology, 2010, 70(9): 1419-1427.

29. Huang Y, Zhu M, Pei Z, et al. A shape memory supercapacitor and its application in smart energy storage textiles[J]. Journal of Materials Chemistry A, 2016, 4(4): 1290-1297.

31. Zhou J, Li H, Liu W, et al. A facile method to fabricate polyurethane based graphene foams/epoxy/carbon nanotubes composite for electro-active shape memory application[J]. Composites Part A: Applied Science and Manufacturing, 2016, 91: 292-300.

32. Patel K K, Purohit R. Future Prospects of shape memory polymer nano-composite and epoxy based shape memory polymer-A review[J]. Materials Today: Proceedings, 2018, 5(9): 20193-20200.

33. Maksimkin A V, Kaloshkin S D, Zadorozhnyy M V, et al. Artificial muscles based on coiled UHMWPE fibers with shape memory effect[J]. Express Polymer Letters, 2018.

34. Bao M, Lou X, Zhou Q, et al. Electrospun biomimetic fibrous scaffold from shape memory polymer of PDLLA-co-TMC for bone tissue engineering[J]. ACS applied materials & interfaces, 2014, 6(4): 2611-2621.

35. Foroughi J, Spinks G M, Aziz S, et al. Knitted carbon-nanotube-sheath/spandex-core elastomeric yarns for artificial muscles and strain

sensing[J]. ACS nano, 2016, 10(10): 9129-9135.

36. Li F, Scarpa F, Lan X, et al. Bending shape recovery of unidirectional carbon fiber reinforced epoxy-based shape memory polymer composites[J]. Composites Part A: Applied Science and Manufacturing, 2019, 116: 169-179.

37. Liu W, Chen H, Ge M, et al. Electroactive shape memory composites with TiO2 whiskers for switching an electrical circuit[J]. Materials & Design, 2018, 143: 196-203.

38. Ge Y, Wang H, Xue J, et al. Programmable humidity-responsive actuation of polymer films enabled by combining shape memory property and surface-tunable hygroscopicity[J]. ACS Applied Materials & Interfaces, 2021, 13(32): 38773-38782.

39. Bai Y, Zhang J, Wen D, et al. A reconfigurable, self-healing and near infrared light responsive thermoset shape memory polymer[J]. Composites Science and Technology, 2020, 187: 107940.

40. Meng H, Li G. A review of stimuli-responsive shape memory polymer composites[J]. polymer, 2013, 54(9): 2199-2221.

41. Lu L, Fan J, Li G. Intrinsic healable and recyclable thermoset epoxy based on shape memory effect and transesterification reaction[J]. Polymer, 2016, 105: 10-18.

42. Peterson G I, Dobrynin A V, Becker M L. Biodegradable shape memory polymers in medicine[J]. Advanced healthcare materials, 2017, 6(21):

1700694.

43. Mirvakili S M, Hunter I W. Fast torsional artificial muscles from NiTi twisted yarns[J]. ACS Applied Materials & Interfaces, 2017, 9(19): 16321-16326.

44. Kanik M, Orguc S, Varnavides G, et al. Strain-programmable fiber-based artificial muscle[J]. Science, 2019, 365(6449): 145-150.

45. Mirvakili S M, Hunter I W. Multidirectional artificial muscles from nylon[J]. Advanced Materials, 2017, 29(4): 1604734.

46. Bhatti M R A, Bilotti E, Zhang H, et al. Ultra-high actuation stress polymer actuators as light-driven artificial muscles[J]. ACS applied materials & interfaces, 2020, 12(29): 33210-33218.

47. Zhang P, Li G. Healing-on-demand composites based on polymer artificial muscle[J]. Polymer, 2015, 64: 29-38.

48. Huang Y, Yu Q, Su C, et al. Light-Responsive Soft Actuators: Mechanism, Materials, Fabrication, and Applications[C]//Actuators. MDPI, 2021, 10(11): 298.

49. Kim M L, Otal E H, Takizawa J, et al. All-Organic Electroactive Shape-Changing Knitted Textiles Using Thermoprogrammed Shape-Memory Fibers Spun by 3D Printing[J]. ACS Applied Polymer Materials, 2022, 4(4): 2355-2364.

50. Liu Y, Chung A, Hu J L, et al. Shape memory behavior of SMPU knitted fabric[J]. Journal of Zhejiang University-Science A, 2007, 8(5):

830-834.

51.Wang L, Zhang F, Liu Y, et al. Shape memory polymer fibers: materials, structures, and applications[J]. Advanced Fiber Materials, 2021: 1-19.

52. Yang Q, Fan J, Li G. Artificial muscles made of chiral two-way shape memory polymer fibers[J]. Applied Physics Letters, 2016, 109(18): 183701.

53. Korkmaz Memiş N, Kaplan S. Smart polyester fabric with comfort regulation by temperature and moisture responsive shape memory nanocomposite treatment[J]. Journal of Industrial Textiles, 2020: 1528083720975652.

54. Kumar B, Hu J, Pan N. Smart medical stocking using memory polymer for chronic venous disorders[J]. Biomaterials, 2016, 75: 174-181.

55. Wu T, Yu S, Chen D, et al. Bionic design, materials and performance of bone tissue scaffolds[J]. Materials, 2017, 10(10): 1187.

56.Wang L, Zhang F, Liu Y, et al. Shape memory polymer fibers: materials, structures, and applications[J]. Advanced Fiber Materials, 2021: 1-19.

57. Kim M T, Rhee K Y, Lee J H, et al. Property enhancement of a carbon fiber/epoxy composite by using carbon nanotubes[J]. Composites Part B: Engineering, 2011, 42(5): 1257-1261.

58. Tang L, He M, Na X, et al. Functionalized glass fibers cloth/spherical BN fillers/epoxy laminated composites with excellent thermal conductivities and electrical insulation properties[J]. Composites

Communications, 2019, 16: 5-10.

59. Xiang Q, Xiao F. Applications of epoxy materials in pavement engineering[J]. Construction and Building Materials, 2020, 235: 117529.

60. Arrabiyeh P A, May D, Eckrich M, et al. An overview on current manufacturing technologies: Processing continuous rovings impregnated with thermoset resin[J]. Polymer Composites, 2021, 42(11): 5630-5655.

61. Hardis R, Jessop J L P, Peters F E, et al. Cure kinetics characterization and monitoring of an epoxy resin using DSC, Raman spectroscopy, and DEA[J]. Composites Part A: Applied Science and Manufacturing, 2013, 49: 100-108.

62. Wazarkar K, Kathalewar M, Sabnis A. Development of epoxy-urethane hybrid coatings via non-isocyanate route[J]. European Polymer Journal, 2016, 84: 812-827.

63. Yang W, Xiong J, Wu L, et al. Methods for enhancing the thermal properties of epoxy matrix composites using 3D network structures[J]. Composites Communications, 2019, 12: 14-20.

64. Rybak A, Nieroda J. Aluminosilicate ‐ epoxy resin composite as novel material for electrical insulation with enhanced mechanical properties and improved thermal conductivity[J]. Polymer Composites, 2019, 40(8): 3182-3188.

65. Jin F L, Li X, Park S J. Synthesis and application of epoxy resins: A review[J]. Journal of Industrial and Engineering Chemistry, 2015, 29: 1-11.

66. Matinlinna J P, Lung C Y K, Tsoi J K H. Silane adhesion mechanism in dental applications and surface treatments: A review[J]. Dental materials, 2018, 34(1): 13-28.
67. Gao W, Bie M, Liu F, et al. Self-healable and reprocessable polysulfide sealants prepared from liquid polysulfide oligomer and epoxy resin[J]. ACS applied materials & interfaces, 2017, 9(18): 15798-15808.
68. Jouyandeh M, Karami Z, Ali J A, et al. Curing epoxy with polyethylene glycol (PEG) surface-functionalized NixFe3-xO4 magnetic nanoparticles[J]. Progress in Organic Coatings, 2019, 136: 105250.
69. Ma Y, Navarro C A, Williams T J, et al. Recovery and reuse of acid digested amine/epoxy-based composite matrices[J]. Polymer Degradation and Stability, 2020, 175: 109125.
70. Oliveux G, Bailleul J L, Gillet A, et al. Recovery and reuse of discontinuous carbon fibres by solvolysis: Realignment and properties of remanufactured materials[J]. Composites Science and Technology, 2017, 139: 99-108.
71. Taniguchi N, Nishiwaki T, Hirayama N, et al. Dynamic tensile properties of carbon fiber composite based on thermoplastic epoxy resin loaded in matrix-dominant directions[J]. Composites Science and Technology, 2009, 69(2): 207-213.
72. Deng S, Djukic L, Paton R, et al. Thermoplastic–epoxy interactions and their potential applications in joining composite structures–A review[J].

Composites Part A: Applied Science and Manufacturing, 2015, 68: 121-132.

73. Kumar K S S, Biju R, Nair C P R. Progress in shape memory epoxy resins[J]. Reactive and Functional Polymers, 2013, 73(2): 421-430.

74. Liu Y, Han C, Tan H, et al. Thermal, mechanical and shape memory properties of shape memory epoxy resin[J]. Materials Science and Engineering: A, 2010, 527(10-11): 2510-2514.

75. Wang W, Liu D, Liu Y, et al. Electrical actuation properties of reduced graphene oxide paper/epoxy-based shape memory composites[J]. Composites Science and Technology, 2015, 106: 20-24.

76. Fan P, Chen W, Hu J, et al. Stress relaxation properties of an epoxy-based shape-memory polymer considering temperature influence: experimental investigation and constitutive modeling[J]. Mechanics of Time-Dependent Materials, 2020, 24(3): 265-284.

77. Luo L, Zhang F, Leng J. Shape Memory Epoxy Resin and Its Composites: From Materials to Applications[J]. Research, 2022, 2022.

78. Liu T, Hao C, Wang L, et al. Eugenol-derived biobased epoxy: shape memory, repairing, and recyclability[J]. Macromolecules, 2017, 50(21): 8588-8597.

79. Squeo E A, Quadrini F. Shape memory epoxy foams by solid-state foaming[J]. Smart Materials and Structures, 2010, 19(10): 105002.

80. Chen L, Li W, Liu X, et al. Carbon nanotubes array reinforced shape -

memory epoxy with fast responses to low‐power microwaves[J]. Journal of Applied Polymer Science, 2019, 136(21): 47563.

81. Li F, Liu Y, Leng J. Progress of shape memory polymers and their composites in aerospace applications[J]. Smart Materials and Structures, 2019, 28(10): 103003.

82. Xu L, Cui L, Li Z, et al. Thermodynamic coupling behavior and energy harvesting of vapor grown carbon fiber/graphene oxide/epoxy shape memory composites[J]. Composites Science and Technology, 2021, 203: 108583.

83. Zhou X, Ma B, Wang X, et al. Study of the interlocking filling–graded composition design method of an asphalt mixture mixed with shape-memory epoxy resin fibers[J]. Journal of Materials in Civil Engineering, 2020, 32(7): 04020186.

84. Jing X, Wei J, Liu Y, et al. Deployment analysis of aramid fiber reinforced shape-memory epoxy resin composites[J]. Engineered Science, 2020, 11(2): 44-53.

85. Guo Y, Liu Y, Liu J, et al. Shape memory epoxy composites with high mechanical performance manufactured by multi-material direct ink writing[J]. Composites Part A: Applied Science and Manufacturing, 2020, 135: 105903.

86. Yu L, Zhang T, Wang W, et al. Carbon fiber fabric/epoxy composites with electric-and light-responsive shape memory effect[J]. Pigment &

Resin Technology, 2020, 50(5): 377-383.

87. Li Y, Goswami M, Zhang Y, et al. Combined light-and heat-induced shape memory behavior of anthracene-based epoxy elastomers[J]. Scientific reports, 2020, 10(1): 1-12.

88. Belmonte A, Russo C, Ambrogi V, et al. Epoxy-based shape-memory actuators obtained via dual-curing of off-stoichiometric “thiol–epoxy” mixtures[J]. Polymers, 2017, 9(3): 113.

89. Lama G C, Cerruti P, Lavorgna M, et al. Controlled actuation of a carbon nanotube/epoxy shape-memory liquid crystalline elastomer[J]. The Journal of Physical Chemistry C, 2016, 120(42): 24417-24426.

90. Huang C, Peng J, Cheng Y, et al. Ultratough nacre-inspired epoxy–graphene composites with shape memory properties[J]. Journal of Materials Chemistry A, 2019, 7(6): 2787-2794.

91. Liu X, Song X, Chen B, et al. Self-healing and shape-memory epoxy thermosets based on dynamic diselenide bonds[J]. Reactive and Functional Polymers, 2022, 170: 105121.

92. Datta S, Henry T C, Sliozberg Y R, et al. Carbon nanotube enhanced shape memory epoxy for improved mechanical properties and electroactive shape recovery[J]. Polymer, 2021, 212: 123158.

93. Chen L, Shen Y, Liu Z, et al. Experimental and modeling investigation on thermodynamic effect of graphene doped shape memory epoxy composites[J]. Polymer, 2022, 239: 124430.

94. Wang X, Zhao X, Chen S, et al. Static and fatigue behavior of basalt fiber-reinforced thermoplastic epoxy composites[J]. Journal of Composite Materials, 2020, 54(18): 2389-2398.
95. Hu B, Xia H, Liu F, et al. Development of thermoplastic epoxy filaments with shape memory properties[J]. Polymer Testing, 2021, 103: 107374.
96. Ai Y F, Xia L, Pang F Q, et al. Mechanically strong and flame-retardant epoxy resins with anti-corrosion performance[J]. Composites Part B: Engineering, 2020, 193: 108019.
97. Kumar S, Krishnan S, Mohanty S, et al. Synthesis and characterization of petroleum and biobased epoxy resins: a review[J]. Polymer International, 2018, 67(7): 815-839.
98. Dean J M, Lipic P M, Grubbs R B, et al. Micellar structure and mechanical properties of block copolymer ‐ modified epoxies[J]. Journal of Polymer Science Part B: Polymer Physics, 2001, 39(23): 2996-3010.
99. Xiang Q, Xiao F. Applications of epoxy materials in pavement engineering[J]. Construction and Building Materials, 2020, 235: 117529.
100. Satapathy A, Jha A K, Mantry S, et al. Processing and characterization of jute-epoxy composites reinforced with SiC derived from rice husk[J]. Journal of Reinforced Plastics and Composites, 2010, 29(18): 2869-2878.
101. Pruksawan S, Lambard G, Samitsu S, et al. Prediction and optimization of epoxy adhesive strength from a small dataset through

active learning[J]. Science and technology of advanced materials, 2019, 20(1): 1010-1021.

102. Liu L, Ying G, Wen D, et al. Aqueous solution-processed MXene (Ti3C2Tx) for non-hydrophilic epoxy resin-based composites with enhanced mechanical and physical properties[J]. Materials & Design, 2021, 197: 109276.

103. Puglia D, Al-Maadeed M A S A, Kenny J M, et al. Elastomer/thermoplastic modified epoxy nanocomposites: The hybrid effect of ‘micro’and ‘nano’scale[J]. Materials Science and Engineering: R: Reports, 2017, 116: 1-29.

104. Chruściel J J, Leśniak E. Modification of epoxy resins with functional silanes, polysiloxanes, silsesquioxanes, silica and silicates[J]. Progress in Polymer Science, 2015, 41: 67-121.

105. Zhao Y, Huang R, Wu Z, et al. Effect of free volume on cryogenic mechanical properties of epoxy resin reinforced by hyperbranched polymers[J]. Materials & Design, 2021, 202: 109565.

106. Thomas R, Yumei D, Yuelong H, et al. Miscibility, morphology, thermal, and mechanical properties of a DGEBA based epoxy resin toughened with a liquid rubber[J]. Polymer, 2008, 49(1): 278-294.

107. Bueno-Ferrer C, Garrigós M C, Jiménez A. Characterization and thermal stability of poly (vinyl chloride) plasticized with epoxidized soybean oil for food packaging[J]. Polymer Degradation and Stability,

2010, 95(11): 2207-2212.
108. Mustafa L M, Ismailov M B, Sanin A F. Study on the effect of plasticizers and thermoplastics on the strength and toughness of epoxy resins[J]. Natsional'nyi Hirnychyi Universytet. Naukovyi Visnyk, 2020 (4): 63-68.
109. Soares B G, Celestino M L, Magioli M, et al. Synthesis of conductive adhesives based on epoxy resin and polyaniline. DBSA using the in situ polymerization and physical mixing procedures[J]. Synthetic Metals, 2010, 160(17-18): 1981-1986.
110. Zavareh S, Samandari G. Polyethylene glycol as an epoxy modifier with extremely high toughening effect: Formation of nanoblend morphology[J]. Polymer Engineering & Science, 2014, 54(8): 1833-1838.
111. Parameswaranpillai J, Ramanan S P, George J J, et al. PEG-ran-PPG modified epoxy thermosets: a simple approach to develop tough shape memory polymers[J]. Industrial & Engineering Chemistry Research, 2018, 57(10): 3583-3590.
112. Wang Y, Nie X, Fang G, et al. Synthesis and application of a novel thermostable epoxy plasticizer based on levulinic acid for poly (vinyl chloride)[J]. Journal of Applied Polymer Science, 2020, 137(36): 49066.
113. Ahmadi-Khaneghah A, Omidi-Ghallemohamadi M, Behniafar H. PEG-based epoxy and epoxy/silica networks: Thermal, mechanical, and thermo-mechanical investigations[J]. International Journal of Adhesion

and Adhesives, 2019, 95: 102430.

114. Gong K, Zhou K, Qian X, et al. MXene as emerging nanofillers for high-performance polymer composites: A review[J]. Composites Part B: Engineering, 2021, 217: 108867.

115. Zhou Y, Yao Y, Chen C Y, et al. The use of polyimide-modified aluminum nitride fillers in AlN@ PI/Epoxy composites with enhanced thermal conductivity for electronic encapsulation[J]. Scientific reports, 2014, 4(1): 1-6.

116. Bai H, Li C, Shi G. Functional composite materials based on chemically converted graphene[J]. Advanced Materials, 2011, 23(9): 1089-1115.

117. D’souza A A, Shegokar R. Polyethylene glycol (PEG): a versatile polymer for pharmaceutical applications[J]. Expert opinion on drug delivery, 2016, 13(9): 1257-1275.

118. Singh M, Verma S K, Biswas I, et al. Effect of molecular weight of polyethylene glycol on the rheological properties of fumed silica-polyethylene glycol shear thickening fluid[J]. Materials Research Express, 2018, 5(5): 055704.

119. Damian F, Blaton N, Naesens L, et al. Physicochemical characterization of solid dispersions of the antiviral agent UC-781 with polyethylene glycol 6000 and Gelucire 44/14[J]. European Journal of Pharmaceutical Sciences, 2000, 10(4): 311-322.

120. B Rahman M A, De Santis D, Spagnoli G, et al. Biocomposites based on lignin and plasticized poly (L‐lactic acid)[J]. Journal of Applied Polymer Science, 2013, 129(1): 202-214.
121. Li S, Cui Z, Zhang L, et al. The effect of sulfonated polysulfone on the compatibility and structure of polyethersulfone-based blend membranes[J]. Journal of Membrane Science, 2016, 513: 1-11.
122. Müller K, Zollfrank C, Schmid M. Natural polymers from biomass resources as feedstocks for thermoplastic materials[J]. Macromolecular Materials and Engineering, 2019, 304(5): 1800760.
123. Falqi F H, Bin-Dahman O A, Hussain M, et al. Preparation of miscible PVA/PEG blends and effect of graphene concentration on thermal, crystallization, morphological, and mechanical properties of PVA/PEG (10 wt%) blend[J]. International Journal of Polymer Science, 2018, 2018.
124. Mohapatra A K, Mohanty S, Nayak S K. Effect of PEG on PLA/PEG blend and its nanocomposites: A study of thermo‐mechanical and morphological characterization[J]. Polymer composites, 2014, 35(2): 283-293.
125. Kelly C A, Jenkins M J, Marsh S H. Rheological analysis of heat labile poly (3-hydroxybutyrate-co-3-hydroxyvalerate): poly (ethylene glycol) blends[J]. Materials Today Communications, 2021, 29: 102787.
126. Soni J, Sahiba N, Sethiya A, et al. Polyethylene glycol: A promising approach for sustainable organic synthesis[J]. Journal of Molecular

Liquids, 2020, 315: 113766.
127. Chieng B W, Ibrahim N A, Yunus W M Z W, et al. Plasticized poly (lactic acid) with low molecular weight poly (ethylene glycol): Mechanical, thermal, and morphology properties[J]. Journal of Applied Polymer Science, 2013, 130(6): 4576-4580.
128. Yu Y, Cheng Y, Ren J, et al. Plasticizing effect of poly (ethylene glycol) s with different molecular weights in poly (lactic acid)/starch blends[J]. Journal of Applied Polymer Science, 2015, 132(16).
129. Sun Y, Sun S, Chen L, et al. Flame retardant and mechanically tough poly (lactic acid) biocomposites via combining ammonia polyphosphate and polyethylene glycol[J]. Composites Communications, 2017, 6: 1-5.
130. Jayan J S, Saritha A, Deeraj B D S, et al. Graphene oxide as a prospective graft in polyethylene glycol for enhancing the toughness of epoxy nanocomposites[J]. Polymer Engineering & Science, 2020, 60(4): 773-781.
131. Müller M, Lee S, Spikes H A, et al. The influence of molecular architecture on the macroscopic lubrication properties of the brush-like co-polyelectrolyte poly (L-lysine)-g-poly (ethylene glycol)(PLL-g-PEG) adsorbed on oxide surfaces[J]. Tribology Letters, 2003, 15(4): 395-405.
132. Sungsanit K, Kao N, Bhattacharya S N. Properties of linear poly (lactic acid)/polyethylene glycol blends[J]. Polymer engineering & science, 2012, 52(1): 108-116.

133. Fortunato G, Guex A G, Popa A M, et al. Molecular weight driven structure formation of PEG based e-spun polymer blend fibres[J]. Polymer, 2014, 55(14): 3139-3148.

134. Nies C W, Messing G L. Effect of glass‐transition temperature of polyethylene glycol‐plasticized polyvinyl alcohol on granule compaction[J]. Journal of the American Ceramic Society, 1984, 67(4): 301-304.

135. Hassouna F, Raquez J M, Addiego F, et al. New approach on the development of plasticized polylactide (PLA): Grafting of poly (ethylene glycol)(PEG) via reactive extrusion[J]. European Polymer Journal, 2011, 47(11): 2134-2144.

136. Guo B L, Ma P X. Synthetic biodegradable functional polymers for tissue engineering: a brief review[J]. Science China Chemistry, 2014, 57(4): 490-500.

137. Martin J R, Patil P, Yu F, et al. Enhanced stem cell retention and antioxidative protection with injectable, ROS-degradable PEG hydrogels[J]. Biomaterials, 2020, 263: 120377.

138. Kargari A, Rezaeinia S. State-of-the-art modification of polymeric membranes by PEO and PEG for carbon dioxide separation: A review of the current status and future perspectives[J]. Journal of Industrial and Engineering Chemistry, 2020, 84: 1-22.

Chapter 2: Shape memory thermoplastic epoxy filaments

2.1 Introduction

As important smart materials, shape memory materials (SMMs) not only have the ability to change into a specific shape, but can also be restored to their original shape by stimulation of external conditions, such as heat [1], electricity [2], light [3], and magnetic field [4]. Thus far, SMMs have been widely used in material science [5], electronic engineering [6], textile science [7], biomedicine, and other fields [8,9]. Among SMMs, shape memory polymers (SMPs) have attracted more attention due to their high flexibility, lightweight, low cost, and high recyclability [10]. They have also shown great potential in applications, such as flexible sensors [11], soft actuators [12], self-healing materials [13], flexible energy harvesters [14], and smart textiles [15].

With the continuous exploration of polymer functions, more and more polymers are reported to have shape memory functions, such as polyurethane [16], polyvinyl alcohol [17], polycaprolactone [18], epoxy resin [19], and their heterophasic copolymers. In recent years, shape memory epoxy polymers (SMEPs) have become a more promising type of smart materials due to their excellent shape memory performance and dimensional stability [20]. Epoxy resins are multifunctional materials and

have been widely used in composite materials [21], coatings [22], sealants [23], etc. In the field of composite materials, epoxy resins are often used as the matrices of composite systems [24,25] and endow composite materials with new functions, such as shape memory and self-healing properties [26,27]. In addition, SMEPs have also been developed in the form of films [28,29] and foams [30] that are used in different fields. It is worth noting that most SMEPs are thermoset polymers and research on the SMEP-TP is rarely reported [31,32].

Shape memory thermosetting epoxy polymers (SMEP-TSs) have relatively low deformability due to their three-dimensional network molecular chain structure. This limits the application range of SMEP-TSs to a certain extent [33,34]. Unlike SMEP-TSs, SMEP-TPs have a linear molecular chain structure, so they have larger deformability, which gives SMEP-TP larger toughness [35]. When the temperature reaches the T_g, the storage modulus of the SMEP-TP will drop rapidly, which is beneficial for shape memory performance with large deformability [36]. In addition, SMEP-TPs can transform from a rubbery state to a melt at a certain high temperature, which gives SMEP-TPs the advantages of melt reprocessing and convenient recycling [37].

In this chapter, a thermoplastic epoxy polymer (EP-TP) with a linear molecular structure was prepared and a shape memory thermoplastic epoxy

filament (SMEF-TP) was successfully developed, for the first time, through a melt-drawing process. The structure of SMEF-TP and the mechanism of the preparation process were characterized by chemical structure and thermal analysis. Then, the static and dynamic mechanical performances of SMEF-TP were analyzed and, based on this an investigation on the mechanism and property of the shape memory of the SMEF-TP was conducted. In the shape memory experiment, the mechanism of shape memory is investigated through shape memory process. Then, the stability of the shape memory performance is analyzed through cyclic experiments. Finally, the shape recovery stress is characterized and the application potential of SMEF-TP in the field of thermal actuation is discussed. The results show that the developed SMEF-TP not only has excellent shape memory performance but also can stably output high recovery stress and shows huge application potential in the fields of artificial muscles and smart textiles.

2.2 Materials and Methods

2.2.1 Materials

The materials used in this study include the main agent of model XNR6850A and the accelerator of model XNH6850B, all provided by Nagase Chemical Industry Co., Ltd. (Japan). The main agent is a white two-component liquid composed of di-functional epoxy resin and di-

functional phenolic with a functional group ratio of 1:1, and its chemical structure is shown below.

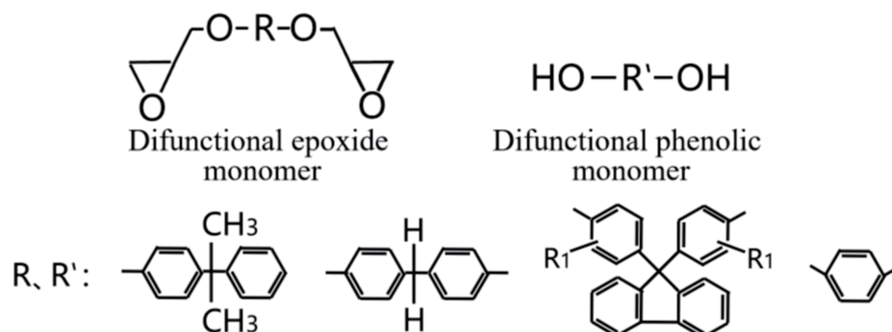

2.2.2 Fabrication of EP-TP and SMEF-TP

A schematic illustrating the fabrication of the EP-TP is shown in Figure 2-1a. 12 g of milky white XNR6850A was weighed in a beaker, which was placed on a hot plate at 160 °C. After heating the XNR6850A until transparent, the temperature of the hot plate was slowly lowered. When the temperature in the beaker dropped to 85 °C, 2wt% of XNH6850B was added. The mixture was stirred for 2 min and transferred to a drying oven, then heated at 150 °C for 40 min to prepare EP-TP, finally cut into pellets as shown in Figure 2-1b.

A twin-screw micro pulverizer (15 ml; DSM Xplore, Netherlands) and supporting equipment were used to prepare the EP-TP into SMEF-TP by the melt-drawing process. The spinning temperatures from entrance zone to extrusion zone were 290 °C, 295 °C, and 300 °C, respectively, the extrusion rate was 40 r/min, drawing was carried out at room temperature with a winding rate of 120 r/min, the spinneret diameter was 0.5 mm, and

the spinning distance was 40 cm. The developed SMEF-TP has good moldability and a smooth surface with an average diameter of 0.285 mm. A photograph, optical microscopy image, and the diameter distribution of the SMEF-TPs are shown in Figure 2-1c. In addition, an electron micrograph of the cross-section of a SMEF-TP is shown in Figure 2-1d.

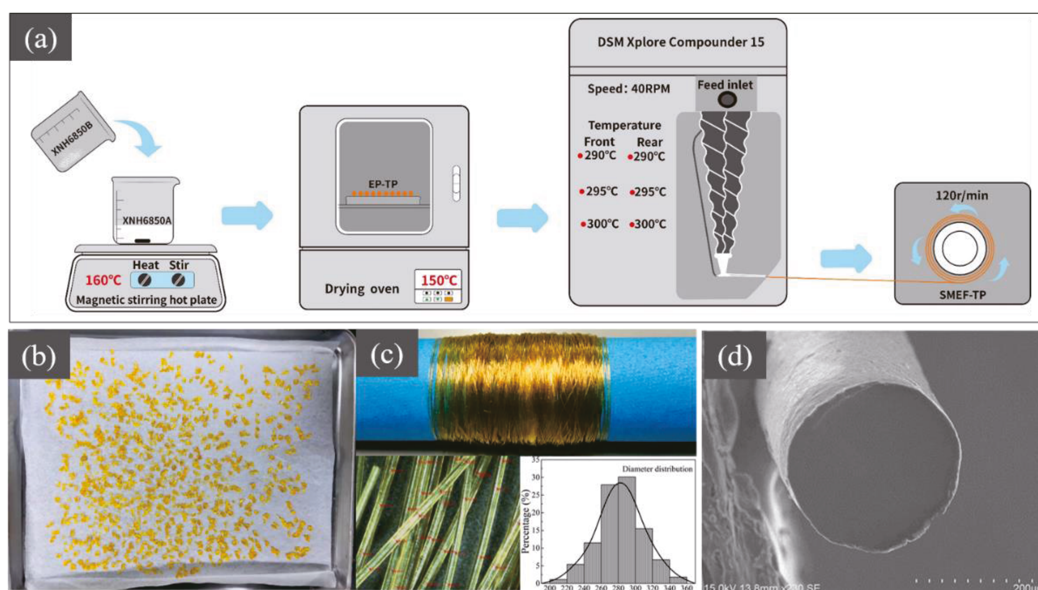

Figure 2-1. (a) Schematic illustrating the fabrication process of EP-TP and SMEF-TP; (b) photograph of EP-TP pellets; (c) photograph of collected SMEF-TP, optical microscope image, and diameter distribution; (d) SEM image of a SMEF-TP cross-section.

2.2.3 Characterization of chemical structure

The chemical structure was analyzed by Fourier transform infrared (FTIR) spectroscopy. The FTIR spectra were measured on a Nicolet 5700 attenuated total reflection FTIR (ATR-FTIR) instrument (Thermo Electron Corp., USA) with a resolution of 4 cm^{-1}.

2.2.4 Thermal analysis

Differential scanning calorimetry (DSC) analysis was performed with a Rigaku Thermo-Plus DSC-8230 system. The measurements were carried out at a heating rate of 10 °C/min in a dry nitrogen atmosphere. For the epoxy resin mixture before the polymerization reaction, the temperature was raised from room temperature (25 °C) to 150 °C, which was the temperature of the polymerization reaction, and then maintained at this temperature for 45 min. For the EP-TP, the temperature was increased from room temperature to 340 °C. For the SMEF-TP, the temperature was increased from room temperature to 110 °C and then the temperature was reduced from 110 °C to room temperature with the same rate as the heating process.

Thermogravimetric analysis (TGA) was performed with a Rigaku Thermo Plus 2 TG-DTA TG8120 system. For the EP-TP, under a nitrogen atmosphere, the temperature was increased from room temperature to 310 °C at a heating rate of 20 °C/min and then maintained at this temperature for 30 min.

2.2.5 Static and dynamic mechanical analysis

Static mechanical tests were conducted at room temperature using a multi-purpose tensile tester (RTC1250A, A&D Company, Ltd, Japan).

SMEF-TP with a length of 20 mm was stretched at a strain speed of 20 mm/min.

A dynamic mechanical analyzer (ITK-DVA225, Japan) was used to investigate dynamic mechanical properties. All samples were investigated in stretching mode at a constant heating rate of 10 °C/min and an oscillation frequency of 10 Hz from 25 °C to 150 °C. The EP-TP film pressed at a temperature of 120 °C and a pressure of 25 MPa is also used to test the dynamic mechanical properties. The test length of EP-TP film and SMEF-TP are both 10 mm. The test width of the EP-TP film is 2 mm and the test thickness is 0.32 mm. Considering the particularity of SMEF-TP as a filament, the test "width" of SMEF-TP is input as 1 mm, and the test "thickness" of SMEF-TP is input as 0.064 mm^2 (the cross-sectional area of SMEF-TP).

2.2.6 Shape memory experiments

The shape memory properties were tested by a thermomechanical analyzer (TMA/SS6100, Hitachi High-Tech Science Corp., Japan). In this paper, the *F* and *L* modes of TMA are selected to test the change of strain and stress, respectively, during the shape memory process.

The test process of the *F* mode is shown in Figure 2-2a. First, under the condition that the SMEF-TP has a certain prestress, the temperature was increased from room temperature (25 °C) to 105 °C and then the stress was

increased at 105 °C to extend the length of the SMEF-TP. Second, the temperature was reduced to room temperature and stress was reduced to the prestress at room temperature. Finally, the temperature was raised again to 105 °C to observe the strain recovery process of the SMEF-TP. The shape fixation rate (R_f) and shape recovery rate (R_r) were obtained by the following equations:

$$R_f = \frac{S_3 - S_1}{S_2 - S_1} \times 100\% \qquad (2-1)$$

and

$$R_r = \frac{S_3 - S_4}{S_3 - S_1} \times 100\%, \qquad (2-2)$$

where S_1 was the strain before the SMEF-TP was stretched, S_2 was the maximum strain after stretching, S_3 was the strain at which the temperature was reduced to room temperature and the tensile stress was released, and S_4 was the strain after reheating and recovery.

The test process of the L mode is shown in Figure 2-2b. First, the temperature was increased to 105 °C and the strain of the SMEF-TP was increased. Second, the temperature was reduced to room temperature and the stress was returned to zero by slightly reducing the strain at room temperature. Finally, the temperature was raised to 105 °C again and output stress in the T_g region is the shape recovery stress of SMEF-TP.

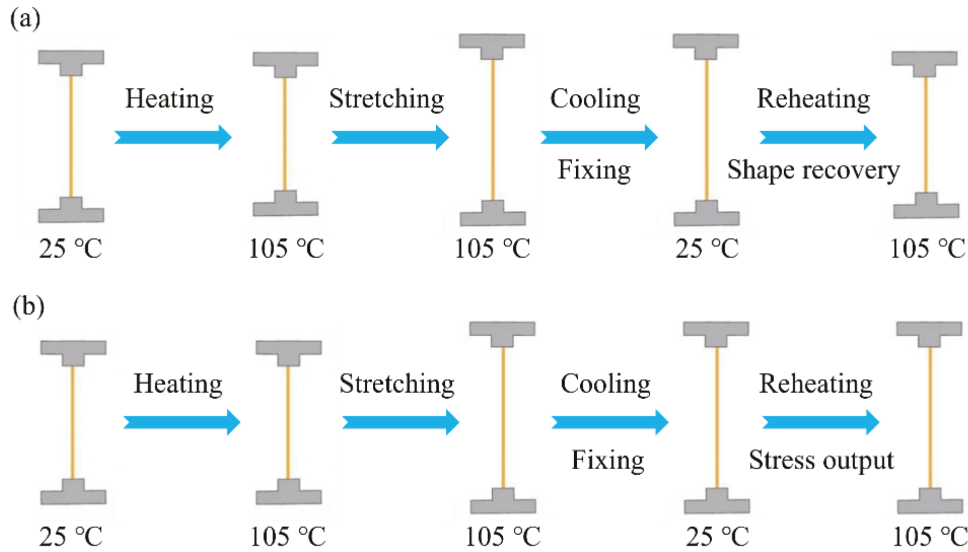

Figure 2-2. (a) Test process of the shape memory with *F* mode, and (b) test process of recovery stress with *L* mode.

2.3 Results and Discussion

2.3.1 Chemical structure

The chemical structure was analyzed using ATR-FTIR spectra. It can be seen from Figure 2-3a that a characteristic peak of an epoxide functional group at 912 cm^{-1} is shown in the spectra of the epoxy resin mixture. This peak in the spectra of EP-TP is obviously weaker, which is because the EP-TP is prepared by an epoxy ring-opening reaction of the epoxy mixture during the polymerization process, as shown in Figure 2-3b. It is worth noting that the polymerization reaction of epoxide monomer and phenolic monomer during heating makes the reaction product has a linear molecular chain structure, as shown in Figure 2-3c. In addition, the spectra of SMEF-TP is almost the same as that of EP-TP, which shows that EP-TP does not

undergo significant chemical structure changes during the melting stage.

The structure of SMEF-TP was further analyzed through the spectra of SMEF-TP. The characteristic peak of the stretching vibration of the C–O bond in the alcohol group is shown at 1035 cm^{-1}. The stretching vibration of the aromatic ether group C–O–C bond is shown between 1150 and 1270 cm^{-1}. The vibration characteristic peaks of the skeleton of the benzene ring are shown at 1500 cm^{-1} and 1600 cm^{-1}. Before and after the polymerization reaction of the epoxy resin mixture, spectra show a difference in position of the characteristic peak of the epoxide functional group while other peaks remain basically unchanged. This is consistent with the expected chemical reaction.

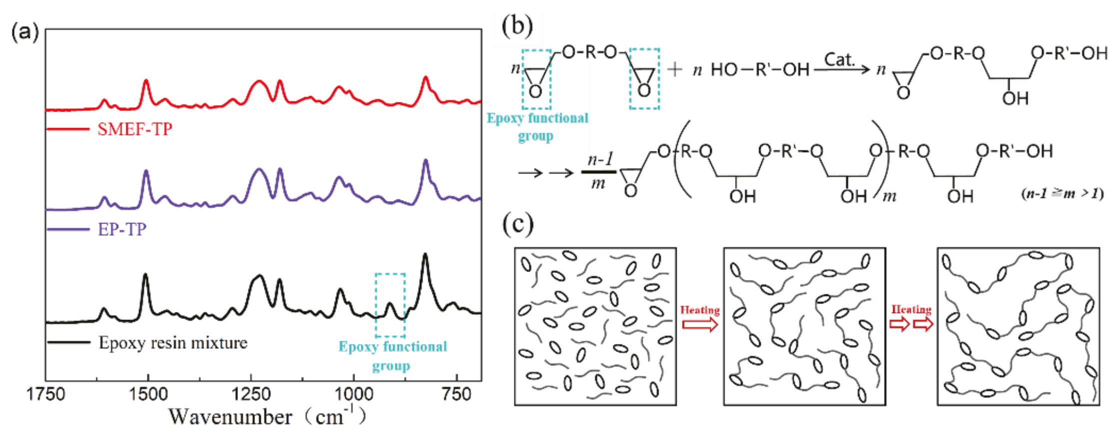

Figure 2-3. (a) FTIR spectra of epoxy resin mixture, EP-TP, and SMEF-TP; (b) diagram of the molecular structure for the polymerization reaction; (c) schematic diagram of the polymerization reaction.

2.3.2 Thermal properties

The polymerization reaction of the epoxy resin mixture is accompanied

by an exothermic effect and an insufficient polymerization reaction will affect the subsequent spinning experiment of the EP-TP. Figure 2-4a is the DSC heating curve of the epoxy resin mixture. It can be seen from Figure 4a that as the temperature increases, the polymerization exotherm of the epoxy resin mixture gradually ends after a heating time of 20 min. Therefore, the polymerization reaction time of the epoxy resin mixture was chosen to be 30 min, which is sufficient for the polymerization reaction to proceed. Figure 2-4b shows the TGA curve of the EP-TP. The EP-TP was kept at a temperature of 300 °C for 30 min and the weight loss was less than 3%. Therefore, the thermal stability of the EP-TP meets the requirements for melt processing at a temperature of 300 °C. Figure 2-4c shows DSC heating curves of the EP-TP and SMEF-TP. It can be seen from Figure 4c that the T_g of the EP-TP ranges from 80 °C to 100 °C and there is no obvious exothermic peak of crystallization. Interestingly, the DSC heating curve of the SMEF-TP has a small exothermic peak near 83 °C. It is speculated that during the cold drawing process of spinning, the developed SMEF-TP is induced to a part of the crystal structure and when the temperature reaches the T_g range again, the crystal structure acquires the ability to rearrange and further crystallize. Therefore, there is a slight exothermic peak at approximately 83 °C. In addition, the DSC cooling curve of SMEF-TP shows a small exothermic peak of crystallization near 64 °C, which further verifies that SMEF-TP has a partial crystal structure.

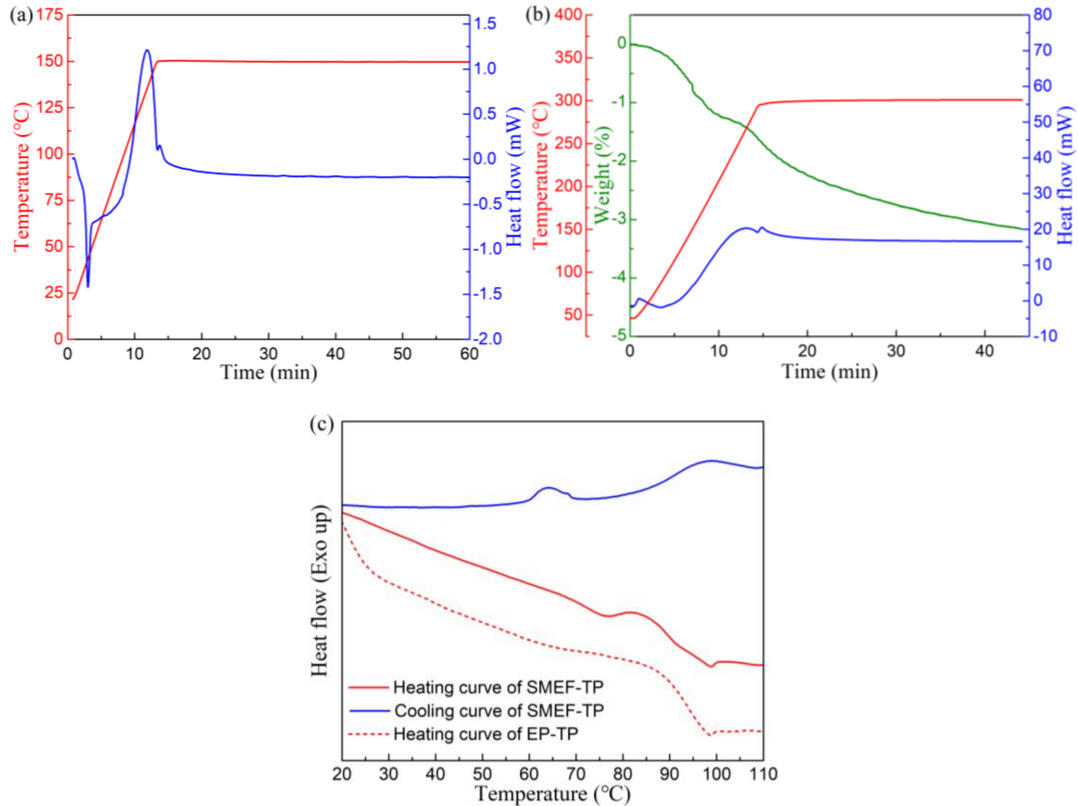

Figure 2-4. (a) DSC curve of epoxy resin mixture, (b) TGA curve of EP-TP, and (c) DSC curve of EP-TP and SMEF-TP.

2.3.3 Static and dynamic mechanical properties

Appropriate drawing in the spinning process is beneficial to improve the mechanical properties of the filament. In this experiment, a drawing rate of 120 r/min was selected. As shown in Figure 2-5a, the initial modulus of the SMEF-TP with a drawing rate of 120 r/min reached 1.89 GPa, yield stress reached 63 MPa, breaking stress reached 78 MPa, and breaking elongation reached 236%. Compared with previous research on EP-TP films by our research group, the yield stress has increased by 54% and the breaking elongation has increased by 133%. For comparison, Figure 2-5a

also shows the stress-strain curves of SMEF-TPs for other drawing rates. On the one hand, the increase in the drawing rate increases the strength of the SMEF-TP. On the other hand, a larger drawing rate may damage the structure of the SMEF-TP, thus reducing its breaking elongation. When the drawing rate reaches 160 r/min, continuous filaments can no longer be obtained in the spinning experiment of SMEF-TP. It can also be found that after reaching the yield point, the tensile stress drops by a “small step.” This is because the tensile movement destroyed the crystalline structure. Interestingly, when the strain reaches approximately 125%, an ascending step appears on the curve. This is because the linear molecules are further oriented, which further increases the tensile stress of the SMEF-TP.

Figure 2-5b is the test result of dynamic mechanical. The storage modulus of SMEF-TP at 25 °C is above 2000 MPa. With the increase of temperature, the storage modulus decreases due to the increase of molecular mobility, gradually decreases before reaching 80 °C, rapidly decreases in the T_g range (80 °C–100 °C), and slowly decreases after 100 °C. After the T_g, the smaller storage modulus is beneficial to the stretching of SMEF-TP while the larger molecular motion energy is beneficial to the recovery of strain in the shape memory process. In addition, compared with EP-TP film, SMEF-TP shows a similar change trend during the temperature increase process, and has a higher initial modulus. In this paper, 105 °C is selected as the strain and recovery

temperature of SMEF-TPs during the shape memory process. The storage modulus at 105 °C is about 70 MPa, as shown in Figure 2-5c.

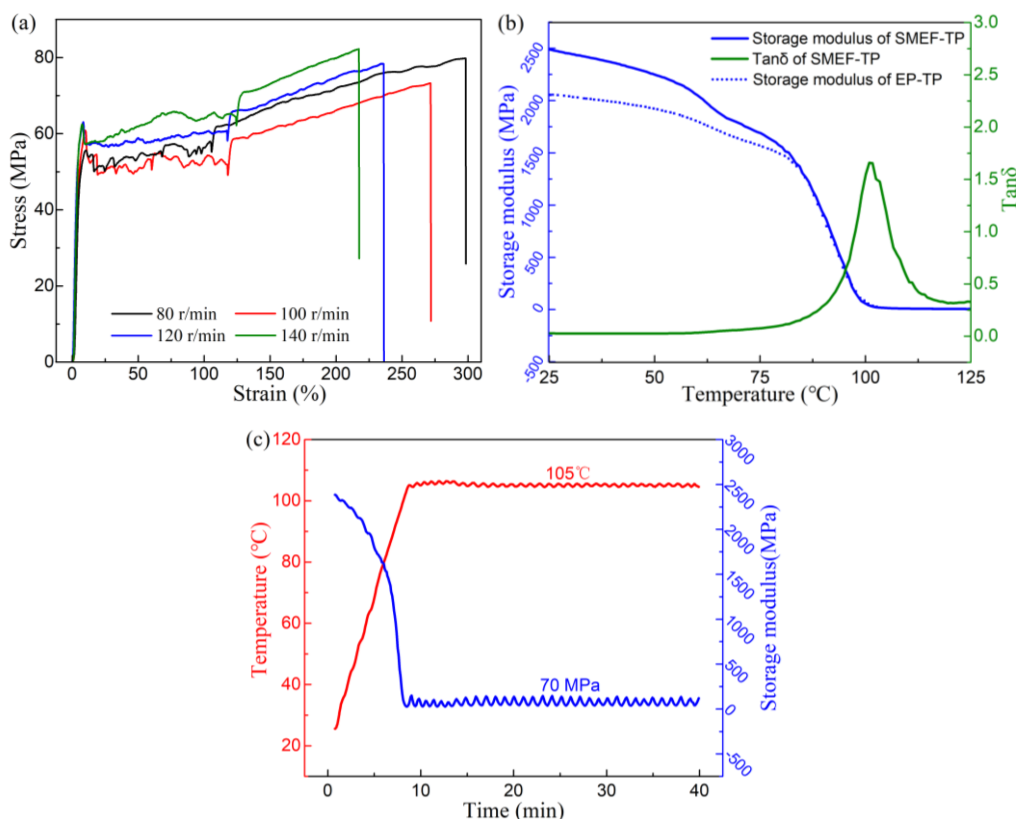

Figure 2-5. (a) Stress-strain curve of SMEF-TP, (b) dynamic mechanical curve of EP-TP and SMEF-TP as a function of temperature, and (c) dynamic mechanical curve of SMEF-TP with time.

2.3.4 Mechanism of shape memory for SMEF-TP

The shape memory process of SMEF-TP with prestresses of 0.1 MPa and 0.4 MPa are shown in Figures 2-6a and 2-6b, respectively. Interestingly, when the prestress is 0.1 MPa, the SMEF-TP continues to undergo heat shrinkage after recovering its length. However, when the prestress is 0.4 MPa, the length of the SMEF-TP is not fully recovered and is extremely

slow in recovering before it is stretched again. In addition, the strain of the SMEF-TP after the recovery stage with different prestress is shown in Figure 2-6c. It can be found that as the prestress increases, the strain of the SMEF-TP after the recovery stage becomes smaller. Obviously, the above situation shows the effect of prestress on recovery for the SMEF-TP. From the perspective of stress, prestress limits the heat shrinkage of SMEF-TP, and SMEF-TP with larger prestress has smaller heat shrinkage under the same conditions, as shown in Figure 2-6d wherein heat shrinkage of the SMEF-TP is shown with different prestress. SMEF-TPs with different prestresses all begin to shrink significantly at around 80 °C; the strain and the slope of the strain with heating time in the stage of heat shrinkage are shown in Table 2-1. When the prestress is less than 0.4 MPa, the slope of the strain of SMEF-TP is relatively high. If the SMEF-TP is stretched at this time, it may cause the SMEF-TP to continue to undergo heat shrinkage after recovering its length, which is not beneficial to the normal progress of the shape memory process. When the prestress is 0.4 MPa, the slope of the strain of SMEF-TP gradually approaches zero, and the relatively stable state is beneficial to the normal progress of the shape memory process, so 0.4 MPa is selected as the prestress of SMEF-TP during the shape memory process. When the prestress is 0.5 MPa, although the slope of the strain of SMEF-TP is relatively low, creep occurs afterwards, making the length of the SMEF-TP slightly increase, which may hinder the recovery process of

the shape memory.

In fact, temperature affects the movability of the molecular chain within the SMEF-TP. Based on the temperature program that has been set, the interaction between different stresses causes the shape memory effect in SMEF-TP. The developed SMEF-TP has a molecular structure in which a benzene ring structure and a linear hydrocarbon structure are alternately arranged. The molecular chain can be regarded as a structure composed of alternately arranged "hard segments" and "soft segments" among which the "hard segments" are composed of a benzene ring structure and the "soft segment" is composed of a straight chain hydrocarbon structure. Before the T_g, the molecular segments inside the SMEF-TP are in a "frozen" state. As the temperature gradually rises to the T_g region, the "soft segments" of the molecular chains gain the ability to move again and make strain occur macroscopically in the SMEF-TP. Because of the existence of "hard segments," this strain is limited to a certain range. As shown in Figure 2-6e, SMEF-TP in a cyclical shape memory process has undergone the stages of heat shrinkage, heat stretching, cold fixing, and heat recovery. The SMEF-TP obtains a molecular structure arranged in the axial direction in the spinning process and an internal stress opposing the drafting direction is generated. As the temperature rises in the stage of heat shrinkage, the "soft segment" shrinks under the action of internal stress and prestress and gradually approaches a state of stress balance, which is expressed as the

heat shrinkage of the SMEF-TP. In the heat stretching stage, the "soft segment" stretches along the direction of the external stress and an internal stress opposite to the external stress is generated. In the cold fixing stage, when the temperature drops to room temperature, the "soft segment" is "frozen," and the internal stress is "stored." In the heat recovery stage, when the temperature rises to the T_g region again, the release of internal stress causes the "soft segment" to shrink, which is expressed as the heat recovery of the length of SMEF-TP.

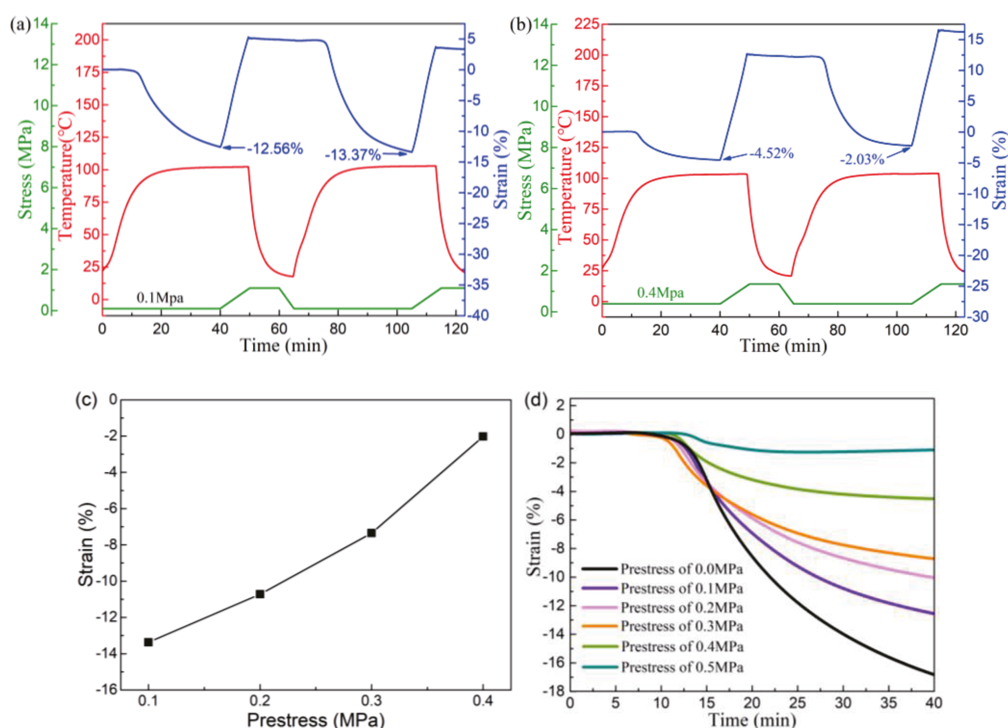

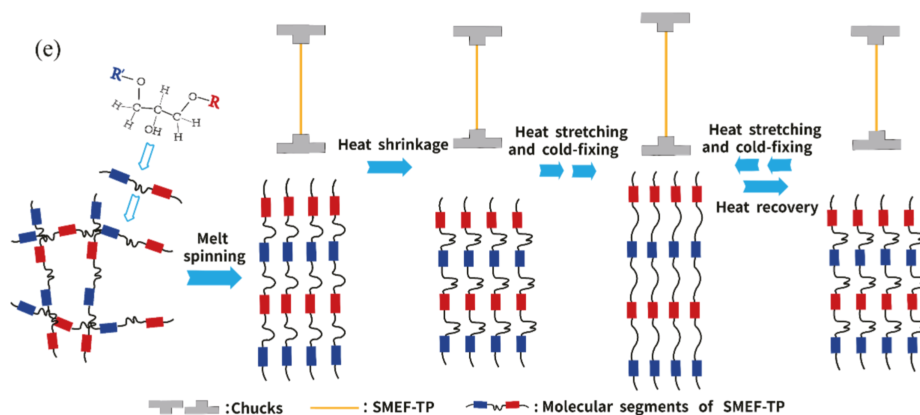

Figure 2-6. TMA curves with prestress values of (a) 0.1 MPa and (b) 0.4 MPa; (c) strain of the SMEF-TP after the recovery stage with different prestress; (d) heat shrinkage curve of TMA with different prestresses; (e) illustration of the shape memory process and strain mechanism of SMEF-TPs.

Table 2-1. Strain (%) and slope (%) of strain with different prestress in the stage of heat shrinkage.

Time	0 MPa		0.1 MPa		0.2 MPa		0.3 MPa		0.4 MPa		0.5 MPa	
(min)	Strain	Slope	Strain	Slope	Strain	Slope	Strain	Slope	Strain	Slope	Strain	Slope
10	-0.02	-12.91	0.03	-8.50	-0.07	-13.75	-0.21	-20.84	0.05	-3.59	0.11	0.05
20	-8.55	79.22	-6.92	-54.56	-5.87	-39.98	-5.61	-32.44	-3.19	-16.70	-1.10	-5.80
30	-13.98	-37.80	-10.79	-24.31	-8.66	-17.89	-7.74	-14.26	-4.20	-5.67	-1.23	0.03
40	-16.82	-21.43	-12.56	-12.03	-10.05	-9.54	-8.72	-5.48	-4.52	-0.83	-1.10	0.99

2.3.5 Cyclic test of shape memory process

Figures 2-7a–2-7c show the shape memory cyclic test results of SMEF-TP with 0.4 MPa prestress and different tensile stresses. SMEF-TP with tensile stresses of 1.0 MPa and 1.3 MPa show good shape memory properties. The shape fixation rate and shape recovery rate with different tensile stresses are shown in Table 2-2. In the stage of cold fixing, the modulus increases rapidly, and the larger tensile stress is beneficial to maintain the shape of the SMEF-TP. Therefore, the SMEF-TP with a tensile stress of 1.3 MPa shows the greatest shape fixation rate (R_f). Moreover, the larger tensile stress is beneficial for the internal molecular chains to obtain a larger axial orientation rate, which makes the SMEF-TP

with a tensile stress of 1.3 MPa also have a larger axial recovery rate during the shape recovery stage. Figure 2-7d shows the average recovery rate (R_r) of the SMEF-TP for two to five cycles with different tensile stresses. Although the SMEF-TP with a tensile stress of 1.6 MPa showed a large R_r, the tensile strain during three to five cycles was relatively large, reaching 35%, and the structure of the SMEF-TP appeared unstable. In the shape memory cycle experiment, the shape recovery performance of the first cycle was relatively ordinary but, after the first training, the shape recovery performance improved. As shown in Figure 2-7e, except for the first cycle, the R_r with a tensile stress of 1.0 MPa and 1.3 MPa is stable at about 94% and 97%, respectively. Figure 2-7f shows the R_r for different heating times. When the temperature was raised for 10 min, although the temperature did not reach 105 °C, the R_r had exceeded 65%. In addition, at 30 min after the temperature rise, the R_r is still increasing, which means that the actual recovery rate is greater than the test value in this experiment. The SMEF-TP shows excellent shape memory performance and good recycling stability; increasing the tensile stress to a certain extent is beneficial to the shape memory performance.

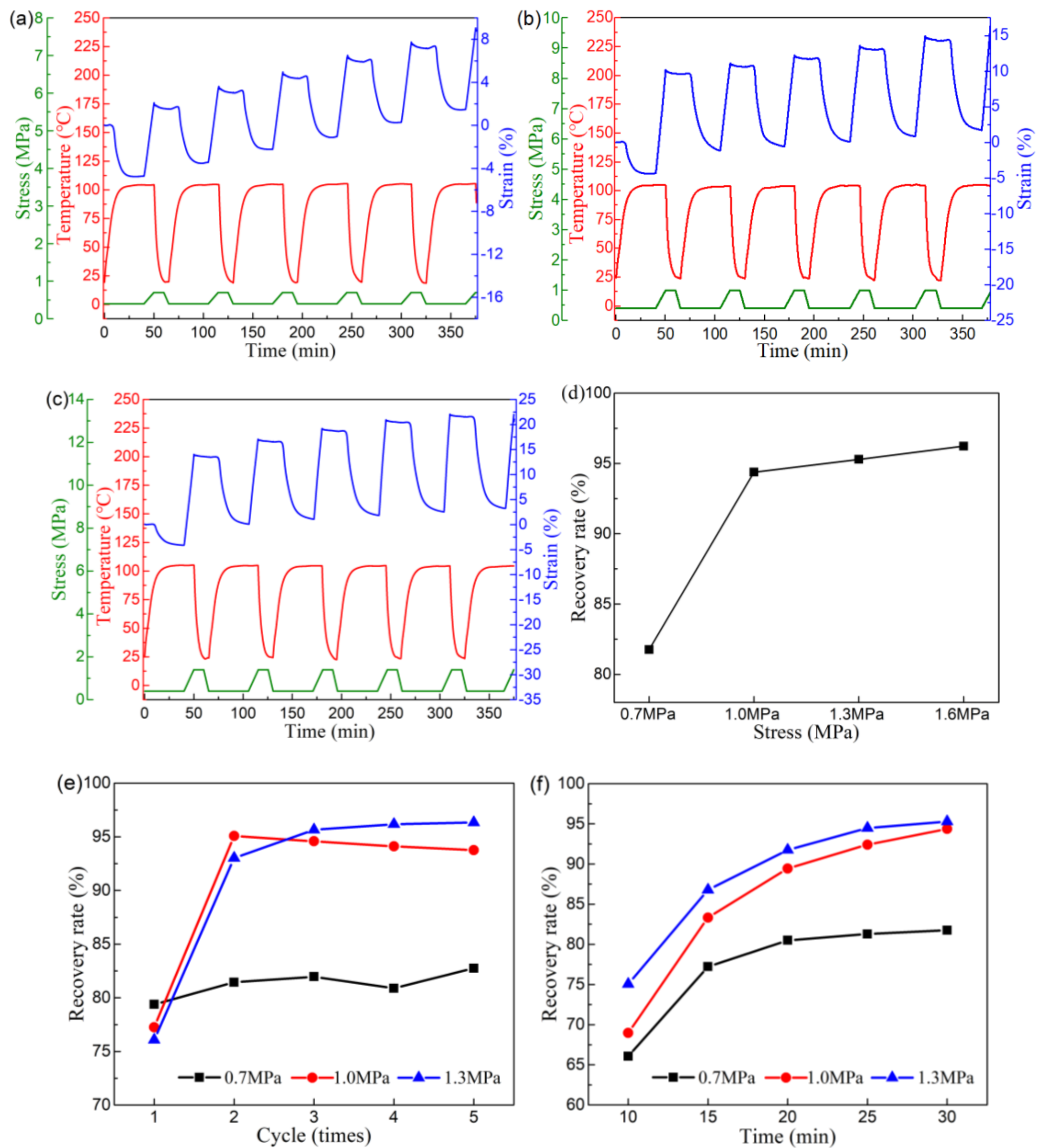

Figure 2-7. TMA cyclic test results with different tensile stresses: cyclic test with tensile stress of (a) 0.7 MPa, (b) 1.0 MPa, and (c) 1.3 MPa; (d) average R_r in two to five cycles with different tensile stresses, (e) R_r by different tensile stresses with different cycles, (f) average R_r in the recovery stage of two to five cycles with heating time.

Table 2-2. R_f and R_r in one to five cycles with different tensile stress.

Stress (MPa)	Cycle-1		Cycle-2		Cycle-3		Cycle-4		Cycle-5	
	R_f (%)	R_r (%)	R_f (%)	R_r (%)	R_f (%)	R_r (%)	R_f (%)	R_r (%)	R_f (%)	R_r (%)
0.7	91.42	79.38	91.41	81.44	91.8	81.96	92.09	80.88	91.79	82.75
1.0	95.74	77.26	95.62	95.08	96.33	94.58	95.7	94.11	97.11	93.75
1.3	96.95	76.08	96.65	93.02	96.90	95.65	97.25	96.17	97.13	96.33

2.3.6 Shape recovery stress of SMEF-TP

The SMEF-TP has stored internal stress during the spinning process and, if it is stretched again, it will store greater internal stress. When the temperature rises, the SMEF-TP releases the internal stress through the change of strain. The strain change of the SMEF-TP during the heating process is shown in Figure 2-8a. The internal stress of the SMEF-TP can be monitored by maintaining the SMEF-TP strain. The shape recovery stress (S_r) of the SMEF-TP during the shape memory process also belongs to the category of internal stress; therefore, S_r can also be monitored. Figure 2-8b shows the response in internal stress of the SMEF-TP to the temperature program, which is a shape memory cycle. The stress change of b_1 to b_3 is due to the internal stress stored in the SMEF-TP during the spinning process changes in response to the increase in temperature. The stress change from b_7 to b_9 occurs because, after the SMEF-TP is stretched, the internal stress stored again changes in response to the increase in temperature. Therefore, the stress changes from b_1 to b_3 and from b_7 to b_9 are the same in the mechanism. In the stage b_8 to b_9, the temperature rises to the glass transition region; the stress monitored at this time is the S_r of

the SMEF-TP during the shape memory process. The S_r first increases with increasing temperature and then slowly decreases due to the stress relaxation effect. It should be noted that the stretching of the SMEF-TP (b_3 to b_4) and the cold fixing of the SMEF-TP (b_4 to b_5) also cause the stress to change. Therefore, in this experiment, the stress is cleared by slightly reducing the strain (b') during the b_5 to b_6 stage to ensure that the SMEF-TP has no initial stress when the temperature is raised again. In addition, the increase in the stress of b_6 to b_7 is caused by the tendency of the SMEF-TP to bend. The decrease in the stress of b_7 to b_8 is caused by the recrystallization inside the SMEF-TP, which makes the SMEF-TP tend to elongate. The increase in strain at b'' is to recover the reduced strain at b' again to ensure that the next cycle of experiments is carried out under the same conditions. Due to the complexity of Figure 2-8b, the test curve shown in Figure 2-8c is selected for the study of S_r in this article, including the strain zone and the recovery zone, and further analyzes its cyclic test. Figure 2-8d is a test of five cycles of S_r with 10% strain. The *S*r of the first cycle can reach 1.12 MPa. As the number of cycles increase, S_r slightly decreases due to the stress relaxation effect and gradually stabilizes at about 0.9 MPa. S_r with different strains was also tested, as shown in Figure 2-8e. Below 35%, the S_r increases with the increase of strain and gradually becomes slower, reaching 1.45 MPa at 35% and then stops increasing. When the strain is 40%, the SMEF-TP at 105 °C is excessively stretched,

resulting in a slight decrease in stress. Therefore, the strain of SMEF-TP at 105 °C should be controlled within 35%. In addition, the SMPU fiber prepared by Shi et al also by the melt-drawing process has been reported to have shape memory properties, but as shown in Figure 2-8f, its shape recovery stress is only 0.33MP [38]. The shape recovery stress of SMEF-TP is more than 5 times that of EP-TP film and almost 4 times that of SMPU fiber prepared by Shi et al. In this research, the developed SMEF-TP can sense temperature and stably output considerable stresses during the shape recovery process.

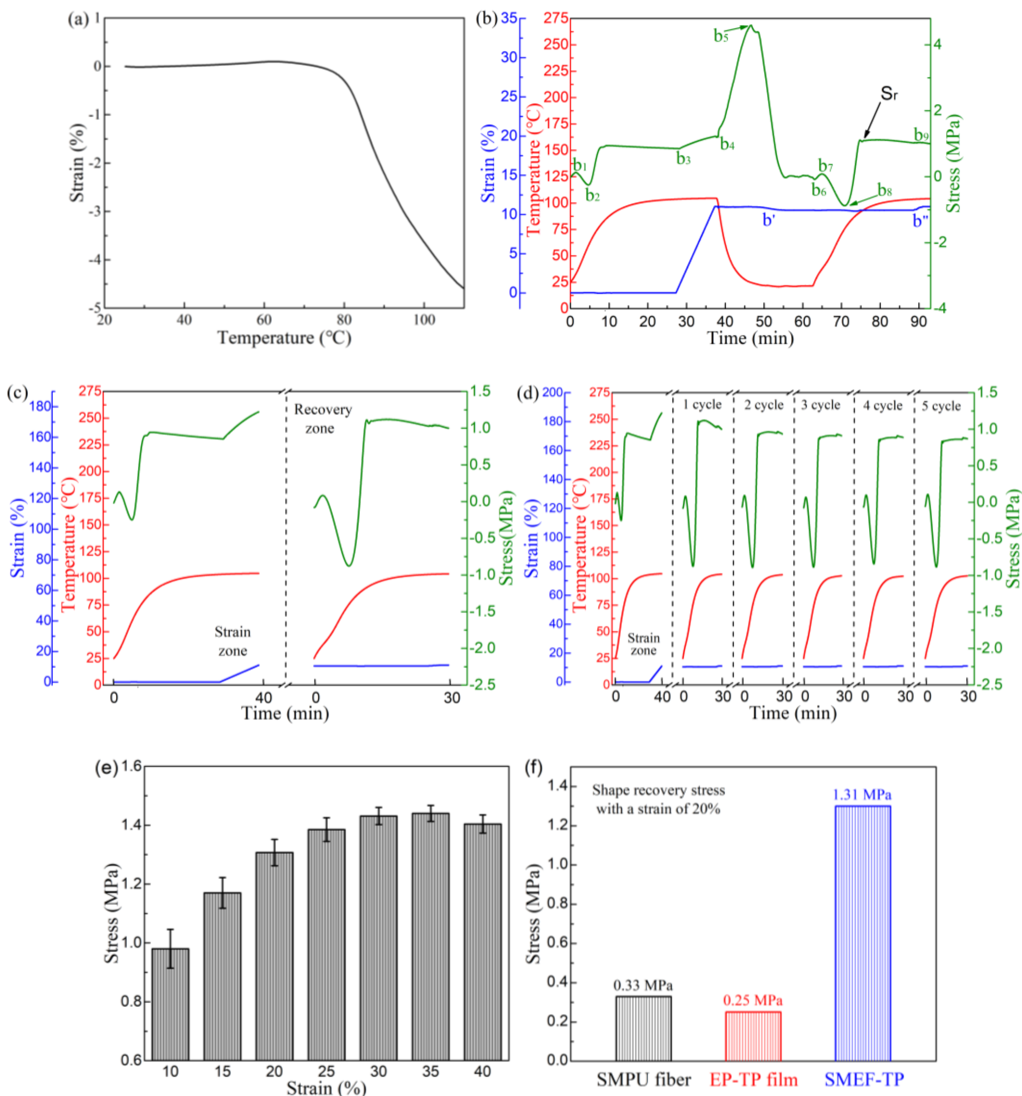

Figure 2-8. (a) Strain as a function of temperature, (b) testing of thermal response stress, (c) one cycle and (d) five cycle test of shape recovery stress, and (e) shape recovery stress with different strains, (f) Shape recovery stress of the samples of SMPU fiber, EP-TP film and SMEF-TP with a strain of 20%.

2.3.7 Application of SMEF-TP in thermal actuation

This paper conducted thermal actuation experiments, and all experiments were conducted inside a heating device (Figure 2-9a). In addition to the single filament (F-1), two-filament twisted yarn (F-2) and three-filament braided yarn (F-3) were also selected for experimental study, as shown in Figure 2-9b. All the samples were 18.0 cm long, the average diameter of the filaments among them was 0.285 mm, and then heat-stretched 30% to 23.4 cm in a temperature atmosphere of 105 °C. Figure 2-9c was the initial state of F-1, F-2, and F-3 in the heating device, and Figure 2-9d was the state of F-1, F-2, and F-3 after 40 s in a temperature atmosphere of 105 °C. The results showed that an F-1 can thermally drive a load of 2.5 g within 40 s to lift a displacement of 31 mm. Here a parameter of energy density (D_e) is introduced to express the actuation ability of the developed filament. D_e of a single SMEF-TP during the thermal actuation reached 0.066 J/cm^3. D_e was obtained by the following equation:

$$D_e = \frac{Hmg}{L\pi r^2}, \qquad (2-3)$$

where H is the rising displacement of F-1 lifting load, m is the total mass borne by F-1, g is approximately equal to 9.81 m/s^2, L is 18cm, π is approximately equal to 3.14, and r is 0.1425 mm.

The thermal actuation results of F-2 shown that an F-2 can thermally drive a load of 5.0 g within 40 s to lift a displacement of 36 mm. The thermal actuation capacity of the F-2 is more than twice that of an F-1. The thermal actuation results of F-3 shown that an F-3 can thermally drive loads of 7.0 g within 40 s to lift displacements of 45 mm. The thermal actuation capacity of the F-3 is more than three times that of the F-1. A single filament exhibits considerable thermal actuation capability, which indicates its application potential in the field of artificial muscles. The capacity of textile processing has also expanded its application in this textile-type thermal actuation.

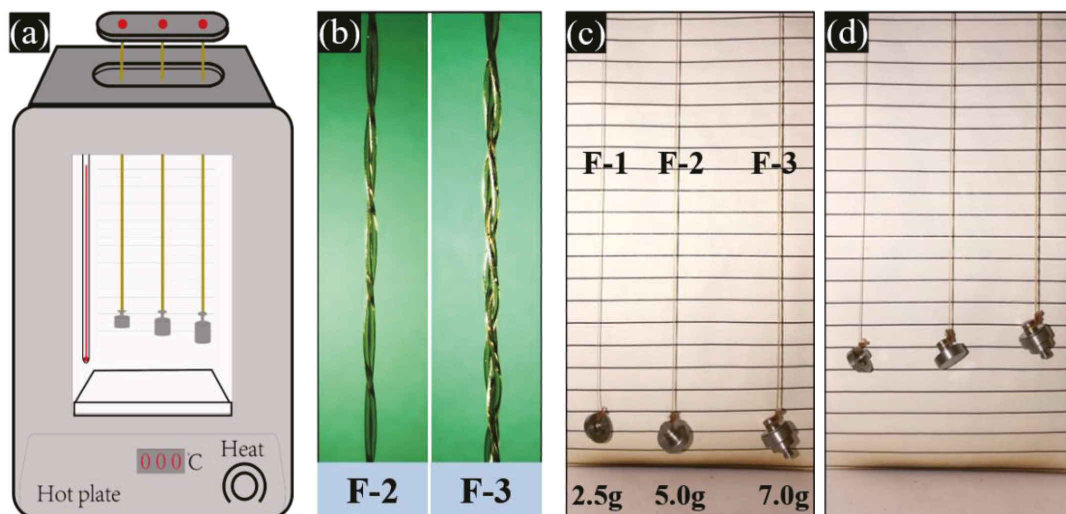

Figure 2-9. (a) Schematic of the thermal actuation test, (b) magnified view of the two-filament twisted yarn and three-filament braided yarn; (c) the

initial state of F-1, F-2, and F-3 in the heating device, and (d) the state of F-1, F-2, and F-3 after 40 s in a temperature atmosphere of 105 °C.

2.4 Conclusions

In this chapter, EP-TP was developed through a polymerization reaction of an epoxy resin mixture composed of epoxy and phenol monomers. Then, SMEF-TP with an average diameter of 0.285 mm was developed by the melt-drawing process. The developed SMEF-TP has a partial crystal structure, a higher T_g range (as high as 80 °C–100 °C), and excellent mechanical properties wherein the yield stress increased by 54% compared to EP-TP films. Through shape memory experiments, it is revealed that the SMEF-TP has excellent shape memory performance. The shape fixation rate can reach 97%, the shape recovery rate can reach more than 97%, and the cyclic test showed good stability. The shape recovery stress of SMEF-TP was further tested to show that it can stably respond to temperature, and the shape recovery stress increases with the increase of strain, reaching 1.45 MPa at a strain of 35%. The thermal actuation experiment of SMEF-TP shows that the energy density can reach 0.066 J/cm^3 and the capacity of textile processing has also expanded its application in textile-type thermal actuation. The developed SMEF-TP shows excellent shape memory performance and can output large shape recovery stress, which is more than 5 times that of EP-TP film. As a new

type of shape memory filament, SMEF-TP has shown huge application potential in the field of artificial muscles and smart textiles.

References

1. Qi, X. *et al.* Design of Ethylene-Vinyl Acetate Copolymer Fiber with Two-Way Shape Memory Effect. *Polymers* **11**, 1599 (2019).
2. Liu, W., Chen, H., Ge, M., Ni, Q.-Q. & Gao, Q. Electroactive shape memory composites with TiO_2 whiskers for switching an electrical circuit. *Mater. Des.* **143**, 196–203 (2018).
3. Cui, X., Chen, J., Zhu, Y. & Jiang, W. Natural sunlight-actuated shape memory materials with reversible shape change and self-healing abilities based on carbon nanotubes filled conductive polymer composites. *Chem. Eng. J.* **382**, 122823 (2020).
4. Ze, Q. *et al.* Magnetic Shape Memory Polymers with Integrated Multifunctional Shape Manipulation. *Adv. Mater.* **32**, 1906657 (2020).
5. Chen, H. *et al.* Flexible Nano positioning actuators based on functional nanocomposites. *Compos. Sci. Technol.* **186**, 107937 (2020).
6. Guan, X. *et al.* Flexible energy harvester based on aligned PZT/SMPU nanofibers and shape memory effect for curved sensors. *Compos. Part B Eng.* **197**, 108169 (2020).
7. Huang, Y. *et al.* A shape memory supercapacitor and its application in smart energy storage textiles. *J. Mater. Chem. A* **4**, 1290–1297 (2016).

8. Hardy, J. G., Palma, M., Wind, S. J. & Biggs, M. J. Responsive Biomaterials: Advances in Materials Based on Shape-Memory Polymers. *Adv. Mater.* **28**, 5717–5724 (2016).
9. Li, F., Liu, Y. & Leng, J. Progress of shape memory polymers and their composites in aerospace applications. *Smart Mater. Struct.* **28**, 103003 (2019).
10. Liu, Y., Du, H., Liu, L. & Leng, J. Shape memory polymers and their composites in aerospace applications: a review. *Smart Mater. Struct.* **23**, 023001 (2014).
11. Li, X. & Serpe, M. J. Understanding the Shape Memory Behavior of Self-Bending Materials and Their Use as Sensors. *Adv. Funct. Mater.* **26**, 3282–3290 (2016).
12. Chen, H., Xia, H., Qiu, Y., Xu, Z. & Ni, Q.-Q. Smart composites of piezoelectric particles and shape memory polymers for actuation and nanopositioning. *Compos. Sci. Technol.* **163**, 123–132 (2018).
13. Li, G. & Uppu, N. Shape memory polymer based self-healing syntactic foam: 3-D confined thermomechanical characterization. *Compos. Sci. Technol.* **70**, 1419–1427 (2010).
14. Liu, R. *et al.* Shape Memory Polymers for Body Motion Energy Harvesting and Self-Powered Mechanosensing. *Adv. Mater.* **30**, 1705195 (2018).
15. Biswas, M. C., Chakraborty, S., Bhattacharjee, A. & Mohammed, Z.

4D Printing of Shape Memory Materials for Textiles: Mechanism, Mathematical Modeling, and Challenges. *Adv. Funct. Mater.* **31**, 2100257 (2021).

16. Guan, X., Dong, Y., Xia, H., Yao, J. & Ni, Q.-Q. Mechanical and shape memory performance of shape memory polyurethane-based aligned nanofibers. *Polym. Test.* **91**, 106778 (2020).
17. Yuan, J. *et al.* Shape memory nanocomposite fibers for untethered high-energy microengines. 5 (2019).
18. Zhang, Q. *et al.* Temperature-controlled reversible pore size change of electrospun fibrous shape-memory polymer actuator based meshes. *Smart Mater. Struct.* **28**, 055037 (2019).
19. Wang, E. *et al.* Effect of graphene oxide-carbon nanotube hybrid filler on the mechanical property and thermal response speed of shape memory epoxy composites. *Compos. Sci. Technol.* **169**, 209–216 (2019).
20. Santhosh Kumar, K. S., Biju, R. & Reghunadhan Nair, C. P. Progress in shape memory epoxy resins. *React. Funct. Polym.* **73**, 421–430 (2013).
21. Chen, Y. *et al.* Enhanced Interfacial Toughness of Thermoplastic–Epoxy Interfaces Using ALD Surface Treatments. *ACS Appl. Mater. Interfaces* **11**, 43573–43580 (2019).
22. Wazarkar, K., Kathalewar, M. & Sabnis, A. Development of epoxy-urethane hybrid coatings via non-isocyanate route. *Eur. Polym. J.* **84**, 812–827 (2016).

23. Gao, W., Bie, M., Liu, F., Chang, P. & Quan, Y. Self-Healable and Reprocessable Polysulfide Sealants Prepared from Liquid Polysulfide Oligomer and Epoxy Resin. *ACS Appl. Mater. Interfaces* **9**, 15798–15808 (2017).

24. Liu, F., Shi, Z. & Dong, Y. Improved wettability and interfacial adhesion in carbon fibre/epoxy composites via an aqueous epoxy sizing agent. *Compos. Part Appl. Sci. Manuf.* **112**, 337–345 (2018).

25. Kim, M. T., Rhee, K. Y., Lee, J. H., Hui, D. & Lau, A. K. T. Property enhancement of a carbon fiber/epoxy composite by using carbon nanotubes. *Compos. Part B Eng.* **42**, 1257–1261 (2011).

26. Zhou, X. Preparation of shape memory epoxy resin for asphalt mixtures and its influences on the main pavement performance. *Constr. Build. Mater.* 11 (2021).

27. Liu, Y. *et al.* Carbon fiber reinforced shape memory epoxy composites with superior mechanical performances. *Compos. Sci. Technol.* **177**, 49–56 (2019).

28. Wang, E. *et al.* A novel reduced graphene oxide/epoxy sandwich structure composite film with thermo-, electro- and light-responsive shape memory effect. *Mater. Lett.* **238**, 54–57 (2019).

29. Liu, T. *et al.* Eugenol-Derived Biobased Epoxy: Shape Memory, Repairing, and Recyclability. *Macromolecules* **50**, 8588–8597 (2017).

30. Squeo, E. A. & Quadrini, F. Shape memory epoxy foams by solid-state

foaming. *Smart Mater. Struct.* **19**, 105002 (2010).

31. Karger-Kocsis, J. & Kéki, S. Review of Progress in Shape Memory Epoxies and Their Composites. *Polymers* **10**, 34 (2017).
32. Xie, F., Huang, L., Leng, J. & Liu, Y. Thermoset shape memory polymers and their composites. *J. Intell. Mater. Syst. Struct.* **27**, 2433–2455 (2016).
33. Sun, Z. *et al.* Enhancing the Mechanical and Thermal Properties of Epoxy Resin via Blending with Thermoplastic Polysulfone. *Polymers* **11**, 461 (2019).
34. Di, C. *et al.* Study of Hybrid Nanoparticles Modified Epoxy Resin Used in Filament Winding Composite. *Materials* **12**, 3853 (2019).
35. Wang, X., Zhao, X., Chen, S. & Wu, Z. Static and fatigue behavior of basalt fiber-reinforced thermoplastic epoxy composites. *J. Compos. Mater.* **54**, 2389–2398 (2020).
36. Bouaziz, R., Roger, F. & Prashantha, K. Thermo-mechanical modeling of semi-crystalline thermoplastic shape memory polymer under large strain. *Smart Mater. Struct.* **26**, 055009 (2017).
37. Taniguchi, N., Nishiwaki, T., Hirayama, N., Nishida, H. & Kawada, H. Dynamic tensile properties of carbon fiber composite based on thermoplastic epoxy resin loaded in matrix-dominant directions. *Compos. Sci. Technol.* **69**, 207–213 (2009).
38. Shi, Y., Chen, H. & Guan, X. High shape memory properties and high

strength of shape memory polyurethane nanofiber-based yarn and coil. *Polym. Test.* **101**, 107277 (2021).

Chapter 3: Multifunctional shape memory epoxy-PEG films

3.1 Introduction

Epoxy resin is widely used in composite materials [1], electrical insulating materials [2], coatings [3], and adhesives [4] because of its excellent mechanical strength [5], dimensional stability [6] and electrical properties [7], and strong adhesion to metals and porcelain [8], et. At present, the more commonly used thermosetting epoxy resins have defects in reprocessing and recycling, which limit their application scope to some extent [9,10]. In recent years, research on the plasticization of thermosetting epoxy resins by elastomers and plasticizers has gradually increased [11,12]. However, thermoplastic epoxy resins, which inherently feature environmentally friendly reprocessing and easy recycling [13,14], are rarely reported.

As a widely used polymer material, epoxy resins have also been developed for various forms of shape memory materials (SMMs) [15,16], and epoxy resins with shape memory properties in the form of films, foams, and stents have been reported [17–19]. SMMs are a class of smart materials that can switch between original and temporary shapes in response to external stimuli [20,21] and have shown great application potential in the fields of aerospace [22], artificial intelligence [23], and biomedicine [24].

Among them, polymer-based SMMs have the advantages of good flexibility [25], lightweight [26], easy processing [27], and good biocompatibility [28], and have huge advantages over shape memory alloys in flexible smart SMMs [29]. The excellent mechanical [30], thermal [31], and electrical properties [32] of epoxy resin make it play an important role in the field of SMMs [33]. However, the analysis of the shape memory properties of thermoplastic epoxy resin is rarely reported.

The low molecular weight state of epoxy resin before curing is favorable for being dispersed by various modifiers for modification [34,35], and this high degree of performance variability endows epoxy resin with the potential to be applied in the field of multifunctional SMMs [36,37]. Based on the modification treatment, it has been reported that epoxy resins can make shape memory responses to external stimuli such as heat [38], electricity [39], light [40], and play an important role in actuation [41], artificial muscle [42], and composite materials [43]. Although it has shown great application potential in the field of shape memory, most of the current research is based on the modification of thermosetting epoxy resins [44,45], and thermoplastic epoxy resins are rarely involved.

In this chapter, based on the research results of thermal and mechanical properties for thermoplastic epoxy in Chapter 2, polyethylene glycol (PEG) with good compatibility for unpolymerized epoxy resin was uniformly and

stably dispersed in epoxy resin by the environmentally friendly way of melting. Through FTIR test, thermal property test, and mechanical test, the regulation of thermal and mechanical properties for thermoplastic epoxy by dispersed PEG molecules were fully confirmed. Based on the regulation of epoxy resin properties by PEG, shape memory epoxy-PEG films ranging from rigid to flexible that can respond to different heat-stimuli temperatures were developed, which expanded the application range of thermoplastic epoxy in the field of SMMs. Heating-based healable and adhesive epoxy-PEG films were also prepared by regulating the PEG content, further demonstrating the application potential of thermoplastic epoxy resins in the field of flexible smart materials.

3.2 Materials and Methods

3.2.1 Materials

The thermoplastic epoxy resin used in this study include the main agent of model XNR6850A and the accelerator of model XNH6850B, all provided by Nagase Chemical Industry Co., Ltd. (Japan). The main agent is a white two-component liquid composed of bifunctional epoxy and bifunctional phenol with a functional group ratio of 1:1. Polyethylene glycol (PEG, molecular weight around 1000) was provided by Wako Pure Chemical Industries (Japan). The physical property statistics of all materials are shown in Table 3-1.

Table 3-1. Physical property statistics.

Statistics category	Main agent	Accelerator	Plasticizer
Model	XNR6850A	XNH6850B	PEG 1000
Chemical classification	Two-component epoxy	Aromatic phosphoric acid ester	Pure PEG
Aspect	White paste	White powder	White waxy
Viscosity at 25℃	220 Pa·s	Solid	Solid
Proportion	100	2	—

3.2.2 Fabrication of epoxy-PEG film

Figure 3-1 shows the fabrication process of epoxy–PEG film. The beaker containing 10 g of main agent was placed on a heating hot plate. When the temperature inside the beaker reached about 85 °C, turned on the stirrer. When the temperature inside the beaker was heated to approximately 105 °C, slowly lowered the temperature of the hot plate. When the temperature stabilized at 85 °C, a certain amount of PEG was added with lower stirring speed. When the temperature stabilized at 85 °C again, 2 wt% accelerator was added with lower stirring speed. After stirring for 3 min, transferred the mixture to the prepared mold first, then transferred the mold containing the mixture to a vacuum oven at 85 °C. After vacuuming for 30 min, the mold containing the mixture was first transferred to a metal plate, which was then covered with another metal plate and pressed by a hot press at a pressure of 5 MPa and 150 °C. After hot pressing for 30 min, first fixed the upper and lower metal plates with metal clips, and then transfer the metal plates as a whole to room temperature for cooling. When the temperature was lowered to room

temperature, the metal plate was removed, and the prepared epoxy-PEG film was taken out from the mold. Epoxy-PEG films (PEG0, PEG10, PEG20, PEG25, PEG30, and PEG40) with PEG content of 0 wt%, 10 wt%, 20 wt%, 25 wt%, 30 wt%, and 40 wt% were prepared by the above process.

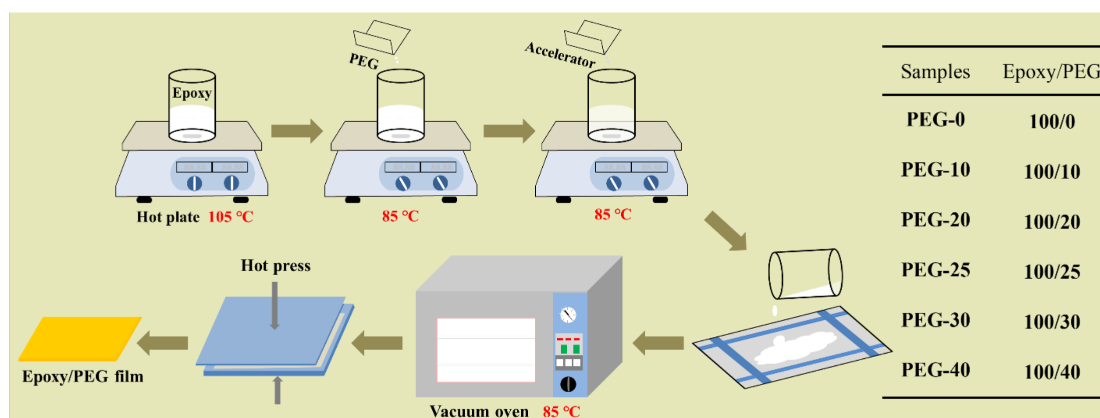

Figure 3-1. The fabrication process of epoxy–PEG film and the names of the prepared samples.

3.2.3 Water contact angle test

The surface water contact angles of epoxy-PEG films were tested using the sessile drop method in air at room temperature using the Drop Master DM500 apparatus (Kyowa Interface Science, Saitama, Japan). The drop size was set as 2 μL, and five specimens for each group were tested to calculate the average value.

3.2.4 Impedance test

The interaction between the epoxy and PEG behavior was investigated using an impedance analyzer, Solartron 1260/1296 (Toyo Technical Ltd.,

Japan). The experiments were carried out in the frequency range of 100-106 Hz at 100 mV. The epoxy-PEG films were cut into circles with a diameter of 14 mm. Each specimen was tested 3 times to calculate the average value.

3.2.5 DSC test

Thermal analysis of the epoxy polymerization reaction was investigated using differential scanning calorimetry (DSC) analysis (Thermo plus EVO2 DSCvesta, Rigaku, Japan). The measurements were performed at a heating rate of 10 °C/min in atmospheric air. One test was to raise the temperature of all mixtures from room temperature to 320 °C. Another test was to raise the temperature of all mixtures from room temperature to 150 °C and maintained at this temperature for 30 min.

3.2.6 FTIR test

The chemical structure was analyzed by Fourier transform infrared (FTIR) spectroscopy. The FTIR spectra were measured on a Nicolet 5700 attenuated total reflection FTIR (ATR-FTIR) instrument (Thermo Electron Corp., USA) with a resolution of 4 cm^{-1}.

3.2.7 TGA test

Thermogravimetric analysis (TGA) for epoxy-PEG was tested using

the Thermo plus TG8120 apparatus (Rigaku, japan). The measurements were performed at a heating rate of 20 °C/min in atmospheric air. The testing temperature of epoxy-PEG was increased from room temperature to 600 °C.

3.2.8 Tensile test

Tensile tests were conducted at room temperature using a multi-purpose tensile tester (RTC1250A, A&D Company, Ltd, Japan). All samples with a length of 20 mm were stretched at a strain speed of 10 mm/min.

3.2.9 Dynamic mechanical test

Dynamic mechanical properties for epoxy-PEG films were tested using the dynamic mechanical analyzer (ITK-DVA225, Japan). All films were investigated in stretching mode at a constant heating rate of 10 °C/min and an oscillation frequency of 10 Hz from room temperature to 150 °C. The test length of all specimens is 10 mm.

3.2.10 Static thermo-mechanical test

The strain of epoxy-PEG films during heat-stretching, cold-fixing and heat-recovery was observed by a thermomechanical analyzer (TMA/SS6100, Hitachi High-Tech Science Corp., Japan). This test was

performed in five steps, and the test program with PEG-0 as an example is shown in Table 3-2 (due to the different T_g) of epoxy-PEG films with different PEG contents, the heating time, temperature and tensile stress of each film are different).

Table 3-2. Thermomechanical program used for the experiments.

Step	Time (min)	Temperature (℃)	Stress (MPa)
1	0-20	Rising: 9 → 104	Keeping: 0.01
	20-25	Keeping: about 104	Stretching: 0.01 → 0.26
2	25-30	Dropping: 104 → 9	Keeping: 0.26
	30-35	Keeping: about 9	Releasing: 0.26 → 0.01
3	35-55	Rising: 9 → 104	Keeping: 0.01
	55-60	Keeping: about 104	Stretching:0.01 → 0.26
4	60-65	Dropping: 104 → 9	Keeping: 0.26
	65-70	Keeping: about 9	Releasing: 0.26 → 0.01
5	70-90	Rising: 9 → 104	Keeping: 0.01
	90-95	Keeping: about 104	Stretching:0.01 → 0.26

3.3 Results and Discussion

3.3.1 Dispersion of PEG in thermoplastic epoxy

The two-component epoxy resin appears as a white emulsion at room temperature, which gradually melts during the heating process, and reaches a completely transparent molten state when heated to about 105 °C. At higher temperatures, PEG may react with oxygen in the air, so PEG was added when the temperature of the epoxy resin was reduced to 85 °C in this experiment. It should be noted that when the epoxy resin was lowered from 105 °C to 85 °C, the epoxy resin was also in a completely transparent molten state. After adding PEG, the PEG is rapidly melted and dispersed

in the epoxy resin, and all epoxy-PEG mixtures with different PEG contents can reach a completely transparent molten state in about 2 min. The melting of epoxy resin, dispersion of PEG, and melting of epoxy-PEG is shown in Figure 3-2a. The epoxy resin before the polymerization reaction is in a low molecular state, and it has a large number of hydroxyl groups like PEG. Therefore, through melt mixing at a lower temperature, the PEG molecules are uniformly dispersed between the epoxy molecules and the phenol molecules, and a stable, transparent mixture is formed. After adding the accelerator to the mixture at 85 °C in the beaker, the epoxy group on the epoxy molecule opens and polymerizes with the phenol molecule, while PEG is wrapped between the polymerized molecular chains. It should be noted that, at 85 °C, the epoxy molecular and the phenol molecular can only be slowly polymerized, and the mixture after adding the accelerator and stirring for 3 min is in a pale-yellow colloidal state. The polymerization reaction process of the epoxy molecule and the phenol molecule is shown in Figure 3-2b. Once the pale-yellow colloidal mixture is transferred to a 150 °C oven, the epoxy and phenol molecules will rapidly polymerize. After heating for about 5 min, all epoxy-PEG mixtures with different PEG contents turn dark yellow, and the color remained essentially unchanged with continued heating. After heating in an oven at 150 °C for 30 min, the fully polymerized epoxy macromolecules encapsulate the PEG molecules to form a stable thermoplastic epoxy-PEG.

The polymerization process of the epoxy-PEG mixture in the oven at 150 °C is shown in Figure 3-2c.

The polymerized epoxy molecular chain contains a large number of hydroxyl groups, which makes the polymerized epoxy have higher hydrophilicity. PEG with a molecular weight of about 1000 has high hydrophilicity, but the hydroxyl group as the main hydrophilic group exists only at both ends of the PEG molecular chain, which is less than the hydroxyl group on the polymerized epoxy molecular chain. When an appropriate amount of PEG is dispersed into the epoxy molecule, the dispersion of PEG causes the reduction of the overall hydroxyl groups of the epoxy-PEG mixture; the hydroxyl groups at the end of PEG form hydrogen bonds with the hydroxyl groups on the epoxy molecule, and the PEG is stably wrapped between oxygen molecular chains; thus the hydrophilicity of the epoxy-PEG mixture first decreases with the increase of PEG content. When the content of PEG is relatively large, the number of hydrogen bonds between epoxy molecular chains decreases due to the dispersion of more PEG, and the epoxy-PEG mixture has more hydroxyl groups that are not involved in forming hydrogen bonds, which makes the hydrophilicity of epoxy-PEG mixture increases with the increasing PEG content. The water contact angle test results of the epoxy-PEG film are shown in Figure 3-2d. When the PEG content does not exceed 20 wt%, the hydrophilicity of the epoxy-PEG film decreases with the increase of PEG

content; when the PEG content exceeds 20 wt%, the hydrophilicity of the epoxy-PEG film increased with the increase of PEG content. The hydrophilicity analysis reflects the interaction between PEG molecules and epoxy molecules, and the hydrophilicity of epoxy-PEG films can be regulated by the content of dispersed PEG to a certain extent.

Although the polymerized epoxy resin contains a large number of hydroxyl groups with relatively large polarity, the hydroxyl groups in the polymerized epoxy molecular chain have relatively large symmetry, which makes the polymerized epoxy resin only weak polarity. When the dispersed PEG content is large enough, the PEG molecule not only reduces the regularity of the aggregated state of the polymerized epoxy molecules but also makes the polymerized epoxy molecules have more hydroxyl groups that are not involved in forming hydrogen bonds, which makes the epoxy-PEG The polarity increases with increasing PEG content. The polarity of epoxy-PEG can be judged by the dielectric constant. As shown in Figure 3-2e, this experiment tested the dielectric constant of epoxy-PEG films at different frequencies. When the PEG content did not exceed 25 wt%, the dielectric constant of epoxy-PEG films did not change much with the increase of PEG content. When the PEG content exceeds 25 wt%, the dielectric constant of epoxy-PEG films increases significantly with the increase of PEG content. As a result, PEG-30 and PEG-40 films showed relatively greater polarity. The dielectric analysis further revealed the

interaction between the PEG molecules and the polymerized epoxy molecules, and the polarity of the epoxy-PEG film showed a relatively large difference before and after the content of dispersed PEG was 30 wt%.

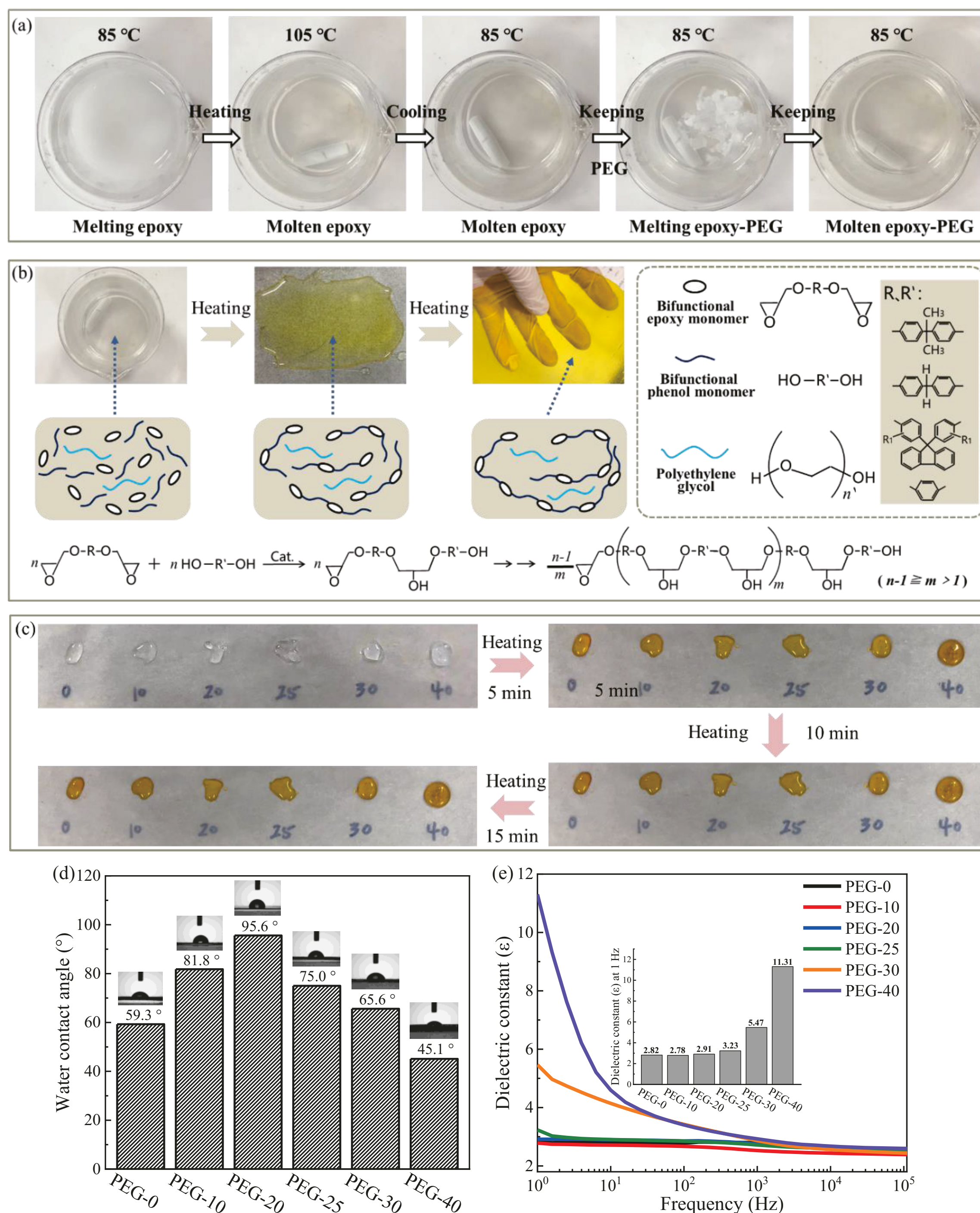

Figure 3-2. (a) Process of the melting for epoxy resin, the dispersion for PEG, and the melting for epoxy-PEG; (b) the polymerization reaction

process of the epoxy molecule and the phenol molecule; (c) the polymerization process of the epoxy-PEG mixture in the oven at 150 °C; (d) water contact angle test result of epoxy-PEG film; (e) impedance test result of epoxy-PEG film.

3.3.2 Thermal analysis of polymerization process

The polymerization of epoxy resins is an exothermic reaction conditioned by temperature and accelerators, during which the epoxy rings open and polymerize with phenol molecules. In the polymerization experiment of pure epoxy resin, the epoxy resin was heated to complete melting, then the accelerator was added at 85 °C, and finally, the polymerization was carried out in an oven at 150 °C. The addition of PEG is an external factor affecting the polymerization reaction to a certain extent. Therefore, in this experiment, all samples of the mixture containing epoxy resin, accelerator and PEG mixed at 85 °C were first collected, and then subjected to thermal analysis from room temperature to 320 °C as shown in Figure 3-3a. Both PEG-0 and PEG-10 mixtures showed obvious exothermic peaks at 80 °C to 160 °C, which were caused by the intense polymerization reaction. The exothermic peak temperature of PEG-0 is around 135 °C, and the exothermic peak temperature of PEG-10 is around 137 °C, which is due to the slightly delayed polymerization reaction of PEG dispersion. PEG-20 and PEG-25 showed significantly flatter

exothermic peaks than PEG-0 and PEG-10, because with the increase of PEG content, not only does the relative content of the epoxy resin in the epoxy-PEG mixture gradually decrease, but also the melting endotherm of PEG melting increases gradually. As the content of PEG continues to increase, the delayed effect of PEG on the polymerization of epoxy resin makes part of the epoxy resin gradually melt due to rapid temperature rise when it is not fully polymerized, so the exothermic peak is extremely insignificant, and there may occur exothermic peaks caused by the oxidation of some epoxy molecules that have not enough time to polymerize with continuous heating. The retardation effect of PEG on epoxy resin polymerization can also be seen in Figure 3-3b, the exothermic peak temperature of the epoxy-PEG mixture increases with the increase of PEG content during the process of heating to 150 °C and then maintaining the temperature for 30 min. In the polymerization experiments, the temperature of epoxy-PEG mixtures of all different PEG contents was first raised to 150 °C and then held for 30 min. The maximum temperature of 150 °C was chosen to avoid the melting and oxidation of insufficiently polymerized epoxy resin caused by excessive temperature. Although PEG has a retarding effect on epoxy resin polymerization, all epoxy-PEG mixtures with different PEG contents reached the exothermic peak within 10 min, and all of them basically completed the polymerization within 20 min.

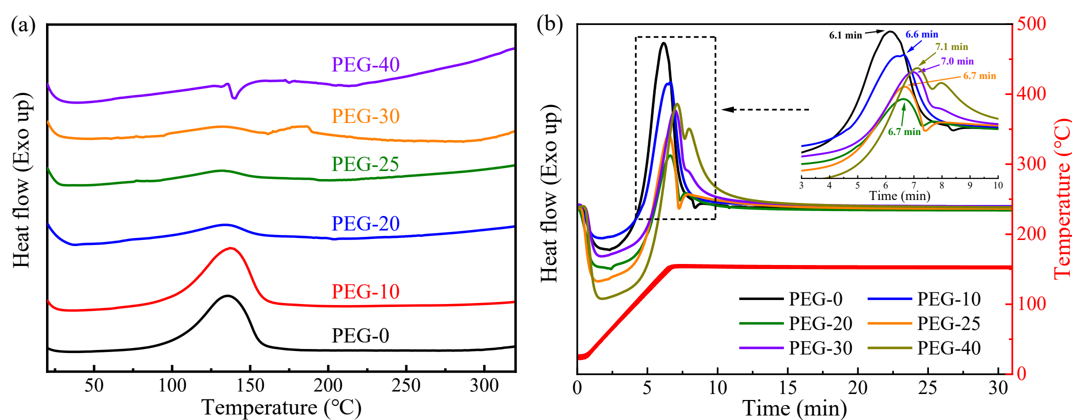

Figure 3-3. (a) DSC test by the process of heating from room temperature to 150 °C, (b) DSC test by the process of heating to 150 °C and then maintaining the temperature for 30 min.

3.3.3 FTIR analysis of thermoplastic epoxy-PEG

Both epoxy resin and PEG have a large number of C-O bonds, and both have hydroxyl groups (the epoxy resin is relatively more), so the epoxy resin and PEG have good compatibility. The functional groups of epoxy resin before and after polymerization and PEG are shown in Figure 3-4a. After the epoxy resin is fully polymerized in an ideal state, the difference from before polymerization is that there is no epoxy group, and the phenolic hydroxyl group on the original phenol is converted into an alcoholic hydroxyl group on the polymerized epoxy molecular chain. Although the phenol group is converted into an aromatic ether group during the polymerization, there is still a lot of R (R')-O bonds in essence. As shown in Figure 3-4b, the FTIR spectrum of the epoxy resin before polymerization showed an obvious epoxy group characteristic peak near

916 cm^{-1}, and the epoxy group characteristic peak disappeared after polymerization. The FTIR spectrum of the epoxy resin before polymerization does not show obvious peaks around 1146 cm^{-1}-1050 cm^{-1}, but the epoxy resin after polymerization and PEG both show characteristic peaks here, which is due to the polymerized epoxy resin has been obtained more C-O bonds in the polymerization. The generation of more C-O bonds also marks the generation of more C-H bonds on saturated C, which can be seen from the difference in the peak intensities at 2870 cm^{-1} in the FTIR spectra of epoxy resins before and after polymerization. Because more C-H bonds on saturated C were generated after polymerization, the polymerized epoxy resin showed a more obvious peak similar to PEG at 2870 cm^{-1}. In addition, due to the difference in the relative number of hydroxyl groups and the difference between phenolic hydroxyl groups and alcoholic hydroxyl groups, the characteristic peaks of hydroxyl groups of epoxy resin and PEG appear around 3370 cm^{-1}, and 3520 cm^{-1}, respectively.

After dispersion into PEG, the peaks at 1100 cm^{-1} and 2870 cm^{-1} of the epoxy-PEG mixture showed differences. As shown in Figure 3-4c, as the PEG content increased, the peaks at 1100 cm^{-1} and 2870 cm^{-1} for the epoxy-PEG mixture became more pronounced, which was due to the dispersion of PEG making the epoxy-PEG mixture have more C-O bonds and C-H bonds on saturated C. In addition, because the epoxy-PEG mixtures with different PEG contents have not been polymerized, there are obvious

epoxy-group characteristic peaks around 916 cm^{-1}. In this experiment, the absorbances of the epoxy-PEG mixtures at 2960 cm^{-1} and 1230 cm^{-1} were used as a reference, and the A_{2870}/A_{2960} values (the ratio of absorbance at 2870 cm^{-1} to 2960 cm^{-1}) and A_{1100}/A_{1230} values (the ratio of absorbance at 1100 cm-1 to 1230 cm^{-1}) of epoxy-PEG mixtures with different PEG contents were calculated respectively to intuitively illustrate the effect of PEG on the chemical structure of epoxy-PEG mixtures. As shown in Figure 3-4d, both the A_{2870}/A_{2960} values and the A_{1100}/A_{1230} values increased nearly linearly with increasing PEG content. This indicates that different contents of PEG are stably dispersed in the epoxy-PEG mixture. The FTIR spectra of the polymerized epoxy-PEG films shown in Figure 3-4e were further analyzed. All the epoxy-PEG films after polymerization did not show the characteristic peak of the epoxy group near 916 cm^{-1}, which indicated that 10 wt%-40 wt% PEG did not reduce the polymerization degree of epoxy resin. It should be noted that PEG does delay the polymerization of epoxy resin, but after heating at 150 °C for 30 min, all epoxy inside epoxy-PEG mixtures with different PEG contents can fully polymerize. In addition, the A_{2870}/A_{2960} values and A_{1100}/A_{1230} values of the polymerized epoxy-PEG film were also calculated in this experiment, and the results are shown in Figure 3-4f. The A_{2870}/A_{2960} and A_{1100}/A_{1230} values of the polymerized epoxy-PEG film also increased almost linearly with the increase of PEG content, which not only indicated that PEG is stably dispersed in the epoxy

resin but also shows that PEG does not occur volatilization and denaturation during the polymerization reaction. This stable, environmentally friendly, and easy-to-operate dispersion of PEG provides a new way for the plasticization and modification of epoxy resins, showing application potential in the fields of flexible films, SMMs, self-healing, and phase change materials.

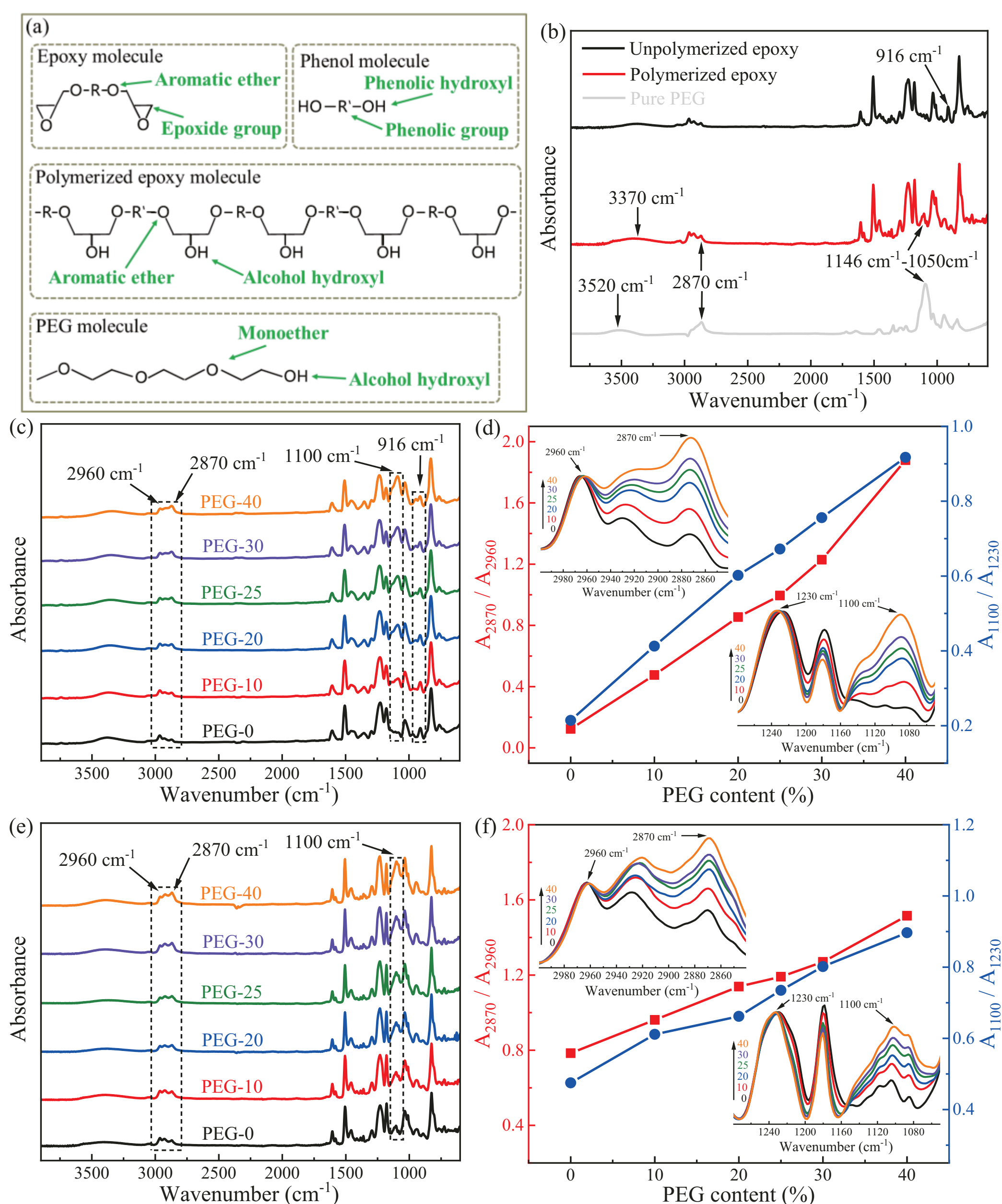

Figure 3-4. (a) The functional groups of unpolymerized epoxy,

polymerized epoxy, and PEG; (b) the FTIR test results of unpolymerized epoxy, polymerized epoxy, and PEG; (c) the FTIR test results of unpolymerized epoxy-PEG mixtures; (d) analysis results of the effect of PEG content on FTIR spectra for unpolymerized epoxy-PEG mixtures; (e) the FTIR test results of polymerized epoxy-PEG films; (f) analysis results of the effect of PEG content on FTIR spectra for polymerized epoxy-PEG films.

3.3.4 Thermal stability analysis of thermoplastic epoxy-PEG

PEG has a low molecular weight, is paraffin-like at room temperature, and has lower thermal stability than epoxy resins. After dispersion into PEG, the stability of the polymerized epoxy-PEG was analyzed by TGA. Figure 3-5a is the thermogravimetric test results of the polymerized epoxy-PEG with different PEG contents. The thermal stability of PEG-0 and PEG-10 was significantly higher. With the increase in PEG content, the thermal stability of the polymerized epoxy-PEG decreased slightly. Nevertheless, the polymerized epoxy-PEGs with different PEG contents all showed excellent thermal stability, and all still maintained a weight loss of less than 3.89% at a high temperature of 300 °C, which indicates that even PEG-40 can meet stable use under the general requirements conditions. After PEG is dispersed into epoxy resin, the hydroxyl groups at both ends can form hydrogen bonds with hydroxyl groups on epoxy molecules, and PEG is

encapsulated between polymerized epoxy molecules with higher molecular weight on the basis of uniform dispersion. That's resulting in that epoxy-PEG exhibiting excellent thermal stability. Figure 3-5b is the DTA curve of epoxy-PEG after polymerization with different PEG contents. It can be found that there is no exothermic peak of oxidation before 350 °C in all curves; after 350 °C, each curve gradually shows an exothermic peak of oxidation, which further proves that PEG can stably exist between polymerized epoxy molecules. The excellent thermal stability of epoxy-PEG further shows its application potential in the fields of heat-stimuli SMMs and heat-repairable polymer materials.

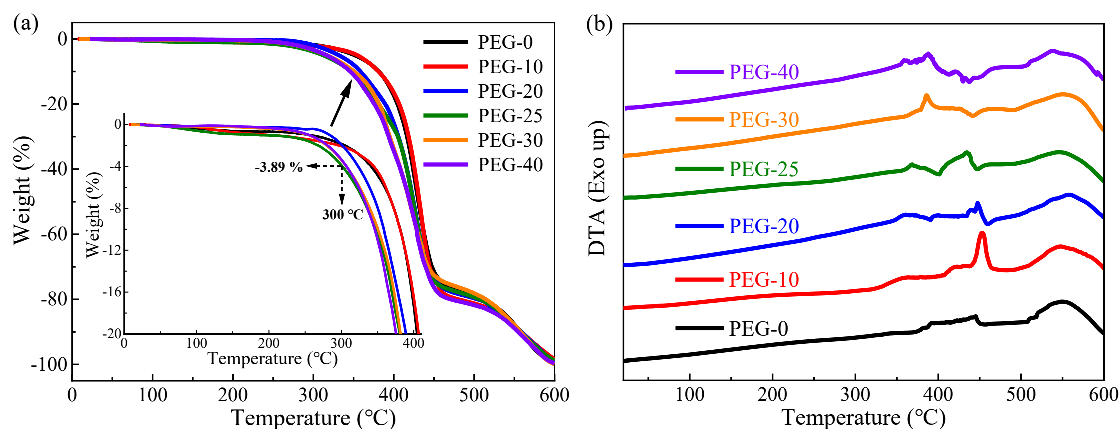

Figure 3-5. (a) Thermogravimetric results of polymerized epoxy-PEG from room temperature to 600 °C, (b) DTA curve of TGA test for polymerized epoxy-PEG.

3.3.5 Mechanical property analysis

The polymerized epoxy resin has a large molecular weight, hydrogen bonds can be formed between molecules, and the molecular chain is

relatively regular, so it has excellent mechanical properties. After dispersing the PEG with a relatively small molecular weight, the epoxy molecular chain in the epoxy-PEG film is relatively reduced, so the mechanical strength is reduced. However, the more flexible PEG can increase the tensile strain to a certain extent. As shown in the stress-strain curve in Figure 3-6a and the statistical results in Figure 3-6b, both the yield stress and the breaking stress of the epoxy-PEG film decreased with the increase of PEG content, and the breaking strain of the epoxy-PEG film increased with the increase of PEG content. In terms of Young's modulus, except for PEG-10, Young's modulus of epoxy-PEG films decreased with the increase of PEG content. The particularity of PEG-10 is due to the weakening of the intermolecular force between the polymerized epoxy molecular chains by PEG. When a small amount of PEG is dispersed, a small amount of PEG will not excessively destroy the regularity of the epoxy molecular chain, and PEG can promote the epoxy molecular chain to be oriented faster in the stretching direction when the epoxy-PEG film is stretched, resulting in an increase in Young's modulus. When the content of PEG is large, the regularity of the epoxy molecular chain is destroyed to a greater extent, and the number of epoxy molecules in the unit area subjected to stress is relatively small when being stretched, resulting in a decrease in Young's modulus. In terms of yield strain, the yield strains of epoxy-PEG films after dispersing PEG are all lower, but the difference is

not significant. It should be emphasized that the yield process of the epoxy-PEG film after dispersing PEG becomes slower, and the difference in the stress-strain curve of PEG-40 before and after the yield point is very small. In addition, Young's modulus, yield stress, yield strain, fracture stress, and fracture strain of each epoxy-PEG film are all listed in Table 3-3. The mechanical strength and flexibility of the epoxy-PEG films prepared in this experiment can be regulated by the content of PEG. With the increase of PEG content, the epoxy-PEG films gradually changed from rigid to flexible. As shown in Figure 3-6c, with the increase of PEG content to 30wt%, PEG-30 can be freely bent at room temperature, showing obvious flexibility, and slowly thinned until breaking during the tensile test, which shows a large breaking strain. Films with different mechanical properties can meet different applications, among which PEG-30 and PEG-40 expand the application of thermoplastic epoxy in flexible smart materials.

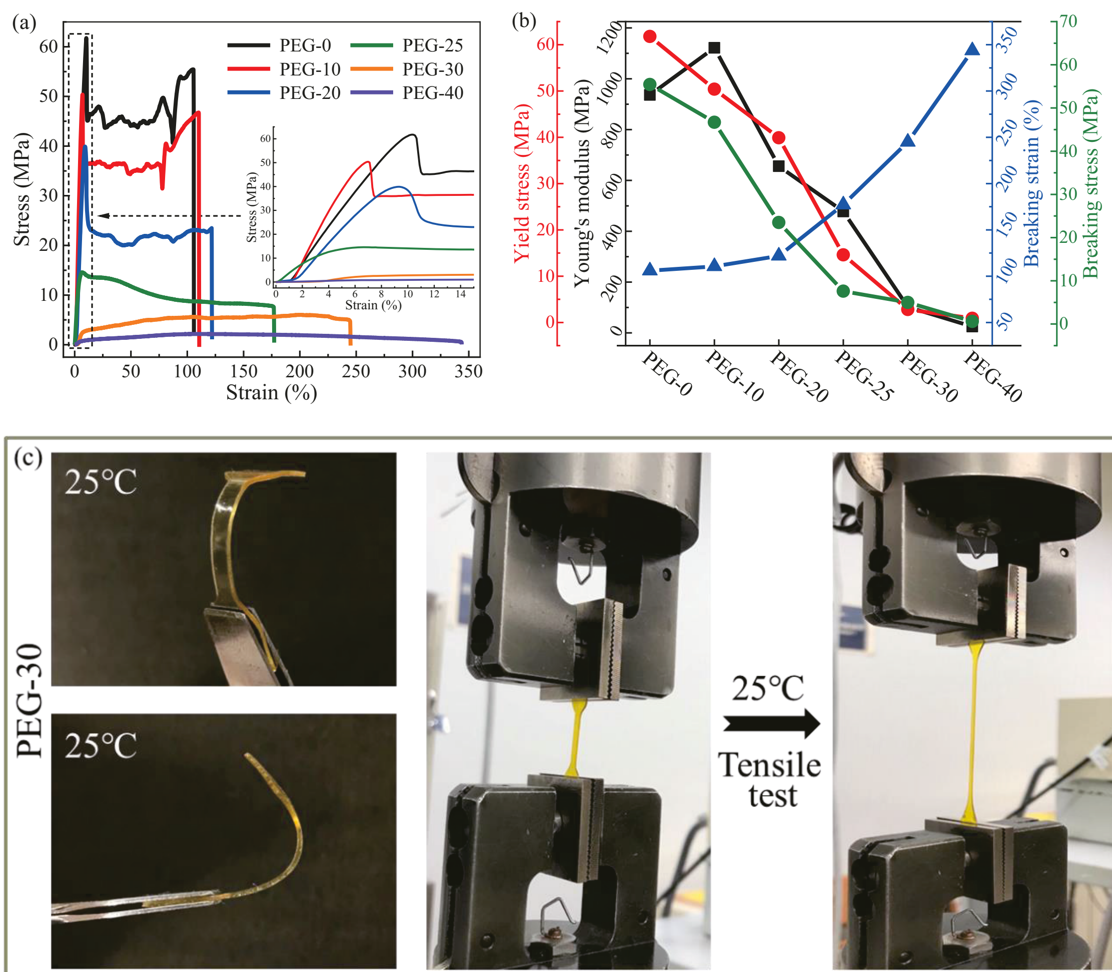

Figure 3-6. (a) Stress-strain curve of epoxy-PEG films, (b) statistical results of stress-strain curves for epoxy-PEG films, (c) bending and tensile test of PEG-30 at room temperature.

Table 3-3. Young's modulus, yield strain, yield stress, breaking strain, and breaking stress.

Samples	Young's modulus (MPa)	Yield Strain (%)	Yield stress (MPa)	Breaking strain (%)	Breaking Stress (MPa)
PEG-0	936.2	9.4	62.0	105.9	55.4
PEG-10	1121.9	6.1	50.5	110.6	46.7
PEG-20	656.0	8.4	40.1	122.0	23.5
PEG-25	477.7	6.2	14.6	177.2	7.6
PEG-30	102.2	-	-	245.0	5.0
PEG-40	24.9	-	-	343.7	0.6

3.3.6 Dynamic mechanical property analysis

In this experiment, a thermoplastic epoxy resin composed of linear macromolecules was generated by the polymerization reaction, and its larger intermolecular force made it's T_g higher. PEG with lower molecular weight has lower T_g, has more active molecular thermal motion at the same temperature than polymerized epoxy resin, and reduces the intermolecular force of polymerized epoxy by blocking the molecular chain of polymerized epoxy. As shown in Figure 3-7a, with the increase of PEG content, the number of PEG molecules between the polymeric epoxy molecular chains increases, so that the intermolecular force of the polymerized epoxy gradually decreased. The temperature-storage modulus curve of the epoxy-PEG film is shown in Figure 3-7b. During the heating process, the PEG molecules first perform the thermal motion, which promotes the thermal motion of the polymerized epoxy molecules, making the storage modulus of epoxy-PEG after adding PEG decreases more rapidly with increasing temperature. Except for PEG-10, the storage modulus at room temperature of epoxy-PEG films decreased with the increase of PEG content. In the tensile test mode of DMA, a relatively small amount of PEG promotes the orientation of the PEG-10 film along the stretching direction on the basis of uniform dispersion, so PEG-10 shows a larger storage modulus at room temperature. However, when the PEG content exceeds 10%, the intermolecular force of the polymerized

epoxy is weakened to a greater extent, resulting in a decrease in the storage modulus at room temperature of the epoxy-PEG film. As shown in Figure 3-7c, due to the effect of PEG on the intermolecular force of the polymerized epoxy, the T_g of each epoxy-PEG film gradually decreased with the increase of PEG content, and the T_g of the PEG-40 film with the largest PEG content had decreased to around room temperature. Statistics of storage modulus (at 25 °C) and T_g for epoxy-PEG films are shown in Table 3-4. The T_g of the epoxy-PEG film is regulated by dispersing PEG. The prepared epoxy-PEG with higher T_g can be used in high-temperature applications, while the epoxy-PEG with lower T_g can be used in the field of flexible materials.

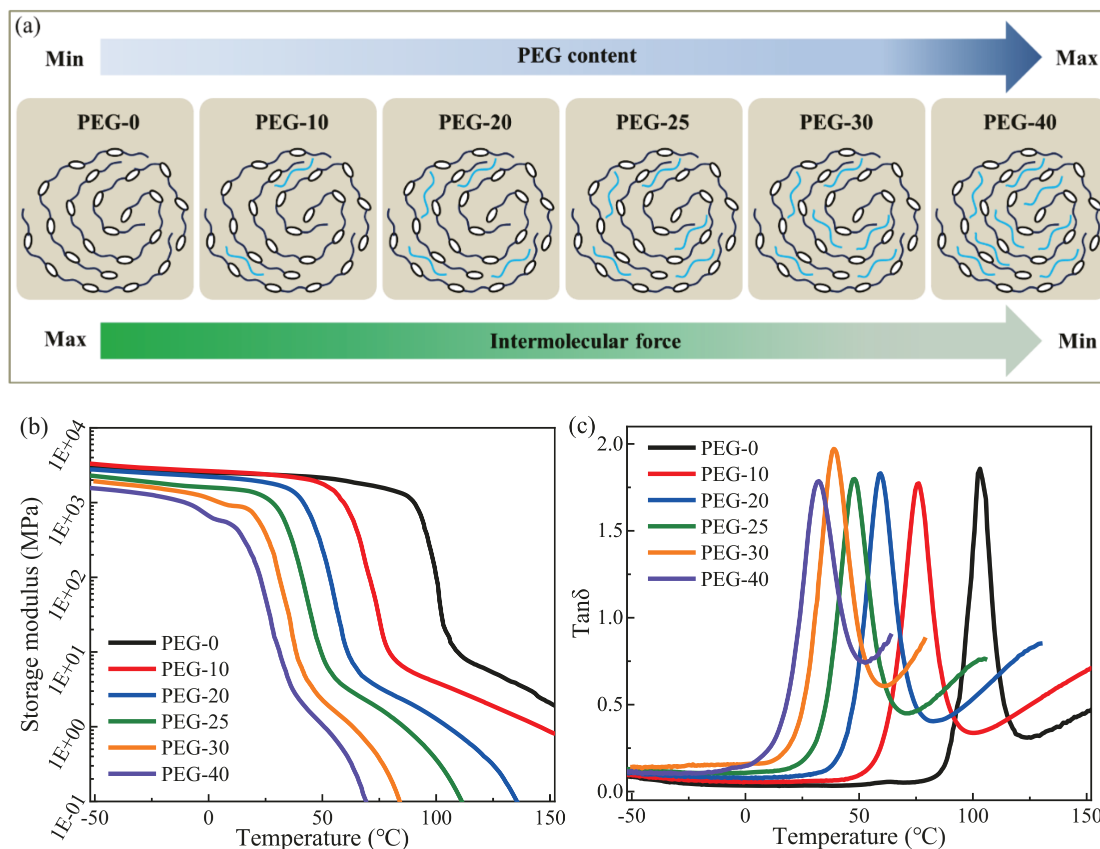

Figure 3-7. (a) Influence of PEG on intermolecular force of polymerized

epoxy, (b) temperature-storage modulus curves and (c) temperature-Tanδ curves of epoxy-PEG films by DMA.

Table 3-4. Storage modulus (at 25 °C) and T_g analyzed by DMA.

Samples	PEG-0	PEG-10	PEG-20	PEG-25	PEG-30	PEG-40
Storage modulus (MPa)	2392.7	2415.1	1890.5	1243.1	406.3	39.7
T_g (℃)	104.7	75.9	59.3	48.2	39.0	32.2

3.3.7 Shape memory properties

In the process of heating from room temperature to the T_g of epoxy-PEG film, the internal molecular chain of epoxy-PEG gradually undergoes thermal motion, which makes the epoxy-PEG film more susceptible to external stretching. When the temperature is near T_g, a temporary shape is obtained by stretching the epoxy-PEG film; but at this time, the internal molecular chain of epoxy-PEG is in an active thermal motion state, and the temporary shape needs to be maintained by external stretching. In order to fix the epoxy-PEG film into a temporary shape, it is necessary to rapidly transfer the epoxy-PEG film from an environment of T_g temperature to a temperature environment below the T_g range on the basis of maintaining external stretching, and at the external stretching was terminated after cooling to environment temperature. In the temperature below the T_g range, the internal molecular chains of epoxy-PEG are “frozen”, so the epoxy-PEG film can be kept in a temporary shape. When the epoxy-PEG film was re-transferred to an environment with a temperature near T_g, the originally

“frozen” molecular chains gradually gained the ability to move, and the thermal motion gradually became active as the temperature increased to near T_g. The originally stretched molecular chains begin to gradually recover to the initial state by active molecular thermal motion, which makes the epoxy-PEG film show shape recovery on a macroscopic scale. The shape memory process of epoxy-PEG is shown in Figure 3-8a. The shape fixation and shape recovery of the epoxy-PEG film can be achieved by external stimuli to meet the demand for different shapes during application.

The T_g of polymerized epoxy as high as 100.4 °C also limits the scope of application to a certain extent. Through the dispersion of PEG, the T_g of epoxy-PEG can be adjusted according to the content of PEG, which further enables the regulation of heat-stimuli temperature for epoxy-PEG shape memory, which provides a new method for the more flexible application of SMMs. As shown in Figure 3-8b, in this experiment, different heat-stimuli temperatures were set according to the T_g of each epoxy-PEG, and each thermal stimulation temperature was slightly higher than its T_g temperature. Figures from 3-8c to 3-8g are shape memory test results of PEG-0 to PEG-30 films. The strain was monitored by setting temperature and external stress conditions to finally achieve the purpose of evaluating the shape memory performance of each epoxy-PEG film. By observation, it can be found that all epoxy-PEG films can produce shape memory recovery at

their respective heat-stimuli temperatures, and all exhibit excellent shape memory effects in the second cycle, with shape recovery rates ranging from 92% to 100%. After training in the first cycle, more molecular chains oriented along the stretching direction were generated inside the epoxy-PEG film, which made the epoxy-PEG film exhibit a higher recovery rate in the second cycle. As shown in Figure 3-8f, the recovery rate of the first cycle is only 66.8%, but the recovery trend is still large before being stretched again, so the relatively small recovery rate of the first cycle can be solved by increasing the recovery time. In terms of fixation rate, each epoxy-PEG membrane exhibited excellent fixation ability in both cycles, and the fixation rate remained between 91% and 100%. The shape fixation rate and shape recovery rate of each epoxy-PEG film within two cycles are summarized in Table 3-5. In addition, the T_g near room temperature makes PEG-40 difficult to fix in shape memory process by a static thermomechanical apparatus, so static thermomechanical testing of PEG-40 films was not performed. In conclusion, the test results of epoxy-PEG films all showed excellent shape memory performance, and the shape memory function under different heat-stimuli temperature conditions was realized through the dispersion of PEG, which expanded the application scope of epoxy resin with shape memory function.

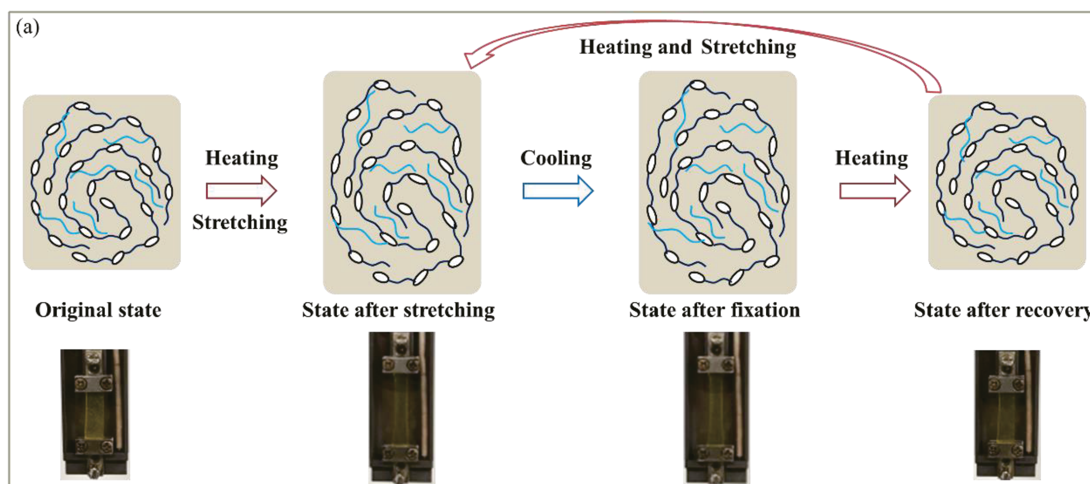

Figure 3-8. (a) Shape memory process of epoxy-PEG films, (b) T_g and shape memory stimulation temperature of epoxy-PEG films, (c) shape

memory test result of PEG-0 film, (d) PEG-10 film shape memory test results, (e) PEG-20 film shape memory test results, (f) PEG-25 film shape memory test results, (g) PEG-30 film shape memory test results.

Table 3-5. Statistics of shape fixation rate (R_f) and recovery rate (R_r) of epoxy-PEG films.

Sample	PEG-0		PEG-10		PEG-20		PEG-25		PEG-30	
	R_f (%)	R_r (%)	R_f (%)	R_r (%)	R_f (%)	R_r (%)	R_f (%)	R_r (%)	R_f (%)	R_r (%)
Cycle-1	97.1	82.8	92.0	72.3	94.6	98.1	96.0	69.8	98.5	82.0
Cycle-2	97.4	96.0	91.9	93.5	95.5	99.0	96.4	92.6	99.1	98.1

3.3.8 Observation for shape memory and healable properties

The epoxy-PEG films changed from rigid to flexible before and after PEG content of 25%. Select representative PEG-25 film with lower flexibility and PEG-30 film with better flexibility as experimental objects to observe their shape memory properties more intuitively. Firstly, the shape of epoxy-PEG was changed by heating and stretching (Perform PEG-25 in 60℃ and PEG-30 in 45℃), and then the temporary shape was fixed by cooling in room temperature, and finally, the shape recovery of heat-stimuli for epoxy-PEG was observed by heating again. As shown in Figures 3-9a and 3-9b, both PEG-25 and PEG-30 film were able to switch between original and temporary shapes by heat-stimuli. Although PEG-25 film is less flexible, it can be changed into a relatively complex temporary shape by heating and external force, and basically recovered by heat-stimuli in about 55 s. It is worth noting that the shape memory heat-stimuli

temperature of PEG-30 is close to that of human skin due to its lower T_g. PEG-30 film can recover shape in response to human skin temperature, and because of its hydrophilicity and flexibility, it has a high degree of adhesion to human skin, which greatly expands the application of thermoplastic epoxies, such as flexible smart materials. Compared with PEG-30, PEG-40 has a lower T_g and greater flexibility, which is difficult to perform cold-fixation at room temperature, but a T_g close to room temperature allows it to undergo shape recovery at room temperature. In this experiment, PEG-40 was changed to a temporary shape at room temperature and then performed cold-fixation on the surface of the ice. As shown in Figure 3-9c, the PEG-40 film fixed in the temporary shape was rapidly transferred to room temperature, and the PEG-40 film almost completely recovered to its original shape in about 75 s. Epoxy-PEG can keep exhibit excellent shape memory properties through successively decreasing heat-stimuli temperatures with increasing PEG content. Epoxy-PEG with different PEG content is suitable for applications with different temperature requirements because of different heat-stimuli temperatures and shows greater application potential in the field of SMMs.

The pure epoxy resin after polymerization has a high modulus and high flow temperature. After dispersing PEG, PEG with a smaller molecular weight can promote the mobility of polymerized epoxy molecules during the heating process. After PEG is dispersed, PEG with a smaller molecular

weight can promote the mobility of polymerized epoxy molecules during the heating process, which is accompanied by the breaking and reorganization of hydrogen bonds (Figure 3-9d) between polymerized epoxy molecules and between polymerized epoxy molecules and PEG molecules. When epoxy-PEG is destroyed, the healing of epoxy-PEG can theoretically be achieved by heating. However, when the PEG content is low, this healing facilitated by the flow of PEG molecules is difficult to achieve. In this experiment, PEG-30 and PEG-40 were selected for healing and adhesion experiments. The unpolymerized epoxy-PEG mixture is colloidal state and can be processed into specific shapes by specific molds. Firstly, the unpolymerized PEG-30 and PEG-40 colloids were poured into a specific mold, and their specific shape of epoxy-PEG was obtained by polymerization, and then a wound was drawn from the specific shape of PEG-30 and PEG-40 with a metal knife in the room temperature; finally, The healing process of epoxy-PEG of specific shape was observed by heating as shown in Figures 3-9e. It is clear that PEG-30 wounds require higher temperatures to achieve healing than PEG-40 wounds. PEG-30 and PEG-40 can achieve excellently healable and adhesion ability at 60 °C for 3h and room temperature for 8h, respectively on the basis of not changing the overall shape. Although the repaired samples all still had the imprint of the scar, they could change shape without showing a defect. In conclusion, PEG with greater fluidity promotes the flow of polymerized epoxy

molecules, and finally achieves the healing and adhesion of epoxy-PEG at a lower temperature through dynamic hydrogen bonding, which expands the application potential of epoxy-PEG in flexible smart materials.

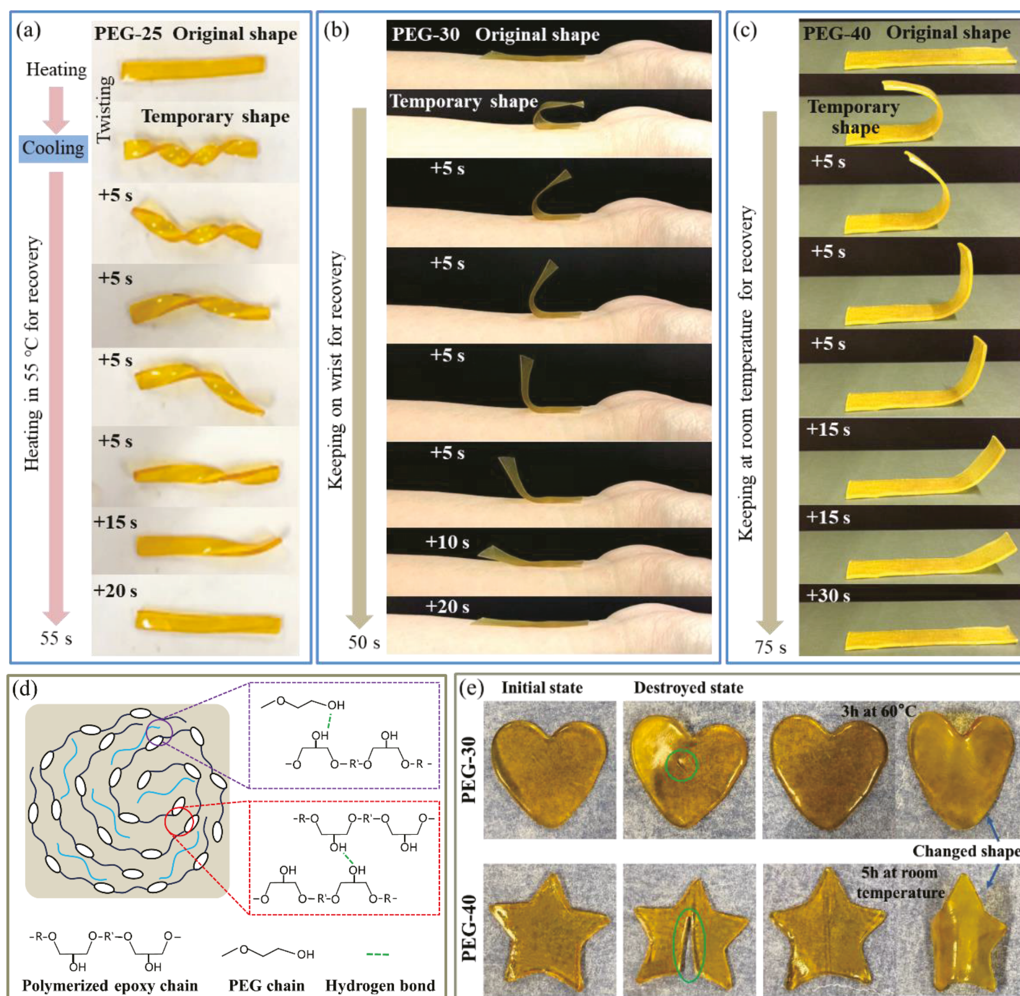

Figure 3-9. (a) SMP observation of PEG-25, (b) shape memory responses of PEG-30 to heat-stimuli based on human skin temperature, (c) shape memory responses of PEG-40 in room temperature, (d) hydrogen bonds of epoxy-PEG, (e) healing and adhesion observations for PEG-30 and PEG-40.

3.4 Conclusions

Through the uniform, stable, and environmentally friendly dispersion of PEG, the mechanical and thermal properties of thermoplastic epoxy were successfully regulated, and the shape memory epoxy-PEG films ranging from rigid to flexible were prepared. Thermal analysis and FTIR analysis showed that epoxy-PEG with different PEG contents were fully polymerized. FTIR analysis also confirmed the distribution of PEG molecules among the polymerized epoxy molecules. Thermal stability analysis showed that PEG did not significantly reduce the thermal stability of epoxy-PEG, and the weight loss at 300 °C remained within 3.89%. Tensile analysis showed that with the increase of PEG content, the epoxy-PEG film gradually changed from a rigid film with high breaking stress and low breaking stress to a gel-like film with low breaking stress and high breaking stress. Thermomechanical analysis showed that the T_g of epoxy-PEG films decreased sequentially with the increase of PEG content. Shape memory analysis showed that epoxy-PEG with different PEG contents all had recovery rates between 92% and 100%, which could be switched between original and temporary shapes by respective stimuli-temperature. In addition, PEG-40 also exhibits excellent healable and adhesive properties. The regulation of thermoplastic epoxy by PEG makes thermoplastic epoxy show greater application potential in the field of shape memory and flexible smart materials.

References

1. Kim, M. T., Rhee, K. Y., Lee, J. H., Hui, D. & Lau, A. K. T. Property enhancement of a carbon fiber/epoxy composite by using carbon nanotubes. Composites Part B: Engineering 42, 1257–1261 (2011).
2. Tang, L. et al. Functionalized glass fibers cloth/spherical BN fillers/epoxy laminated composites with excellent thermal conductivities and electrical insulation properties. Composites Communications 16, 5–10 (2019).
3. Wazarkar, K., Kathalewar, M. & Sabnis, A. Development of epoxy-urethane hybrid coatings via non-isocyanate route. European Polymer Journal 84, 812–827 (2016).
4. Gao, W., Bie, M., Liu, F., Chang, P. & Quan, Y. Self-Healable and Reprocessable Polysulfide Sealants Prepared from Liquid Polysulfide Oligomer and Epoxy Resin. ACS Appl. Mater. Interfaces 9, 15798–15808 (2017).
5. Hardis, R., Jessop, J. L. P., Peters, F. E. & Kessler, M. R. Cure kinetics characterization and monitoring of an epoxy resin using DSC, Raman spectroscopy, and DEA. Composites Part A: Applied Science and Manufacturing 49, 100–108 (2013).
6. Yang, W., Xiong, J., Wu, L. & Du, Y. Methods for enhancing the thermal properties of epoxy matrix composites using 3D network structures. Composites Communications 12, 14–20 (2019).
7. Rybak, A. & Nieroda, J. Aluminosilicate-epoxy resin composite as novel

material for electrical insulation with enhanced mechanical properties and improved thermal conductivity. Polym. Compos. 40, 3182–3188 (2019).

8. Matinlinna, J. P., Lung, C. Y. K. & Tsoi, J. K. H. Silane adhesion mechanism in dental applications and surface treatments: A review. Dental Materials 34, 13–28 (2018).

9. Ma, Y., Navarro, C. A., Williams, T. J. & Nutt, S. R. Recovery and reuse of acid digested amine/epoxy-based composite matrices. Polymer Degradation and Stability 175, 109125 (2020).

10. Oliveux, G., Bailleul, J.-L., Gillet, A., Mantaux, O. & Leeke, G. A. Recovery and reuse of discontinuous carbon fibres by solvolysis: Realignment and properties of remanufactured materials. Composites Science and Technology 139, 99–108 (2017).

11. Jouyandeh, M. et al. Curing epoxy with polyethylene glycol (PEG) surface-functionalized NixFe3-xO4magnetic nanoparticles. Progress in Organic Coatings 136, 105250 (2019).

12. Vijayan P., P., Puglia, D., Al-Maadeed, M. A. S. A., Kenny, Jose. M. & Thomas, S. Elastomer/thermoplastic modified epoxy nanocomposites: The hybrid effect of 'micro' and 'nano' scale. Materials Science and Engineering: R: Reports 116, 1–29 (2017).

13. Taniguchi, N., Nishiwaki, T., Hirayama, N., Nishida, H. & Kawada, H. Dynamic tensile properties of carbon fiber composite based on

thermoplastic epoxy resin loaded in matrix-dominant directions. Composites Science and Technology 69, 207–213 (2009).

14. Deng, S., Djukic, L., Paton, R. & Ye, L. Thermoplastic–epoxy interactions and their potential applications in joining composite structures – A review. Composites Part A: Applied Science and Manufacturing 68, 121–132 (2015).

15. Luo, L., Zhang, F. & Leng, J. Shape Memory Epoxy Resin and Its Composites: From Materials to Applications. Research 2022, 1–25 (2022).

16. School of Chemical Engineering and Technology, Harbin Institute of Technology, Harbin 150001, China et al. Deployment Analysis of Aramid Fiber Reinforced Shape-Memory Epoxy Resin Composites. Eng. Sci. (2020) doi:10.30919/es8d1120.

17. Squeo, E. A. & Quadrini, F. Shape memory epoxy foams by solid-state foaming. Smart Mater. Struct. 19, 105002 (2010).

18. Liu, T. et al. Eugenol-Derived Biobased Epoxy: Shape Memory, Repairing, and Recyclability. Macromolecules 50, 8588–8597 (2017).

19. Zhang, F. et al. Thermosetting epoxy reinforced shape memory composite microfiber membranes: Fabrication, structure and properties. Composites Part A: Applied Science and Manufacturing 76, 54–61 (2015).

20. Mohd Jani, J., Leary, M., Subic, A. & Gibson, M. A. A review of shape memory alloy research, applications and opportunities. Materials & Design (1980-2015) 56, 1078–1113 (2014).

21. Lei, M., Chen, Z., Lu, H. & Yu, K. Recent progress in shape memory polymer composites: methods, properties, applications and prospects. Nanotechnology Reviews 8, 327–351 (2019).
22. Li, F., Liu, Y. & Leng, J. Progress of shape memory polymers and their composites in aerospace applications. Smart Mater. Struct. 28, 103003 (2019).
23. Liu, J. A.-C., Gillen, J. H., Mishra, S. R., Evans, B. A. & Tracy, J. B. Photothermally and magnetically controlled reconfiguration of polymer composites for soft robotics. Sci. Adv. 5, eaaw2897 (2019).
24. Zhao, W., Liu, L., Zhang, F., Leng, J. & Liu, Y. Shape memory polymers and their composites in biomedical applications. Materials Science and Engineering: C 97, 864–883 (2019).
25. Yi, H. et al. Ultra-Adaptable and Wearable Photonic Skin Based on a Shape-Memory, Responsive Cellulose Derivative. Adv. Funct. Mater. 29, 1902720 (2019).
26. Zhu, S. et al. Modulating electromagnetic interference shielding performance of ultra-lightweight composite foams through shape memory function. Composites Part B: Engineering 204, 108497 (2021).
27. Xia, Y., He, Y., Zhang, F., Liu, Y. & Leng, J. A Review of Shape Memory Polymers and Composites: Mechanisms, Materials, and Applications. Adv. Mater. 33, 2000713 (2021).
28. Chen, X. et al. Harnessing 4D Printing Bioscaffolds for Advanced

Orthopedics. Small 2106824 (2022) doi:10.1002/smll.202106824.

29. Guan, X. et al. Flexible energy harvester based on aligned PZT/SMPU nanofibers and shape memory effect for curved sensors. Composites Part B: Engineering 197, 108169 (2020).

30. Cui, Y., Li, D., Gong, C. & Chang, C. Bioinspired Shape Memory Hydrogel Artificial Muscles Driven by Solvents. ACS Nano 15, 13712–13720 (2021).

31. Kong, D., Li, J., Guo, A., Zhang, X. & Xiao, X. Self-healing high temperature shape memory polymer. European Polymer Journal 120, 109279 (2019).

32. Panahi-Sarmad, M. et al. Programing polyurethane with rational surface-modified graphene platelets for shape memory actuators and dielectric elastomer generators. European Polymer Journal 133, 109745 (2020).

33. Santhosh Kumar, K. S., Biju, R. & Reghunadhan Nair, C. P. Progress in shape memory epoxy resins. Reactive and Functional Polymers 73, 421–430 (2013).

34. Paluvai, N. R., Mohanty, S. & Nayak, S. K. Synthesis and Modifications of Epoxy Resins and Their Composites: A Review. Polymer-Plastics Technology and Engineering 53, 1723–1758 (2014).

35. Bazrgari, D. et al. Mechanical properties and tribological performance of epoxy/Al2O3 nanocomposite. Ceramics International 44, 1220–1224 (2018).

36. Behl, M., Razzaq, M. Y. & Lendlein, A. Multifunctional Shape-Memory Polymers. Adv. Mater. 22, 3388–3410 (2010).
37. Fan, P. et al. Stress relaxation properties of an epoxy-based shape-memory polymer considering temperature influence: experimental investigation and constitutive modeling. Mech Time-Depend Mater 24, 265–284 (2020).
38. Guo, Y. et al. Shape memory epoxy composites with high mechanical performance manufactured by multi-material direct ink writing. Composites Part A: Applied Science and Manufacturing 135, 105903 (2020).
39. Zhou, J. et al. A facile method to fabricate polyurethane based graphene foams/epoxy/carbon nanotubes composite for electro-active shape memory application. Composites Part A: Applied Science and Manufacturing 91, 292–300 (2016).
40. Li, Y. et al. Combined light- and heat-induced shape memory behavior of anthracene-based epoxy elastomers. Sci Rep 10, 20214 (2020).
41. Chen, H. et al. Flexible nanopositioning actuators based on functional nanocomposites. Composites Science and Technology 186, 107937 (2020).
42. Zhang, P. & Li, G. Healing-on-demand composites based on polymer artificial muscle. Polymer 64, 29–38 (2015).
43. Li, F. et al. Bending shape recovery of unidirectional carbon fiber reinforced epoxy-based shape memory polymer composites. Composites

Part A: Applied Science and Manufacturing 116, 169–179 (2019).
44. Kumar Patel, K. & Purohit, R. Future Prospects of shape memory polymer nano-composite and epoxy based shape memory polymer- A review. Materials Today: Proceedings 5, 20193–20200 (2018).
45. Lu, L., Fan, J. & Li, G. Intrinsic healable and recyclable thermoset epoxy based on shape memory effect and transesterification reaction. Polymer 105, 10–18 (2016).

Chapter 4: Heat-stimuli controllable shape memory epoxy-PEG filaments

4.1 Introduction

Shape memory polymers (SMPs), as intelligent shape-memory materials, can respond to stimuli from external conditions such as heat [1], electricity [2], light [3], magnetism [4], and humidity [5]. Compared with shape memory alloys, SMPs have the advantages of flexibility, lightweight, easy processing, and biocompatibility [6]. With the continuous exploration of SMPs functions, SMPs play an important role in actuation [7], self-healing [8], composite [9], and flexible smart materials [10], as well as shown significant potential in applications, such as aerospace [11], artificial intelligence [12], and biomedicine [13].

Epoxy resin is a common polymer material used in coatings [14], adhesives [15], and composite materials [16]. The more commonly used epoxy resin is thermosetting, but there are drawbacks in reprocessing and recycling that limit its application range [17]. Compared with thermosetting epoxy resin, thermoplastic epoxy resin has the characteristics of melt reprocessing and recycling, allowing it to be used in a wider range of applications [18]. Epoxy resin has also been widely developed as a SMPs in the form of film and foam because of its excellent

mechanical strength and dimensional stability [19–22]; however, the thermoplastic shape memory epoxy resin is rarely reported. Unlike thermosetting SMPs, thermoplastic SMPs can be converted into fibrous shape memory materials (SMMs) through thermomechanical drawing and textile processing [23–25]. Recently, the application of fibrous SMMs in artificial muscles and smart textiles has become one of the research hotspots [26–28]. The molecular chain inside the fiber has a higher axial orientation rate and can be further increased by stretching [29,30]. The highly axially oriented molecular chain makes the fiber material has excellent mechanical properties and high actuation capability [31,32].

The controllable glass transition temperature (T_g) of temperature-stimuli SMPs, can allow the material to adapt to more temperature-environment requirements [33,34]. Polyethylene glycol (PEG) has excellent compatibility with many polymers and is widely used in biomedicine, cosmetics, and textiles [35–38]. PEG with lower molecular weight can improve the plasticity of the polymer materials and the spinnability of polymers during the spinning process [39,40]. The T_g of the polymer materials can also be adjusted by adding PEG[41]. However, the thermal stability of PEG-doped polymer materials has been reduced, and it also influences mechanical strength, limiting the application range of PEG-doped polymers [42–44].

Based on the research results of thermal and mechanical properties of thermoplastic epoxy regulated by PEG in Chapter 3, this chapter describes shape memory thermoplastic TEP–PEG filaments with heat-stimuli controllability of shape memory function. The dispersion of PEG in unpolymerized epoxy resin (UEP) is performed in a molten state, and after adding accelerator, a uniform PEG-modified thermoplastic epoxy (TEP–PEG) is obtained through the polymerization reaction of UEP. PEG controls T_g and melts spinning temperature of TEP-PEGs, resulting in shape memory TEP–PEG filaments prepared with controllable spinning temperature, which also have controllable stimuli temperature. By modifying the PEG, TEP–PEG filaments have a higher Young's modulus as the TEP–PEG spinning effect improves. Furthermore, all TEP–PEG filaments with different PEG content have excellent shape memory effects with higher shape fixation rate and recovery stress, indicating greater application prospects in the fields of thermal actuation, smart textiles, and so on.

4.2 Materials and Methods

4.2.1 Materials

The UEP of model XNR6850A and accelerator (aromatic phosphoric acid ester) of model XNH6850B were provided by Nagase Chemical Industry Co., Ltd. (Japan). UEP is a white two-component liquid composed

of bifunctional epoxy and phenol in a 1:1 functional group ratio. PEG with a molecular weight of 1000 was provided by Wako Pure Chemical Industries (Japan). The chemical structures of bifunctional epoxy, bifunctional phenol, and PEG are shown in Figure 4-1.

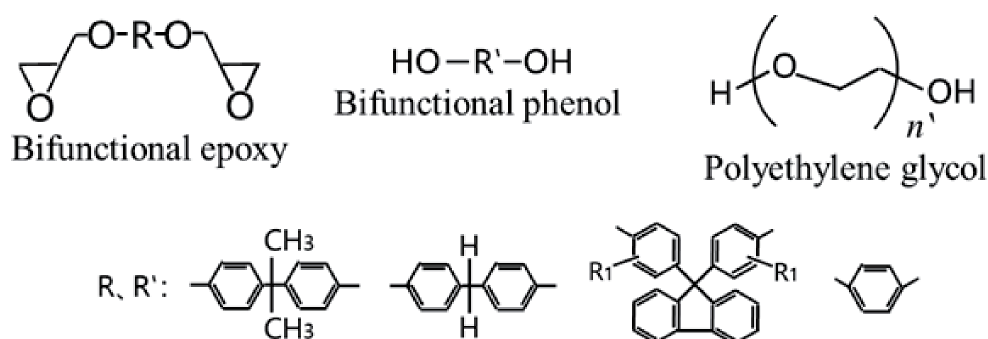

Figure 4-1. Chemical structures of bifunctional epoxy, bifunctional phenol, and PEG.

4.2.2 Fabrication of TEP–PEG pellets and TEP–PEG filaments

Figure 4-2a shows the fabrication process of TEP–PEG pellets. A beaker containing 12 g of XNR6850A (UEP) was weighed and was placed on a hot plate set at 165 °C. When the temperature inside the beaker reached 85 °C, turned on the stirrer of the hot plate. When the temperature inside the beaker was heated to approximately 105 °C, XNR6850A became transparent, then slowly lowered the temperature of the hot plate. When the temperature inside the beaker dropped to 85 °C, a certain amount of PEG was added while stirring. Continue to maintain the temperature inside the beaker at 85 °C, when the mixture became transparent again, poured out a portion of the mixture (after melt mixing of UEP and PEG) for later testing,

and then added 2 wt% XNH6850B (accelerator) to the remaining mixture while stirring. After continued stirring for 3 min, poured out a portion of the mixture (after the addition of accelerator) for later testing, and heated the remaining mixture in a drying oven at 150 °C for 30 min before cutting it into pellets (Figure 4-2b). TEP–PEG (TEP–PEG0, TEP–PEG5, TEP–PEG10, and TEP–PEG15) pellets with PEG content of 0 wt%, 5 wt%, 10 wt%, and 15 wt% were prepared for the next melt processing.

Figure 4-2c shows that a twin-screw micro pulverizer (15 ml; DSM Xplore, Netherlands) and supporting equipment were used to prepare the TEP–PEG pellets for melt-drawing into TEP–PEG filament. The spinning temperatures for TEP–PEG0, TEP–PEG5, TEP–PEG10, and TEP–PEG15 pellets were 300 °C, 280 °C, 250 °C, and 220 °C, respectively. The extrusion rate was set to 10 r/min, and drawing was performed at room temperature with a winding rate of 140 r/min, the spinneret diameter was 0.5 mm, and the spinning distance was 90 cm. The continuously collected TEP–PEG filaments and their average diameters are shown in Figures 4-2d and 4-2e, respectively. The names of all samples used for testing in this study along with their composition and formulation are shown in Table 4-1.

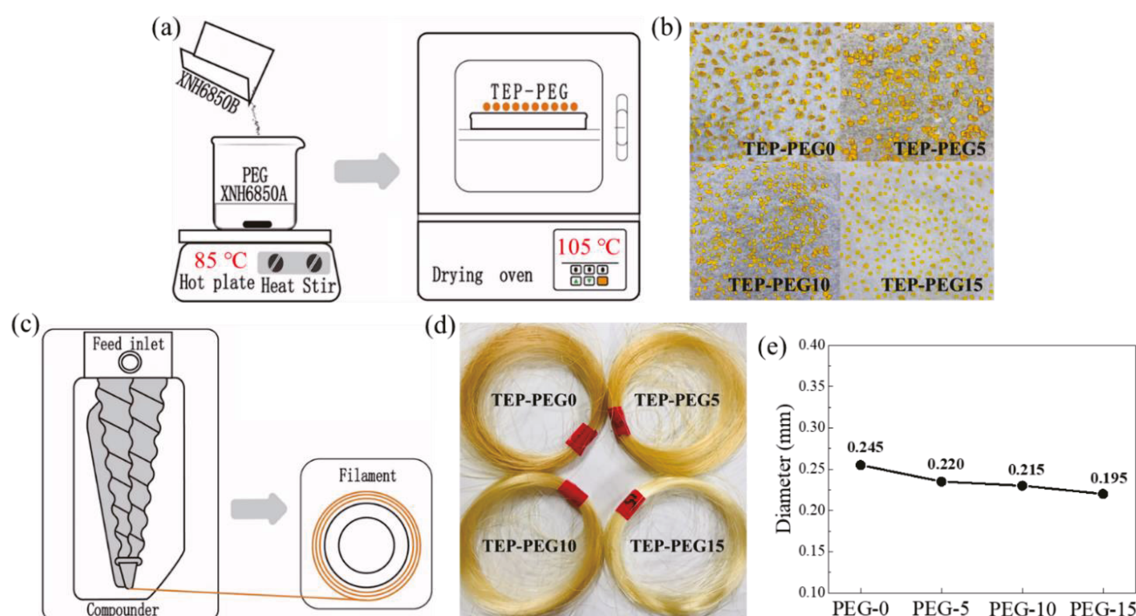

Figure 4-2. (a) Schematic illustrating the fabrication process and (b) photographs of TEP–PEG pellets, (c) schematic illustrating the fabrication process, (d) photographs and (e) average diameters of TEP–PEG filaments.

Table 4-1. The names of the samples used for subsequent testing in this study along with their composition and formulation.

Samples	**UEP/PEG 100/0**	**UEP/PEG 100/5**	**UEP/PEG 100/10**	**UEP/PEG 100/15**
Mixtures (After melt mixing)	UEP-PEG0 (UEP)	UEP-PEG5	UEP-PEG10	UEP-PEG15
Pellets (After polymerization)	TEP-PEG0 (PEP)	TEP-PEG5	TEP-PEG10	TEP-PEG15
Filaments (After spinning)	TEP-PEG0	TEP-PEG5	TEP-PEG10	TEP-PEG15

4.2.3 Chemical structure analysis by FTIR

The chemical structure was analyzed using Fourier transform infrared (FTIR) spectroscopy. The FTIR spectra were measured on a Nicolet 5700 attenuated total reflection FTIR (ATR-FTIR) instrument (Thermo Electron

Corp., USA) with a resolution of 4 cm^{-1}.

4.2.4 Thermal analysis

A Thermo plus EVO2 DSCvesta (Rigaku) was used for differential scanning calorimetry (DSC) analysis. The measurements were performed at a heating rate of 10 °C/min in atmospheric air. The temperature of the mixture of UEP and PEG was raised from 25 °C to 150 °C, which was the temperature of the polymerization reaction for UEP, and then maintained at this temperature for 30 min. The temperature of the TEP–PEG pellets and filaments was raised from 25 °C to 140 °C with a heating rate of 10 °C/min.

A Rigaku Thermo plus TG8120 was used for Thermogravimetric analysis (TGA). The measurements were performed at a heating rate of 20 °C/min in atmospheric air. The testing temperature of TEP–PEG filaments was increased from room temperature to 500 °C. Additionally, filaments of TEP–PEG0, TEP–PEG5, TEP–PEG10, and TEP–PEG15 were tested, in which the temperature was raised from room temperature to 300 °C, 280 °C, 250 °C, and 220 °C, respectively, which is individually held for 30 min.

4.2.5 Tensile and dynamic mechanical analysis

A multi-purpose tensile tester (RTC1250A, A&D Company, Ltd, Japan)

was used for tensile tests at room temperature. All samples with a length of 20 mm were stretched with a speed of 10 mm/min.

A dynamic mechanical analyzer (DMA, ITK-DVA225, Japan) was used to investigate dynamic mechanical properties. All samples were tested in the tensile mode at a constant heating rate of 10 °C/min and an oscillation frequency of 10 Hz. The test temperature of all samples was raised from room temperature to 150 °C. The test length of all samples is 10 mm.

4.2.6 Shape memory experiments

A thermomechanical analyzer (TMA/SS6100, Hitachi High-Tech Science Corp., Japan) was used to measure the shrinkage strain, tensile strain, recovery strain, and recovery stress (S_r) of the shape memory process. The test processes are shown in Figure 4-3. The shrinkage strain of heat-shrinkage in the shape memory process, as shown in P_1, was tested by increasing the temperature from room temperature to its shape memory stimuli temperature (T_s) of the filament, which is slightly higher than its T_g. After testing the shrinkage strain, perform heat-stretching at T_s as shown in P_1-P_2 to test the tensile strain in the shape memory process.

The test of recovery strain in the shape memory process is as follows (P_1-P_2-P_3-P_{4-1}). First, under the condition that the TEP–PEG filament has a

certain prestress, the temperature was increased from room temperature to T_s and then the stress was increased at T_s to extend the length of the TEP–PEG filament. Second, the temperature was reduced to room temperature and stress was reduced to the prestress. Finally, the temperature was raised again to T_s to observe the recovery strain of the TEP–PEG filament. The following equations were used to obtain the shape fixation rate (R_f) and shape recovery rate (R_r):

$$R_f = \frac{S_3 - S_1}{S_2 - S_1} \times 100\% \qquad (4-1)$$

and

$$R_r = \frac{S_3 - S_4}{S_3 - S_1} \times 100\%, \qquad (4-2)$$

where S_1 was the strain before the TEP–PEG filament was stretched, S_2 was the maximum strain after stretching, S_3 was the strain at which the temperature was reduced to 25 °C and the tensile stress was released, and S_4 was the strain after reheating and recovery.

The test of recovery stress in the shape memory process is as follows (P_1-P_2-P_3-$P_{4\text{-}2}$). First, the temperature was increased to T_s and the strain of the TEP–PEG filament was increased. Second, the temperature was reduced to room temperature and the stress was reduced to zero by slightly reducing the strain. Finally, the temperature was raised to T_s again, and the S_r output by the TEP–PEG filament was tested.

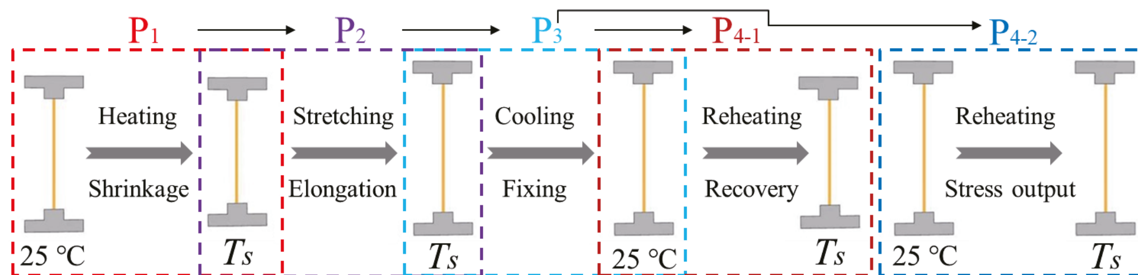

Figure 4-3. The tests of shrinkage strain (P_1), tensile strain (P_1-P_2), recovery strain (P_1-P_2-P_3-P_{4-1}), and recovery stress (P_1-P_2-P_3-P_{4-2}) in the shape memory process.

4.3 Results and Discussion

4.3.1 FTIR analysis

In this study, UEP and PEG are mixed at 85 °C in a molten state for 3 min to obtain a uniform and transparent melt (Figure 4-4a). The lower melting temperature and shorter mixing time help to prevent PEG oxidation by oxygen in the air. After the polymerization reaction of UEP, the shorter PEG molecular chains are uniformly dispersed between the longer molecular chains of polymerized epoxy resin (PEP), yielding a stable TEP–PEG (Figure 4-4b and Figure 4-4c). Figure 4-4d shows FTIR spectra of PEG and UEP-PEG mixtures (after melt mixing of UEP and PEG). Spectra of PEG shows a characteristic peak of hydroxyl group near 3520 cm^{-1}, and a characteristic peak of C–H bond near 2870 cm^{-1}. The peaks of the UEP–PEG mixtures at 2870 cm^{-1} (relative to the peak at 2960 cm^{-1}) and 1100 cm $^{-1}$ are more significant after PEG dispersion, and the

characteristic peaks of the epoxide functional group and hydroxyl group are shown at approximately 912 $cm^{-1}$and 3370 cm^{-1}, respectively. The bifunctional phenol and PEG molecule contain hydroxyl groups that can form hydrogen bonds. Because of the combination of epoxy-phenol in polymerization, the content of intermolecular hydrogen bonds is relatively reduced, causing the characteristic peaks of the TEP–PEG hydroxyl to move slightly to the high band than that of UEP. UEP and TEP–PEGs show a characteristic peak of hydroxyl around 3370 cm^{-1} and 3400^{-1}, respectively (Figure 4-4e). The stretching vibration of C–H is also shown in Figure 4e. All spectra except for pure PEG show peaks caused by C–H bonds on unsaturated C near 3030 cm^{-1}. PEG and TEP–PEGs show a peak caused by the C–H bond on saturated C near 2870 cm^{-1}. The opening of the epoxy group increases the C–H bonds on saturated C; therefore, the peak of the TEP–PEG0 at 2870 cm^{-1} become significant (relative to the peak of UEP at 2960 cm^{-1}). The peaks of the TEP–PEGs at 2870 cm^{-1} are more significant after PEG modification, which make the peak of TEP–PEG15 at 2870 cm^{-1} higher than the peak at 2960 cm^{-1}. After the polymerization reaction, the peak near 912 cm^{-1} (Figure 4-4f) in all spectra of TEP–PEG disappeared because of the epoxy ring-opening reaction during the polymerization process, which also indicates that the dispersion of PEG does not hinder the polymerization reaction. The UEP contains the C–O bond on saturated C and the C–O bond on unsaturated C. Therefore,

the characteristic peak of the C–O bond for UEP is more complicated, which is displayed between 1000 cm^{-1} and 1350 cm^{-1}. PEG only contains C–O bonds on saturated C, resulting in characteristic peaks of C–O bonds being displayed in a relatively low band. After the polymerization reaction, the epoxy ring opens to increase the C–O bond on the saturated C, thus the peak near 1100 cm^{-1} is strengthened and becomes more significant with an increase in PEG content. The peak near 1100 cm^{-1} of TEP–PEG15 is the strongest (Figure 4-4f), followed by TEP–PEG10 and TEP–PEG5. The FTIR spectra of TEP–PEG before and after melt spinning is shown in Figure 4-4g, and the FTIR spectra of TEP–PEG with different PEG content are consistent with their filaments, indicating that melt spinning does not significantly damage the chemical structure of TEP–PEG.

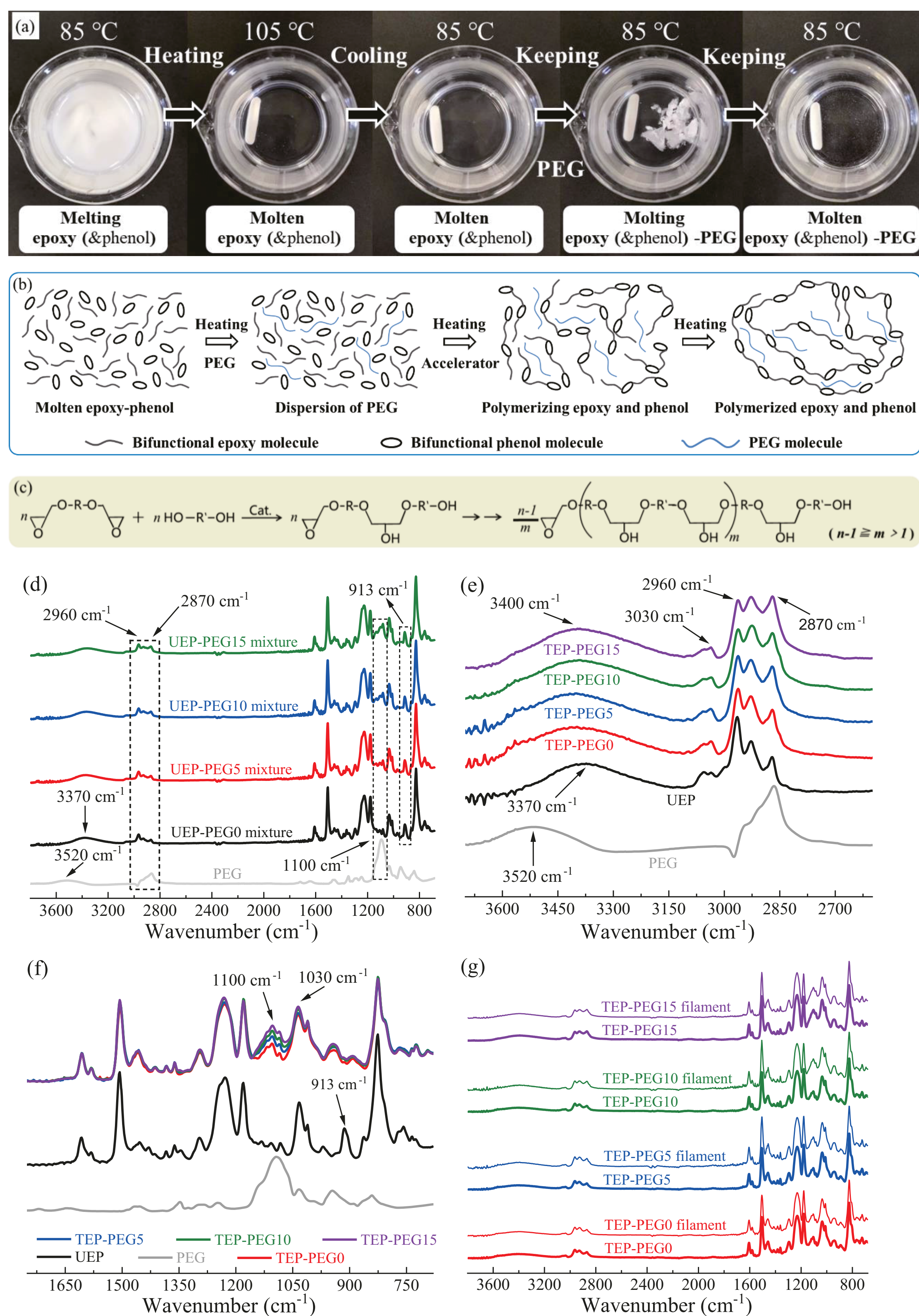

Figure 4-4. (a) The mixing process of UEP and PEG, (b) the dispersion process of PEG molecular and polymerization process of UEP, (c) the

polymerization reaction of UEP; (d) FTIR spectra of the UEP-PEG mixtures (after melt mixing of UEP and PEG); partial FTIR spectra of PEG, UEP, and TEP–PEG (TEP–PEG0, TEP–PEG5, TEP–PEG10, and TEP–PEG15) in (e) higher wavenumber and (f) lower wavenumber; (g) FTIR spectra of TEP–PEG and their filaments.

4.3.2 Thermal analysis

Intermolecular forces are factors that affect the thermal properties of polymers. Because of many hydroxyl groups (Figure 4-5a), hydrogen bonds can be formed between the molecular chains of PEP. For the TEP–PEG (Figure 4-5b), PEG with a shorter molecular chain hinders the formation of hydrogen bonds among PEP molecular chains, and it weakens the intermolecular force of the PEP. A new hydrogen bond is also formed between the PEG molecular chain and PEP molecular chains by the hydroxyl groups, indicating that PEG molecular is more stably dispersed among the molecular chains of PEP. PEP molecular chains are blocked by an increasing number of PEG molecules as PEG content is increased (Figure 4-5c), resulting in a gradual decrease in the intermolecular force of PEP. The thermal properties of pellets and filaments were investigated using DSC analysis. Note that all pellets here are prepared using sufficient polymerization, and subsequent thermal analysis will not be affected by insufficient polymerization. PEG did not significantly hinder the

polymerization reaction of PEP in all TEP–PEG mixtures after the addition of accelerator (Figure 4-5d), and the polymerization exotherm ended after 10 min, which was much less than 30 min of the fabrication process. When TEP–PEG is heated, the PEG molecular chain first exhibits thermal movement and promotes the thermal movement of the PEP molecular chain whose intermolecular force is weakened, making the T_g of TEP–PEG pellets and filaments decrease gradually as the content of PEG increases (Figures 4-5e and 4-5f). The thermal stability of polymer materials is an important factor for melt spinning. When heated to 300 °C, which is the highest spinning temperature in this study, the thermal weight loss of pellets with different PEG content are all less than 3%, showing excellent thermal stability (Figure 4-5g). When pellets with different PEG contents were heated to their spinning temperature and held for 10 min (Figure 4-5h), the thermal weight loss of all pellets was also less than 3%, which is stable enough to be used to melt spinning with a melt mixing time of 10 min. When TEP–PEG is continuously heated above T_g, the PEG molecular chain first has fluidity and promotes the fluidity of the PEP molecular chain whose intermolecular force is weakened, making the melt flow temperature of the TEP–PEG decrease as PEG content increases, which means that pellets with more PEG content can be melt-processed at lower spinning temperatures. When the screw rotation speed is constant, the extrusion force indirectly reflects the fluidity of the melt. With a screw rotation rate

of 10 r/min for 10 min in melt processing, pellets of TEP–PEG0, TEP–PEG5, TEP–PEG10, and TEP–PEG15 reached extrusion force of approximately 1900 N at 300 °C, 280 °C, 250 °C, and 220 °C, respectively (Figure 4-5i). Although the spinning temperature of the pellets with more PEG content was lower, all pellets had similar extrusion forces at their spinning temperature, which means that their melt fluidity properties were also approximately the same. In addition, the temperature of the extruded melts are rapidly reduced to room temperature in the drawing process, and the filaments with more PEG content can be more fully drawn because of the weakening effect of PEG molecules on the intermolecular force of PEP, thereby making filaments with more PEG content have slightly lower diameters. In summary, after the modification of PEG, TEP–PEG obtains a controllable melt spinning temperature, which significantly improves its spinnability. TEP–PEG filaments also obtain a controllable T_g, which extends their range of application, such as heat-stimuli controllability for shape memory function.

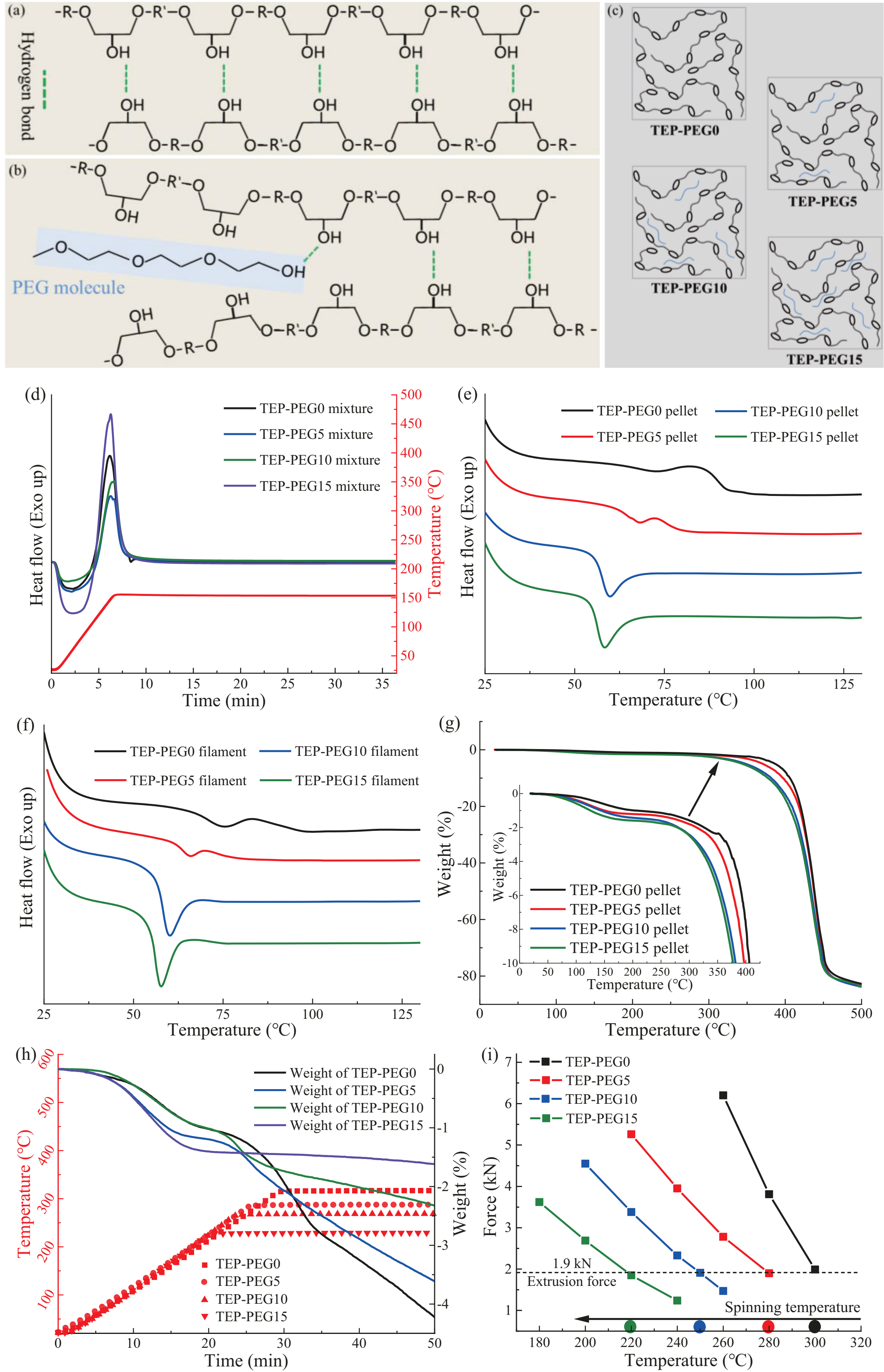

Figure 4-5. (a) Hydrogen bonds of PEP molecular chains, (b) hydrogen

bond between PEP molecular chain and PEG molecular chain, (c) molecular chains of TEP–PEGs, (d) DSC curves of TEP–PEG mixtures after the addition of accelerator, (e) DSC curves of TEP–PEG pellets, (f) DSC curves of TEP–PEG filaments, (g) TGA curve of TEP–PEG pellets, (h) TGA curves of TEP–PEG pellets for keeping 20 min, (i) extrusion force of TEP–PEG pellets during melt processing.

4.3.3 Mechanical analysis

PEG acts as a plasticizer and generally reduces the modulus of the plasticized polymer. The main purpose of adding PEG in this study is to control the T_g of TEP–PEG filaments, but not to reduce their modulus. Interestingly, PEG in this study, in addition to lowering the T_g of TEP–PEG filaments, Young's modulus was slightly increased, which was attributed to the increased spinning effect of the TEP–PEG by PEG. The PEP has relatively poor fluidity in the molten state, which affects the drawing effect of the melt during the spinning process. PEG increases the fluidity of the spinning melt, making the spinning process of PEG-modified filaments more continuous. The improvement of melt fluidity by PEG can be verified from the statistics of extrusion force for TEP–PEG pellets. The stress-strain curve of TEP–PEG filaments at room temperature is shown in Figure 4-6a. TEP-PEG whose intermolecular force is weakened by PEG can obtain more molecular chains oriented along the axis during the drawing process.

Therefore, Young’s modulus and yield stress of PEG-modified filaments are higher than TEP–PEG0 filament (pure TEP filament). The Young's modulus, yield strain, yield stress, breaking strain, and breaking stress of TEP–PEG filaments are shown in Table 4-2. The yield stress of TEP–PEG15 filaments is 8.77 MPa higher than that of TEP–PEG0 filament. Furthermore, PEG reduces the intermolecular forces of PEP, making the molecular chains of the PEG-modified filaments oriented along the axial direction faster during the tensile process. The stress of filaments with more PEG content increased faster because of the faster further orientation (Figure 4-6a), showing a relatively smaller breaking strain. Nonetheless, the TEP–PEG filaments have enough elongation characterization with more than 179% breaking strain. In a word, the PEG-modified filaments obtained higher Young's modulus and yield stress, and still had a large breaking strain.

The mechanical properties of filaments were further investigated through DMA measurement. The PEG-modified filaments demonstrated a higher storage modulus than the TEP–PEG0 filament at 25 °C (Figure 4-6b), which is because PEG improved the spinning effect of TEP–PEG. The modulus of the filaments with more PEG content decreased faster and gradually lower than filaments with less PEG content during the process of gradual heating from room temperature because of their relatively lower T_g. The different contents of PEG obtain different T_g of TEP-PEGs to

prepare shape memory TEP–PEG filaments that can be stimulated at different temperatures. The T_g of the filament decreased as the PEG content increased, and the T_g of the TEP–PEG15 filament decreased by 37 °C compared with that of the TEP–PEG0 filament (Figure 4-6c). Additionally, the shape memory stimuli temperature of TEP–PEG filament in this study is set to a temperature slightly higher than its T_g. The storage modulus (at 25 °C) and T_g of TEP–PEG filaments are listed in Table 4-2, indicating PEG through modification, not only TEP–PEG filaments with different T_g were obtained, but also the storage modulus at 25 °C of TEP–PEG filaments was improved.

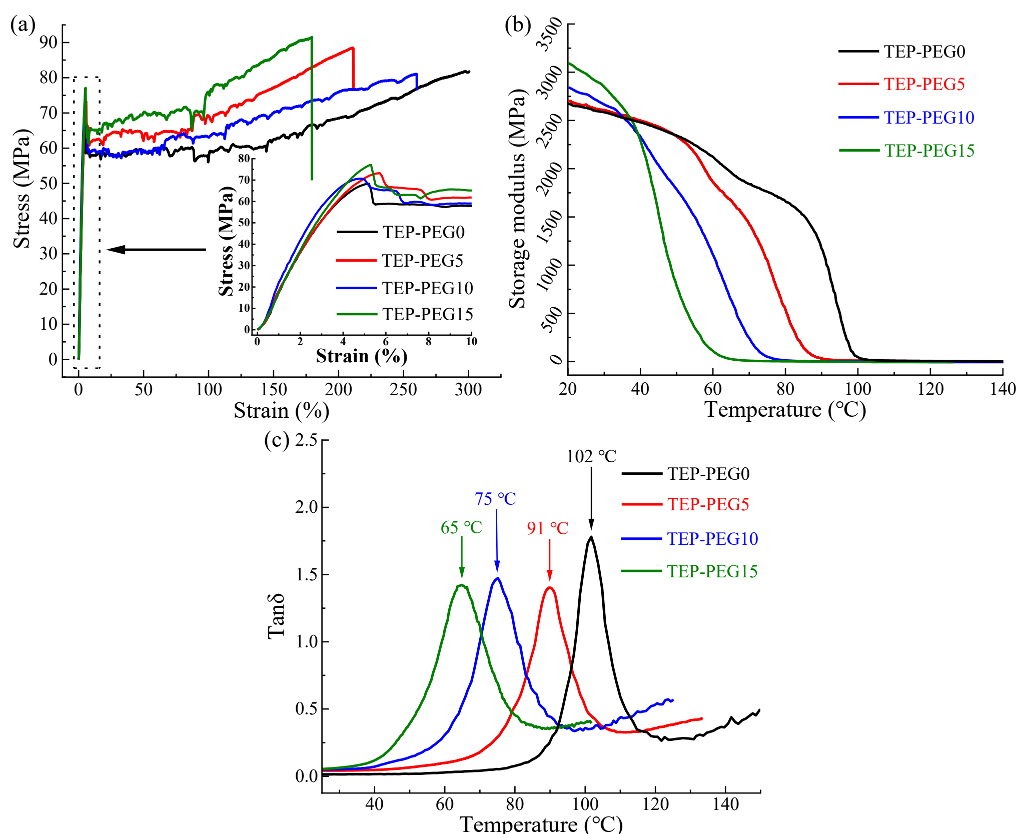

Figure 4-6. (a) Stress-strain curve of TEP–PEG filaments, (b) temperature-modulus curve of TEP–PEG filaments by DMA, (c) temperature-Tanδ

curve of TEP–PEG filaments by DMA.

Table 4-2. Young's modulus, yield strain, yield stress, breaking strain, and breaking stress were analyzed from the stress-strain curves; storage modulus (at 25 °C) and T_g analyzed by DMA.

Filaments	Young's modulus (MPa)	Yield Strain (%)	Yield stress (MPa)	Breaking strain (%)	Breaking Stress (MPa)	Storage modulus (MPa)	T_g (℃)
TEP-PEG0	1907	5.21	68.32	300.61	81.77	2632	102
TEP-PEG5	1918	5.71	73.29	210.81	88.51	2665	91
TEP-PEG10	2218	4.90	70.68	260.11	81.01	2775	75
TEP-PEG15	1959	5.09	77.09	179.41	91.56	2983	65

4.3.4 Shape memory performance

4.3.4.1 Investigation and selection of prestress and tensile stress

The filament is drawn in the axial direction during the spinning process, and the internal molecular chain obtains the axial orientation. When the processed filament is heated again, the thermal movement of the internal molecular chain causes the filament to exhibit heat-shrinkage. The prestress is a necessary factor affecting the shape memory process of filament-type samples. In this experiment, the effect of different prestresses on the heat-shrinkage process was investigated, and a prestress was selected for each filament for subsequent shape memory experiments. The shrinkage curves of TEP–PEG filaments with different PEG content during heating to their stimuli temperatures are shown in Figures 4-7(a–d). All filaments begin to quickly shrink when the temperature rises to its T_g region

and gradually slows. Appropriate prestress straightens the filament before heating, while also limiting the shrinkage of the filament to a certain range to achieve the expected effect of experimental programming. When the prestress of the filament is relatively small, the shrinkage strain of the filament is large, and it still has a large strain rate when heated for 25 min. When the prestress is relatively large, the filament shrinks slowly and even tends to elongate at a later stage, such as the TEP–PEG0 filament with a prestress of 0.5 MPa shown in Figure 4-7a. The final shrinkage strain and its rate for TEP–PEG filaments with different prestress after 25 min are shown in Table 4-3. This experiment selected a prestress that maintains the filament heat shrinking throughout the heating process with a relatively small shrinkage strain rate at the end of the heating. The prestress of TEP–PEG0, TEP–PEG5, TEP–PEG10, and TEP–PEG15 filaments were selected as 0.4, 0.3, 0.3, and 0.3 MPa, respectively, for subsequent shape memory experiments.

Unlike the lower elastic elongation of TEP–PEG filaments at room temperature, the filaments show greater elastic elongation at stimuli temperature (from Figures 4-7e to 4-7h). Tensile stress is an important factor affecting the shape memory process. In this experiment, the appropriate tensile stresses on the heat-stretching process were selected by investigating the tensile strains of the filaments for subsequent shape memory experiments. Appropriate tensile stress is beneficial to the strain

recovery of the shape memory, whereas excessive tensile stress may obtain a small recovery rate because the filament is overstretched. TEP–PEG0 filaments with tensile stresses of 1.3 and 1.5 MPa showed non-uniformly increasing strains at the later stage because of overstretching (Figures 4-7e), whereas PEG-modified filaments with different tensile stress did not exhibit this phenomenon because of their relatively excellent mechanical properties. The tensile strain of filaments with different PEG content is also different because of the difference in mechanical and thermal properties. In this experiment, the stress that makes the strain slightly higher than 15% is selected as the tensile stress of filament in the subsequent shape memory process. The final tensile strain for TEP–PEG filaments with different tensile stresses after 5 min is shown in Table 4-4. According to the statistical results, the tensile stress of the TEP–PEG0 and TEP–PEG10 filaments was chosen to be 1.2 MPa and1.0 MPa respectively, and the tensile stress of both TEP–PEG5 and TEP–PEG15 filaments was chosen to be 1.1 MPa for the subsequent shape memory experiments.

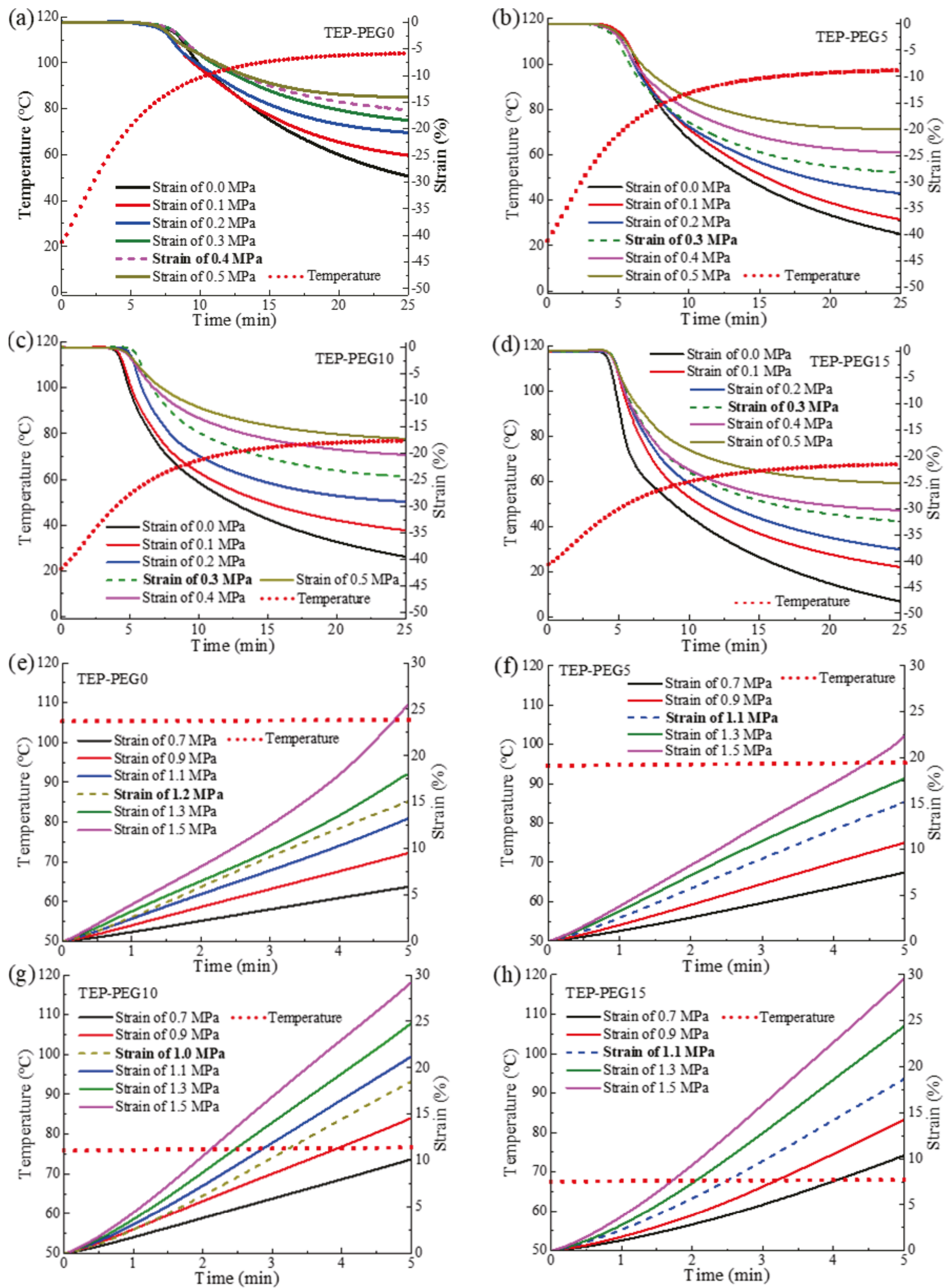

Figure 4-7. Shrinkage curves of filaments with different prestresses, (a) TEP–PEG0, (b) TEP–PEG5, (c) TEP–PEG10, (d) TEP–PEG15; strain curves of filaments with different tensile stresses, (e) TEP–PEG0, (f) TEP–

PEG5, (g) TEP–PEG10, (h) TEP–PEG15.

Table 4-3. Final shrinkage strain (%) and its rate (%/min) with different prestresses.

Filaments	0.0MPa		0.1 MPa		0.2 MPa		0.3 MPa		0.4 MPa		0.5 MPa	
	Strain	Rate	Strain	Rate	Strain	Rate	Strain	Rate	Strain	Rate	Strain	Rate
TEP-PEG0	28.9	0.67	24.9	0.29	20.7	0.21	18.4	0.24	**16.5**	0.18	14.0	-0.14
TEP-PEG5	40.0	0.76	37.2	0.56	32.2	0.30	**28.2**	0.12	24.4	0.07	20.0	0.00
TEP-PEG10	39.5	0.51	34.5	0.29	29.1	0.14	**24.4**	0.11	20.3	0.02	17.2	0.00
TEP-PEG15	47.7	0.56	41.2	0.40	37.8	0.37	**32.4**	0.20	30.4	0.11	25.1	0.08

Table 4-4. Strain (%) with different tensile stresses

Filaments	0.7 MPa	0.9 MPa	1.0 MPa	1.1 MPa	1.2 MPa	1.3 MPa	1.5 MPa
TEP-PEG0	5.9	9.5	—	13.3	**15.1**	18.0	25.6
TEP-PEG5	7.4	10.7	—	**15.2**	—	17.7	22.4
TEP-PEG10	10.1	14.6	**18.5**	21.2	—	24.8	29.2
TEP-PEG15	10.4	14.2	—	**18.7**	—	24.4	29.6

4.3.4.2 Investigation of shape memory function

Compared with TEP–PEG pellets, TEP–PEG filaments have an axially oriented molecular chain structure because of the drawing of the melt. The shape memory mechanism of TEP–PEG filament is shown in Figure 4-8a. When the TEP–PEG filament is heated, the molecular chain stretched during the previous spinning process shrinks at the T_g region. When the TEP–PEG filament is heat stretched, the internal molecular chain is stretched again, and then the internal molecular chain is fixed by quickly lowering the temperature to room temperature while maintaining the tensile stress, and the length of the TEP–PEG filament is also fixed in the stretched state. When the TEP–PEG filament is heated to the glass transition region again, the heat-shrinkage of the internal molecular chain

causes the length of the TEP–PEG filament to recover. During the heat-stretching process, the PEG molecules first move in the tensile direction, promoting the movement of the PEP molecular chain along the tensile direction. During the heat recovery process, the PEG molecules first move in the shrinking direction and promote the heat shrinking movement of the PEP molecular chain. The more the PEG content, the more significant the promoting effect of PEG on the movement of the PEP molecular chain, and the lower the T_g of the TEP–PEG. Therefore, the shape memory stimuli temperature of TEP–PEG filaments can be controlled using the content of PEG, thereby realizing the heat-stimuli controllability of the shape memory function. The shape memory test curves of TEP–PEG filaments performed two cycles based on selected prestress and tensile stresses (from Figures 4-8b to 4-8e). The shape memory stimuli temperature of TEP–PEG15, TEP–PEG10, TEP–PEG5, and TEP–PEG0 filament in this shape memory experiment are 69 °C, 78 °C, 94 °C, and 105 °C, respectively. Despite the different stimuli temperature, all TEP–PEG filaments show excellent shape memory properties. The fixation rates of TEP–PEG filaments with different PEG content demonstrate high average shape fixation rates (R_f) ranging from 95.8% to 99.1% (Figure 4-8f). Note that the PEG-modified filaments have higher fixation rates because the modulus of TEP–PEG filaments after adding PEG increases faster during the cold fixing process as the temperature drops to room temperature, whereas the filaments with

high modulus are relatively difficult to be deformed by the external environment. The higher the PEG content in the previous thermomechanical analysis, the faster the modulus of the filament changes with temperature, and the higher the modulus is at room temperature. The fixation rates of TEP–PEG filaments with different PEG content are shown in Figure 4-8g. TEP–PEG0 filament show a shape recovery rate (R_r) of not less than 96.1% in each cycle and the R_r increased slightly in the second cycle after training for one cycle. The R_r of both TEP–PEG5 and TEP–PEG15 filaments was larger than 98.2% in the first cycle due to a larger shrinkage tendency before the stretching of the first cycle. However, the R_r of both TEP–PEG5 and TEP–PEG15 filaments was relatively smaller in the second cycle due to the gentler recovery tendency before the stretching of the second cycle. Although the shrinkage tendency of TEP–PEG10 filament before the stretching of the first cycle is larger, the larger tensile strain increases the difficulty of recovery in the first cycle, which makes TEP–PEG10 filament trained for one cycle shows a relatively larger R_r in the second cycle. Overall, with different stimuli temperatures, the average R_r of TEP–PEG filaments has R_r ranging from 93.1% to 99.0%, achieving heat-stimuli controllability of the shape memory function based on the excellent shape memory performance.

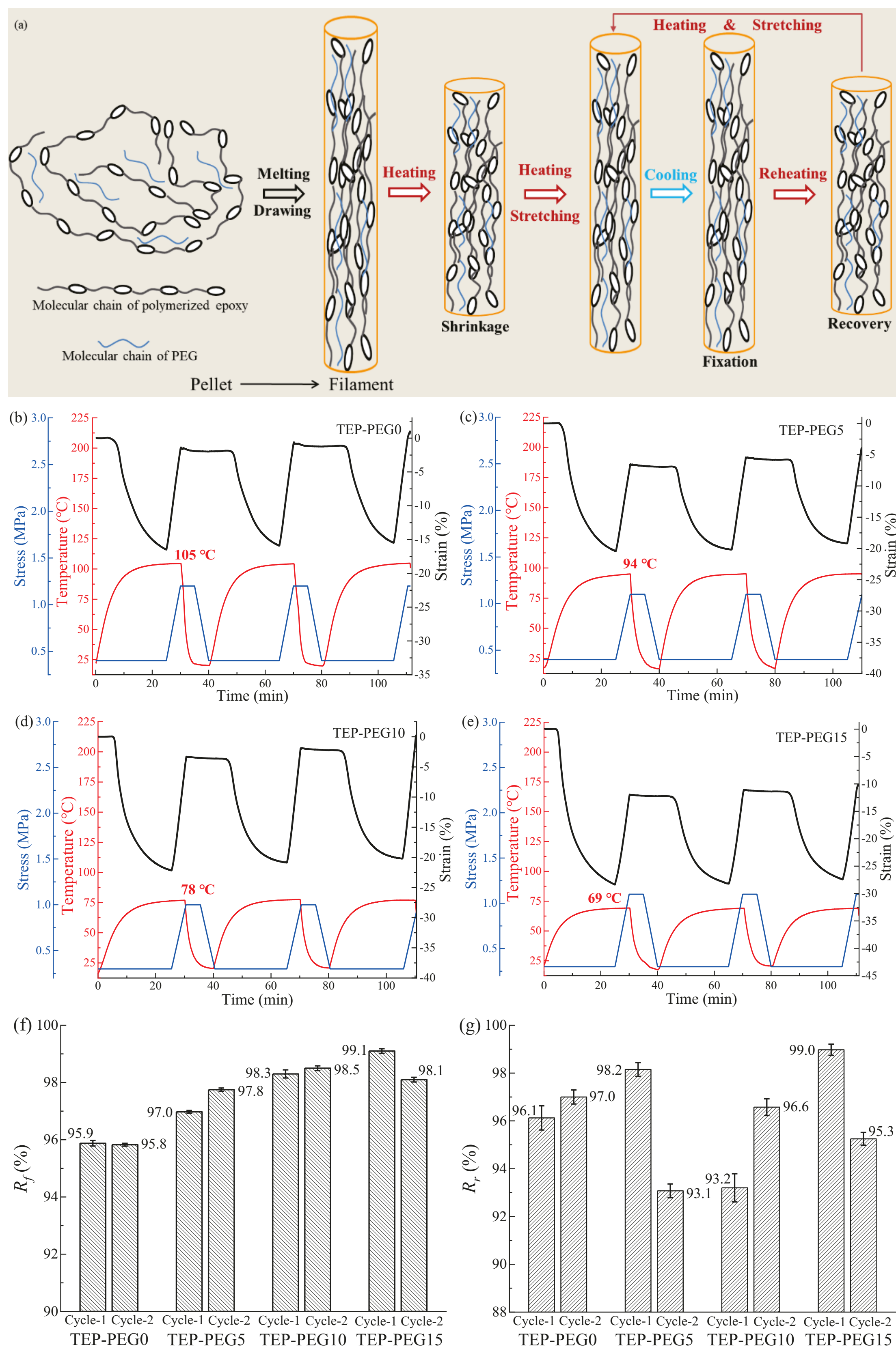

Figure 4-8. (a) Illustration of the shape memory mechanism of TEP–PEG filaments; shape memory curves of (b) TEP–PEG0 filament, (c) TEP–

PEG5 filament, (d) TEP–PEG10 filament and (e) TEP–PEG15 filament; statistical results of (f) R_f and (g) R_r for TEP–PEG filaments.

4.3.4.3 Recovery stress in shape recovery process

The analysis of shape memory shows that TEP–PEG filaments have very high R_r on the basis of maintaining the prestress of 0.3 MPa and above, so it is particularly important to investigate the recovery stress of TEP–PEG filament in the shape memory process. When the filaments drawn during the spinning process are heated again, shrinkage stress will be generated because of heat-shrinkage. In the shape recovery process of shape memory, the heat stretched filament will output S_r. The process of S_r from generation to output is shown in Figure 4-9a. After the filament is heat stretched, the S_r is "frozen" by rapid cooling that can be output again by temperature stimulation. The shrinkage stress of TEP–PEG filaments is shown in Figures 4-9b. The output process of S_r for TEP–PEG filaments is shown in Figures 4-9 (c–f). Before the stress recovery test, the tensile strain of all filaments was 15%. All filaments generate S_r as the temperature rises, which gradually stabilize after reaching the peak in the T_g region, and have a slight downward trend because of the mechanical relaxation effect over time. Note that TEP–PEG0 filament outputs opposite stress before outputting S_r, which is related to temperature and molecular structures. The heat-stretching temperature of the TEP–PEG0 filament is relatively high,

which is different from the room temperature of cold fixation, causing part of the molecular chain to be “frozen” while retaining the elongation trend. When the temperature rises to the T_g region again, the partially “frozen” TEP–PEG0 filament molecular chain tends to elongate and first generates a stress opposite to the direction of the S_r. For PEG-modified filaments, the temperature difference during the cold fixation process is relatively small, and PEG molecules with greater thermal mobility reduce the elongation tendency of the PEP molecules in the heat recovery process. Therefore, none of the PEG-modified filament output a stress opposite to S_r (from Figures 4-9d to 4-9f), improving the output efficiency of the TEP–PEG filament during the shape memory process. Note that the filaments undergo a slight stress change because of mechanical clamping in the initial stage. PEG improved the drawing effect of TEP–PEG melts, resulting in higher S_r of PEG-modified filaments. Additionally, PEG reduces the temperature at maximum recovery stress (S_m), which is due to the decrease in T_g of TEP–PEG filaments by PEG. For the TEP–PEG15 filament, its S_m was 0.45 MPa higher than that of the TEP–PEG0 filament, and the temperature at S_m is 39 °C lower than that of TEP–PEG0 filament (Figure 4-9g). The initial temperature (T_i) at which each filament begins to output S_r is shown in Figure 4-9h. Because PEG not only reduces the T_g of the TEP–PEG filament but also improves the stress output efficiency of the TEP–PEG filament, the PEG-modified filaments output S_r at a lower T_i and an earlier

time. Compared with the TEP–PEG0 filament, T_i and the time at T_i for the TEP–PEG15 filament were reduced by 62 °C and 9.4 min, respectively. In a word, through PEG modification, TEP–PEG filaments have higher stress output efficiency and greater S_r on the basis of obtaining the heat-stimuli controllability of shape memory function and show excellent thermal actuation potential over a wider range of temperature options.

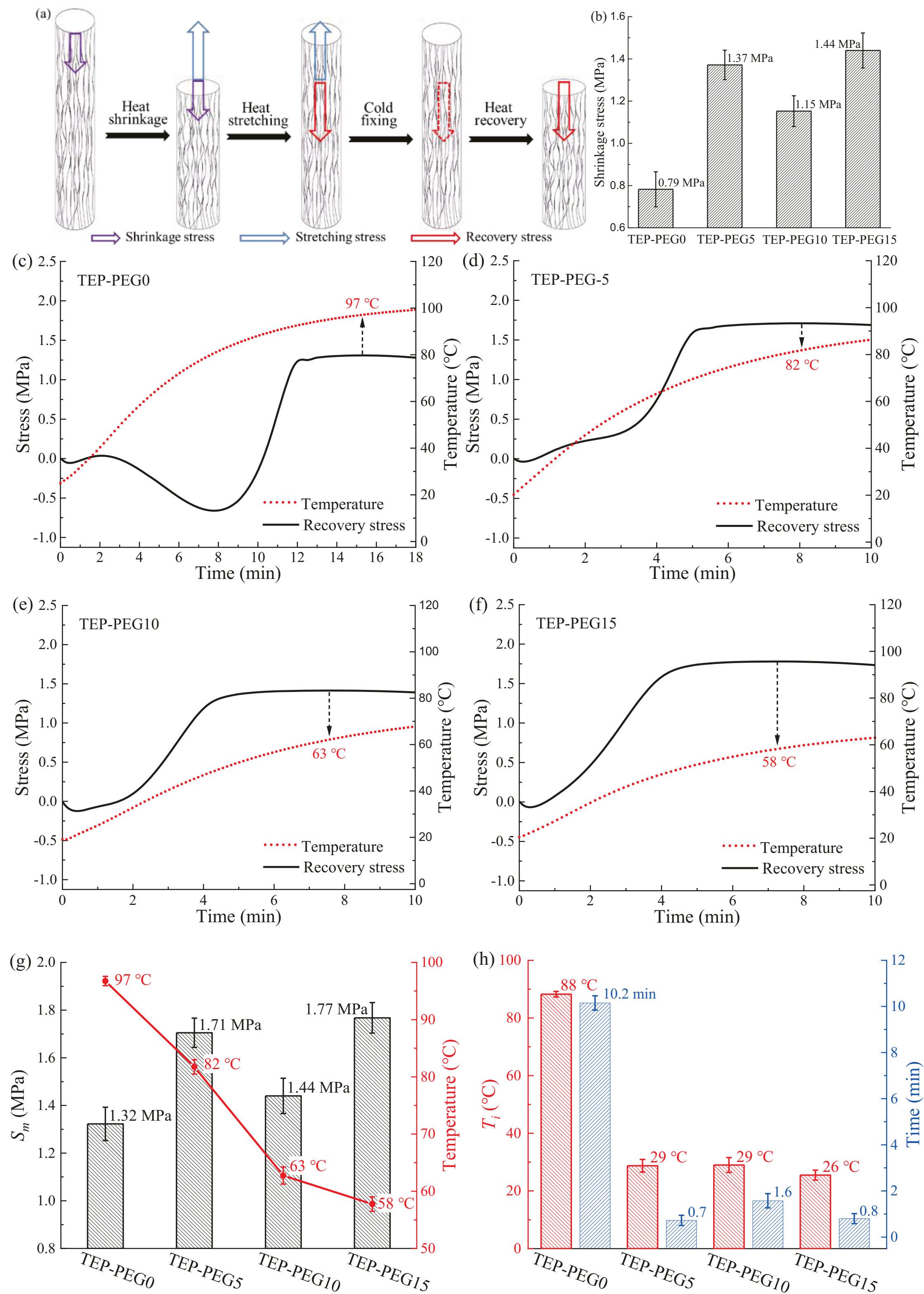

Figure 4-9. (a) The generation, freezing, and output of S_r for TEP–PEG filament; (b) statistics of shrinkage stress for each filament; S_r output process of (c) TEP–PEG0 filament, (d) TEP–PEG5 filament, (e) TEP–

PEG10 filament and (f) TEP–PEG15 filament; statistical results of (g) S_m and temperature at S_m, (h) T_i and time at T_i.

4.3.5 Discussion in thermal actuation

The TEP–PEG filaments prepared in this study have excellent shape memory properties. Furthermore, PEG improves the melt spinnability, mechanical strength at room temperature, R_f, S_r, stress output effects, and so on. The shape memory stimuli temperature of TEP–PEG filaments can also be adjusted according to the PEG content. For example, the shape memory stimuli temperature of TEP–PEG15 filament can be reduced to 69 °C, which is 36 °C lower than that of TEP–PEG0 filament. The significant effect is that the PEG-modified filaments can output greater S_r at a lower temperature and a shorter time. Among them, the TEP–PEG15 filament has the highest S_r, showing its greater application potential in the field of thermal actuation. In this experiment, a TEP–PEG15 filament of a length (L) of 13 cm and a radius (r) of 0.1 mm with a load (m = 2 g) was selected for the thermal actuation experiment (Figure 4-10a). TEP–PEG15 filament can lift the load by 36 mm (statistical error within 2 mm) through heat-shrinkage in a temperature atmosphere of 69 °C. The TEP–PEG15 filaments were then stretched to 15 cm with a larger load (7.2 g) at 69 °C. When the load was changed back to the original 2 g, the load can be lifted by height (H) of 45 mm through heat-recovery in a temperature atmosphere

of 69 °C, and an energy density (= $Hmg/L\pi r^2$) for thermal actuation can reach 0.22 J/cm^3. Depending on the drawing during the spinning process, TEP–PEG15 filament exhibits excellent thermal actuation ability through heat-shrinkage, which can be further improved by heat-stretching. Additionally, TEP–PEG15 yarn stretched approximately 15% woven from three TEP–PEG15 filaments can lift the load of 7 g by 57 mm (Figure 4-10b), demonstrating better thermal actuation capability than single TEP–PEG15 filament, and recovery force of TEP–PEG15 yarn tested using TMA measurement is also more than three times that of single TEP–PEG15 filament (Figure 4-10c). Further analysis of the recovery stresses with different strains is shown in Figure 4-10d; as the strain increases from 10% to 35%, S_r shows an increasing trend and gradually becomes slower after a tensile strain of 15%. A test of S_r of TEP–PEG15 filament with a tensile strain of 15% for 5 cycles is shown in Figure 10e. The S_r of the second cycle is relatively significantly reduced, and the reduction of S_r becomes insignificant. Additionally, this study tested the shape memory process of TEP–PEG15 filament in 5 cycles (Figure 4-10f). The R_f of the TEP-PEG15 filament has higher stability, except in the first cycle which is due to the faster cooling. The R_r of the TEP-PEG15 filament fluctuates somewhat due to the slightly different recovery tendency in the previous cycle and the tensile strain in its own cycle. Overall, TEP-PEG15 filament with a high R_f of 98.1% -99.1% and a high R_r of 94.8%–99.0% has shown

excellent shape memory performance (Figure 4-10g). The filament-type material for thermal actuation has the advantage of being woven. TEP–PEG15 filament shows excellent shape memory performance and thermal actuation ability and can be further woven and processed to be suitable for more applications, showing great application potential in the fields of thermal actuation, smart textiles, and artificial muscles.

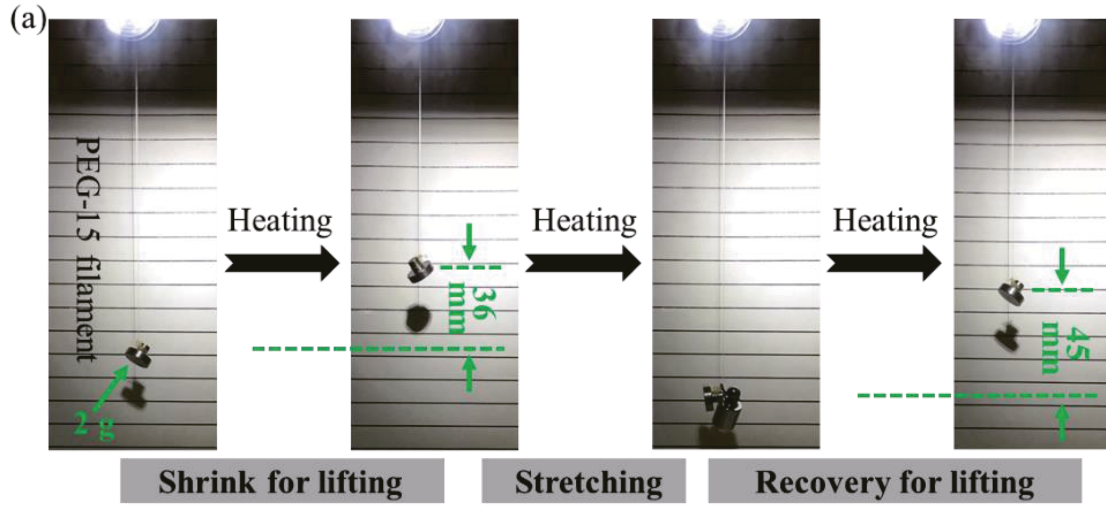
(a)
PEG-15 filament
2 g
Heating
36 mm
Heating
Heating
45 mm
Shrink for lifting
Stretching
Recovery for lifting

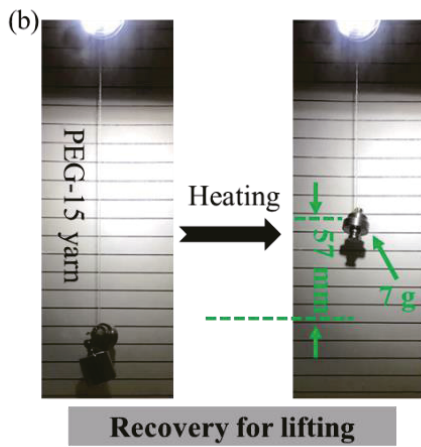
(b)
PEG-15 yarn
Heating
57 mm
7 g
Recovery for lifting

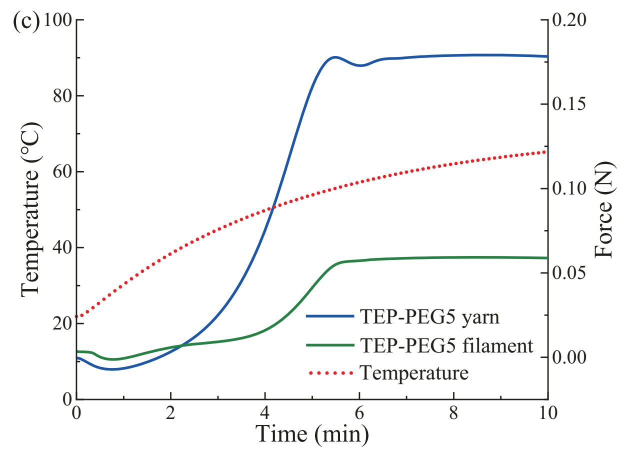
(c)
Temperature (°C)
Force (N)
Time (min)
TEP-PEG5 yarn
TEP-PEG5 filament
Temperature

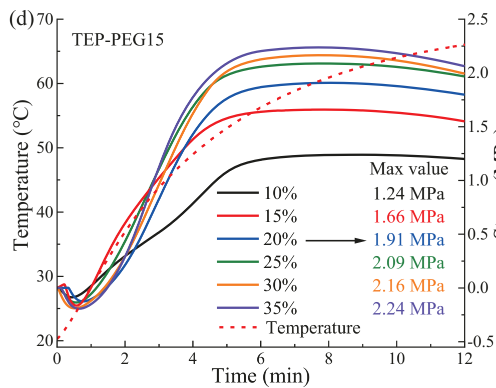
(d)
TEP-PEG15
Temperature (°C)
Stress (MPa)
Time (min)
Max value
10% 1.24 MPa
15% 1.66 MPa
20% 1.91 MPa
25% 2.09 MPa
30% 2.16 MPa
35% 2.24 MPa
Temperature

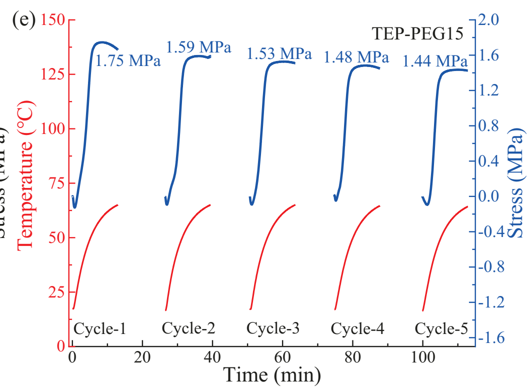
(e)
TEP-PEG15
1.75 MPa
1.59 MPa
1.53 MPa
1.48 MPa
1.44 MPa
Temperature (°C)
Stress (MPa)
Cycle-1
Cycle-2
Cycle-3
Cycle-4
Cycle-5
Time (min)

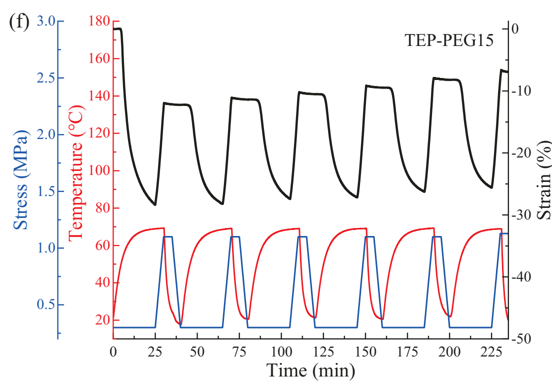
(f)
TEP-PEG15
Stress (MPa)
Temperature (°C)
Strain (%)
Time (min)

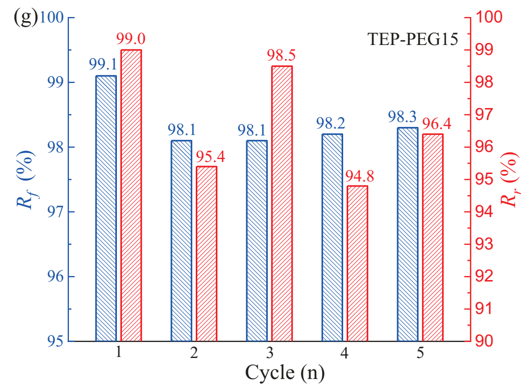
(g)
TEP-PEG15
99.1
99.0
98.1
95.4
98.1
98.5
98.2
94.8
98.3
96.4
R_f (%)
R_r (%)
Cycle (n)

Figure 4-10. (a) Thermal actuation process of TEP–PEG15 filament, (b) thermal actuation process of TEP–PEG15 yarn, (c) recovery forces of TEP–PEG15 filament and TEP–PEG15 yarn with a tensile strain of 15%, (d) S_r of TEP–PEG15 filament with different tensile strains, (e) S_r of TEP–PEG15 filament with a tensile strain of 15% for 5 cycles, (f) shape memory curve and its (g) statistical results (R_f and R_r) for TEP–PEG15 filament within 5 cycles.

4.4. Conclusions

To achieve heat-stimuli controllability of shape memory function, shape memory TEP–PEG filaments with controllable stimuli temperature were prepared. The chemical structure analysis revealed that the dispersion of PEG did not hinder the polymerization reaction of UEP. Thermal analysis showed that both the T_g and melt spinning temperatures of TEP–PEG filaments could be adjusted based on the PEG content. Mechanical analysis showed that PEG enhanced both Young's modulus and yield stress of TEP–PEG filaments. Shape memory analysis showed that TEP–PEG filaments exhibit excellent shape memory performance with a shape fixation rate range of 95.8%–99.1% and a shape recovery rate range of 93.1%–99.0%. The TEP–PEG filaments have obtained controllable stimuli temperature and greater their shape fixation rates after PEG modification. Furthermore, the recovery stress test showed that TEP–PEG filaments have

higher recovery stress at lower temperatures after PEG modification. The difficulty of melt processing for TEP was reduced in a more environmentally friendly way, and shape memory TEP–PEG filaments with different stimuli temperature were developed without reducing Young's modulus. With the addition of PEG, TEP–PEG filaments not only realized the heat-stimuli controllability of shape memory function but also showed greater thermal actuation ability, indicating a wider range of applications, such as thermal actuation, smart textiles, and artificial muscles.

References

1. Zhao, Q., Zou, W., Luo, Y. & Xie, T. Shape memory polymer network with thermally distinct elasticity and plasticity. *Sci. Adv.* **2**, e1501297 (2016).
2. Liu, W., Chen, H., Ge, M., Ni, Q.-Q. & Gao, Q. Electroactive shape memory composites with TiO_2 whiskers for switching an electrical circuit. *Mater. Des.* **143**, 196–203 (2018).
3. Bai, Y. *et al.* A reconfigurable, self-healing and near infrared light responsive thermoset shape memory polymer. *Compos. Sci. Technol.* **187**, 107940 (2020).
4. Yue, C. *et al.* Three-dimensional printing of cellulose nanofibers reinforced PHB/PCL/Fe_3O_4 magneto-responsive shape memory polymer

composites with excellent mechanical properties. *Addit. Manuf.* **46**, 102146 (2021).

5. Ge, Y. *et al.* Programmable Humidity-Responsive Actuation of Polymer Films Enabled by Combining Shape Memory Property and Surface-Tunable Hygroscopicity. *ACS Appl. Mater. Interfaces* **13**, 38773–38782 (2021).

6. Liu, Y., Du, H., Liu, L. & Leng, J. Shape memory polymers and their composites in aerospace applications: a review. *Smart Mater. Struct.* **23**, 023001 (2014).

7. Chen, H. *et al.* Flexible nanopositioning actuators based on functional nanocomposites. *Compos. Sci. Technol.* **186**, 107937 (2020).

8. Li, G. & Uppu, N. Shape memory polymer based self-healing syntactic foam: 3-D confined thermomechanical characterization. *Compos. Sci. Technol.* **70**, 1419–1427 (2010).

9. Meng, H. & Li, G. A review of stimuli-responsive shape memory polymer composites. *Polymer* **54**, 2199–2221 (2013).

10. Guan, X. *et al.* Flexible energy harvester based on aligned PZT/SMPU nanofibers and shape memory effect for curved sensors. *Compos. Part B Eng.* **197**, 108169 (2020).

11. Li, F., Liu, Y. & Leng, J. Progress of shape memory polymers and their composites in aerospace applications. *Smart Mater. Struct.* **28**, 103003 (2019).

12. Liu, J. A.-C., Gillen, J. H., Mishra, S. R., Evans, B. A. & Tracy, J. B.

Photothermally and magnetically controlled reconfiguration of polymer composites for soft robotics. *Sci. Adv.* **5**, eaaw2897 (2019).

13. Zhao, W., Liu, L., Zhang, F., Leng, J. & Liu, Y. Shape memory polymers and their composites in biomedical applications. *Mater. Sci. Eng. C* **97**, 864–883 (2019).

14. Wazarkar, K., Kathalewar, M. & Sabnis, A. Development of epoxy-urethane hybrid coatings via non-isocyanate route. *Eur. Polym. J.* **84**, 812–827 (2016).

15. Gao, W., Bie, M., Liu, F., Chang, P. & Quan, Y. Self-Healable and Reprocessable Polysulfide Sealants Prepared from Liquid Polysulfide Oligomer and Epoxy Resin. *ACS Appl. Mater. Interfaces* **9**, 15798–15808 (2017).

16. Kim, M. T., Rhee, K. Y., Lee, J. H., Hui, D. & Lau, A. K. T. Property enhancement of a carbon fiber/epoxy composite by using carbon nanotubes. *Compos. Part B Eng.* **42**, 1257–1261 (2011).

17. White, J. E., Silvis, H. C., Winkler, M. S., Glass, T. W. & Kirkpatrick, D. E. Poly(hydroxyaminoethers): A New Family of Epoxy-Based Thermoplastics. *Adv. Mater.* **12**, 1791–1800 (2000).

18. Taniguchi, N., Nishiwaki, T., Hirayama, N., Nishida, H. & Kawada, H. Dynamic tensile properties of carbon fiber composite based on thermoplastic epoxy resin loaded in matrix-dominant directions. *Compos. Sci. Technol.* **69**, 207–213 (2009).

19. Squeo, E. A. & Quadrini, F. Shape memory epoxy foams by solid-state foaming. *Smart Mater. Struct.* **19**, 105002 (2010).

20. Liu, T. *et al.* Eugenol-Derived Biobased Epoxy: Shape Memory, Repairing, and Recyclability. *Macromolecules* **50**, 8588–8597 (2017).

21. Zhang, F. *et al.* Thermosetting epoxy reinforced shape memory composite microfiber membranes: Fabrication, structure and properties. *Compos. Part Appl. Sci. Manuf.* **76**, 54–61 (2015).

22. Santhosh Kumar, K. S., Biju, R. & Reghunadhan Nair, C. P. Progress in shape memory epoxy resins. *React. Funct. Polym.* **73**, 421–430 (2013).

23. Bao, M. *et al.* Electrospun Biomimetic Fibrous Scaffold from Shape Memory Polymer of PDLLA- *co* -TMC for Bone Tissue Engineering. *ACS Appl. Mater. Interfaces* **6**, 2611–2621 (2014).

24. Yuan, J. *et al.* Shape memory nanocomposite fibers for untethered high-energy microengines. *Science* **365**, 155–158 (2019).

25. Tawfick, S. & Tang, Y. Stronger artificial muscles, with a twist. *Science* **365**, 125–126 (2019).

26. Huang, Y. *et al.* A shape memory supercapacitor and its application in smart energy storage textiles. *J. Mater. Chem. A* **4**, 1290–1297 (2016).

27. Mirvakili, S. M. & Hunter, I. W. Fast Torsional Artificial Muscles from NiTi Twisted Yarns. *ACS Appl. Mater. Interfaces* **9**, 16321–16326 (2017).

28. Kanik, M. *et al.* Strain-programmable fiber-based artificial muscle. *Science* **365**, 145–150 (2019).

29. Mirvakili, S. M. & Hunter, I. W. Multidirectional Artificial Muscles from Nylon. *Adv. Mater.* **29**, 1604734 (2017).

30. Maksimkin, A. V. *et al.* Artificial muscles based on coiled UHMWPE fibers with shape memory effect. *Express Polym. Lett.* **12**, 1072–1080 (2018).

31. Bhatti, M. R. A. *et al.* Ultra-High Actuation Stress Polymer Actuators as Light-Driven Artificial Muscles. *ACS Appl. Mater. Interfaces* **12**, 33210–33218 (2020).

32. Foroughi, J. *et al.* Knitted Carbon-Nanotube-Sheath/Spandex-Core Elastomeric Yarns for Artificial Muscles and Strain Sensing. *ACS Nano* **10**, 9129–9135 (2016).

33. Liang, R. *et al.* Highly Tough Hydrogels with the Body Temperature-Responsive Shape Memory Effect. *ACS Appl. Mater. Interfaces* **11**, 43563–43572 (2019).

34. Basak, S. Redesigning the modern applied medical sciences and engineering with shape memory polymers. *Adv. Compos. Hybrid Mater.* **4**, 223–234 (2021).

35. Banpean, A., Takagi, H., Shimizu, N., Igarashi, N. & Sakurai, S. Small- and wide-angle X-ray scattering studies on confined crystallization of Poly (ethylene glycol) in Poly (L-lactic acid) spherulite in a PLLA/PEG blend. *Polymer* **229**, 123971 (2021).

36. Cho, H., Liu, P., Boyle, A. J., Reilly, R. M. & Winnik, M. A. Synthesis of a

metal-chelating polymer with NOTA pendants as a carrier for 64Cu, intended for radioimmunotherapy. *Eur. Polym. J.* **125**, 109501 (2020).

37. Grenier, L. *et al.* Enabling Indium Channels for Mass Cytometry by Using Reinforced Cyclam-Based Chelating Polylysine. *Bioconjug. Chem.* **31**, 2103–2115 (2020).

38. Naidoo, L., Kanchi, S., Drexel, R., Meier, F. & Bisetty, K. Measurement of TiO_2 Nanoscale Ingredients in Sunscreens by Multidetector AF4, TEM, and spICP-MS Supported by Computational Modeling. *ACS Appl. Nano Mater.* **4**, 4665–4675 (2021).

39. Kfoury, G. *et al.* Recent advances in high performance poly(lactide): from “green” plasticization to super-tough materials via (reactive) compounding. *Front. Chem.* **1**, (2013).

40. Im, Y. M., Nathanael, A. J., Jung, M. H., Lee, S. O. & Oh, T. H. Effect of Polyethylene Glycol on Melt Spinning of Poly (Acrylonitrile-co-1-Vinylimidazole). *Fibers Polym.* (2021) doi:10.1007/s12221-021-0180-1.

41. Byun, Y., Kim, Y. T. & Whiteside, S. Characterization of an antioxidant polylactic acid (PLA) film prepared with α-tocopherol, BHT and polyethylene glycol using film cast extruder. *J. Food Eng.* **100**, 239–244 (2010).

42. Norazlina, H. & Kamal, Y. Elucidating the plasticizing effect on mechanical and thermal properties of poly (lactic acid)/carbon nanotubes nanocomposites. *Polym. Bull.* **78**, 6911–6933 (2021).

43. Tian, M. *et al.* Largely improved actuation strain at low electric field of dielectric elastomer by combining disrupting hydrogen bonds with ionic conductivity. *J Mater Chem C* **2**, 8388–8397 (2014).
44. Taib, R. M., Ramarad, S., Mohd Ishak, Z. A. & Todo, M. Properties of kenaf fiber/polylactic acid biocomposites plasticized with polyethylene glycol. *Polym. Compos.* NA-NA (2009) doi:10.1002/pc.20908.

Chapter 5: General conclusions

This study fully discusses the performance regulation of thermoplastic epoxy by the dispersion of PEG. The study aims to develop multifunctional, multimodal SMMs that have applications in thermal actuation, artificial muscles, smart textiles, flexibility, and healable materials based on thermoplastic epoxy resins by investigating the thermal and mechanical properties of PEG-modified thermoplastic epoxy. The method of PEG-dispersed thermoplastic epoxy shows great potential for application, and PEG-modified thermoplastic epoxy is expected to develop higher performance, composite materials for more functions and applications. The results of the research conducted are summarized below, respectively.

In chapter 2, thermoplastic epoxy was developed through a polymerization reaction of an epoxy resin mixture composed of epoxy and phenol monomers. Then, thermoplastic epoxy filament with an average diameter of 0.285 mm was developed by the melt-drawing process. The developed SMEF-TP has a partial crystal structure, a higher T_g range from 80 °C to 100 °C, and excellent mechanical properties wherein the yield stress increased by 54% compared to thermoplastic epoxy films. Through shape memory experiments, it is revealed that the thermoplastic epoxy filament has excellent shape memory performance. The shape fixation rate

can reach 97%, the shape recovery rate can reach more than 97%, and the cyclic test showed good stability. The shape recovery stress of thermoplastic epoxy filament was further tested to show that it can stably respond to temperature, and the shape recovery stress increases with the increase of strain, reaching 1.45 MPa at a strain of 35%. The thermal actuation experiment of thermoplastic epoxy filament shows that the energy density can reach 0.066 J/cm^3 and the capacity of textile processing has also expanded its application in textile-type thermal actuation. The developed thermoplastic epoxy filament shows excellent shape memory performance and can output large shape recovery stress, which is more than 5 times that of thermoplastic epoxy film. As a new type of shape memory filament, thermoplastic epoxy filament has shown huge application potential in the field of artificial muscles and smart textiles.

In chapter 3, the mechanical and thermal properties of thermoplastic epoxy were successfully regulated by the uniform, stable, and environmentally friendly dispersion of PEG, and the shape memory epoxy-PEG films ranging from rigid to flexible were furtherly developed. Thermal analysis and FTIR analysis showed that epoxy-PEG with different PEG contents were fully polymerized. FTIR analysis also confirmed the distribution of PEG molecules among the polymerized epoxy molecules. Thermal stability analysis showed that PEG did not significantly reduce the thermal stability of epoxy-PEG, and the weight loss at 300 °C remained

within 3.89%. Tensile analysis showed that with the increase of PEG content, the epoxy-PEG film gradually changed from a rigid film with high breaking stress and low breaking stress to a gel-like film with low breaking stress and high breaking stress. Thermomechanical analysis showed that the T_g of epoxy-PEG films decreased sequentially with the increase of PEG content. Shape memory analysis showed that epoxy-PEG with different PEG contents all had recovery rates between 92% and 100%, which could be switched between original and temporary shapes by respective stimuli-temperature. In addition, PEG-40 also exhibits excellent healable and adhesive properties. The regulation of thermoplastic epoxy by PEG makes thermoplastic epoxy show greater application potential in the field of shape memory and flexible smart materials.

In chapter 4, to achieve heat-stimuli controllability of shape memory function, shape memory thermoplastic epoxy-PEG filaments with controllable stimuli temperature were prepared. The chemical structure analysis revealed that the dispersion of PEG did not hinder the polymerization reaction of epoxy resin. Thermal analysis showed that both the T_g and melt spinning temperatures of epoxy-PEG filaments could be adjusted based on the PEG content. Mechanical analysis showed that PEG enhanced both Young's modulus and yield stress of epoxy-PEG filaments. Shape memory analysis showed that epoxy-PEG filaments exhibit excellent shape memory performance with a shape fixation rate range from

95.8% to 99.1% and a shape recovery rate range from 93.1% to 99.0%. The TEP–PEG filaments have obtained controllable stimuli temperature and greater their shape fixation rates after PEG modification. Furthermore, the recovery stress test showed that epoxy-PEG filaments have higher recovery stress at lower temperatures after PEG modification. The difficulty of melt processing for thermoplastic epoxy was reduced in a more environmentally friendly way, and shape memory epoxy-PEG filaments with different stimuli temperature were developed without reducing Young's modulus. With the addition of PEG, epoxy-PEG filaments not only realized the heat-stimuli controllability of shape memory function but also showed greater thermal actuation ability, indicating a wider range of applications, such as thermal actuation, smart textiles, and artificial muscles.

In conclusion, thermoplastic epoxy-PEG has excellent shape memory function and shows application potential in healable and adhesive fields. In future research, multi-stimuli responsive and multifunctional composites including flexible smart materials will be developed based on thermoplastic epoxy.

List of publications

[1] **Baoji Hu**, Hong Xia, Fan Liu, Qing-Qing Ni. Development of thermoplastic epoxy filaments with shape memory properties[J]. Polymer Testing, 2021,103:107374.

[2] **Baoji Hu**, Hong Xia, Fan Liu, Qing-Qing Ni. Heat-stimuli controllability of shape memory thermoplastic epoxy filaments by adding polyethylene glycol[J]. Polymer, 2022,250:124818.

[3] **Baoji Hu**, Hong Xia, Fan Liu, Hao Wang, Qing-Qing Ni. Development of shape memory thermoplastic epoxy films with human skin temperature response and self-healing function through the regulation of thermal and mechanical properties by PEG. Progress in Organic Coatings, Under review.

[4] Hao Wang, Hong Xia, Zhenzhen Xu, **Baoji Hu**, et al. Heat-stimuli shape memory effect of poly(ε-caprolactone)-cellulose acetate composite tubular scaffolds[J]. Biomacromolecules. Accept.

Scientific presentation

Baoji Hu, Hong Xia, Fan Liu, Qing-Qing Ni, Development of thermoplastic epoxy filaments with shape memory properties. China-Japan Composite Materials Academic and Technology Exchange Conference, Wuhu, China.

Acknowledgements

I would like to thank Prof. Qing-Qing Ni for his continued support, guidance, and concern. His profound knowledge and rich experience helped me overcome many research difficulties. Under his guidance, my research gradually entered the hall of scientific research, and successfully obtained a doctorate degree.

Many thanks also to Prof. Toshiaki Natsuki, Prof. Yasuo Gotoh, Prof. Toshihisa Tanaka, and Prof. Ick-Soo Kim, for their continued support of my research.

I would like to thank Dr. Hong Xia who has been assisting my experiments and has been guiding my subject experiments. She also provided me with a lot of creative ideas and paper writing skills. She has been a great help to my research at Shinshu University and my life in Ueda City.

I would like to thank the teachers including Liu Fan, Zhang Heng, Li Wei, and Cheng Xiaoying for their support in my research.

I would like to thank the many staff at Shinshu University, including Katayama Yukari and Saito Yuki. I would like to especially thank Katayama Yukari, the international student in charge, who has always supported and helped me in my studies.

I would like to thank my colleagues in our laboratory: Chen Hairong,

Guan Xiaoyu, Hong Jun, Xu Ping, Hui Jin, Liu Yajun, Cui Lina, Huang Canyi, Li Chongchao, Piw Piw, Yan Yongjie, Xing Jian, Qu Jingyan, Chen Si, Li Fengyu, Wang Hao, Jing Yinan, Su Guangyu, Wang Xinchen, Yang Wendan, and Nakazawa Kodai. They have always supported my research and cared about my life. Among them, I would like to especially thank Chen Hairong, Guan Xiaoyu, Hong Jun, Liu Yajun and Hui Jin, who provided valuable suggestions for my research. I would also like to express my special thanks to Li Fengyu and Chen Si, they have given me a lot of company, and I wish them better achievements in the future. I would also like to wish Wang Hao and Qu Jingyan to graduate as soon as possible, and especially thank them for their incredible support and care for my life in Ueda City and my studies at Shinshu University.

I would like to thank many laboratory staff, including Okada Yusuke, Sugawara Kousuke, Yoshioka Sachiko, Muto Yuichi, Nakamura Isao, Takeda Masaaki. They have helped me tremendously in the use of the equipment and also provided valuable advice. Among them, I would like to especially thank Okada Yusuke, who taught me the use of the equipment very kindly, and has always been able to solve my doubts during the test. We often communicated about the test.

I would like to thank the students in the research groups of Prof. Yasuo Gotoh and Prof. Ick-Soo Kim, for their help and support for my research.

I would like to thank my friends at Shinshu University, they are Wang

Feifei, Jiang Bin, Li Fang, Weng Kai, Liu Shizhu, Zhu Pengbo, Wang Jiaan, Sun Ye, Yu Yongtao, Wang Mingxu, and Fu Jiajia, who have always supported my research and life. Among them, I would like to especially thank Wang Feifei and Jiang Bin, they have provided tremendous help to my research and life at Shinshu University, respectively.

I would like to thank two students, Sonobe Miki and Sudo Kanako. I instructed their experimental projects and assist with their graduation assignments. They have similar research to me and have done a lot of experiments together. They helped me a lot with my research at Shinshu University and my life in Ueda City. I hope they work well and achieve better results in the future.

I would like to thank the Japanese teachers at Shinshu University, Teacher IDE, and Teacher KATASHO who have taught me Japanese seriously and professionally.

I would like to thank the Shinshu University Chinomori Fund for its support with scholarships and grants.

Huge thanks to the Japan Society for the Promotion of Science (JSPS KAKENHI 20H00288 and 21K04675) and National Natural Science Foundation of China (No.52073259), which supported my research.

I would like to thank every teacher, student, and friend who helped me during my Ph.D. program at Shinshu University.

I also want to thank the time. I gradually become my ideal person.

Lastly, and most importantly, so many thanks to my family. I want to enter 1,000 words about gratitude here because the miss happened in the past 1,000 days and nights, and I also know that they miss me in these 1,000 days and nights.